ADVANCED SELF-HEALING POLYMER COMPOSITES FOR WIND TURBINE BLADES

by

Arun Kumar Koralagundi Matt

A Thesis Submitted in

Partial Fulfillment of the

Requirements for the Degree of

Master of Science

in Engineering

at

The University of Wisconsin- Milwaukee

August 2016

ABSTRACT

ADVANCED SELF-HEALING POLYMER COMPOSITES FOR WIND TURBINE BLADES

by

Arun Kumar Koralagundi Matt

The University of Wisconsin-Milwaukee, 2016
Under the Supervision of Professor Ryoichi S. Amano

Wind energy is one of the prime sources of energy among the renewable sources of energy. Wind power has been one of the most promising sources of long-term, clean energy. Materials and design approach in commercial wind turbines have not seen a momentous change in the recent years. In this study, an intriguing bio-mimetic design approach is sought after, which is to heal damages as they arise in a composite material. Self-healing material systems in wind turbine blades have the potential to fulfill the requirement as an added safety mechanism to heal damages and prevent catastrophic failures. Effectively supplying healing agent throughout the composite structure without degrading essential properties is of core interest in this study. Several cost efficient and straightforward techniques to produce vascular channels are attempted in this study. Millimeter and micro scale Borosilicate tubes are used to store and supply the healing agent in glass fiber reinforced thermoset polymer composites with an effort to strengthen and retain the mechanical properties of the composite material. Tensile and bending tests are performed to compare the mechanical properties of polymer composites with tubes to that of without-tubes composite material. Also, Glass transition temperature, the effect of fiber orientation and effect of vacuum infusion process on a conventional composite material (without

tubes) were studied. An attempt was also made to mold and test for mechanical properties of a woven fiberglass reinforced thermoplastic polymer composite material.

Wind turbine blades are under continuous bending forces, and hence, the self-healing of woven fiberglass reinforced thermoset composite material was demonstrated using three-point bending tests. An Ultra Violet (UV) light sensitive dye was mixed with the healing agent to observe the breakage of vascular Borosilicate tubes (500μm outer diameter) and flow of healing agent into the cracks during the bending tests. The flow of healing agent during the flexural test clearly demonstrated discharge of healing agent at the damage site, flow of the healing agent into material cracks and spreading of the healing agent throughout the thickness of the composite at the damage site. A minimum average of 84% healing of maximum flexural strength under three-point bending was obtained among three different vascular channel layouts in the composite material. A prototype of a wind turbine with self-healing Borosilicate vascular tubes embedded in woven fiberglass reinforced thermoset composite blade was also fabricated and tested in a wind tunnel. Depletion of healing agent within the tubes after wind tunnel testing verified the usefulness and potential for self-healing in future wind turbine blades.

To

my parents,

and my sister

TABLE OF CONTENTS

LIST OF FIGURES

LIST OF TABLES

LIST OF EQUATIONS

LIST OF ABBREVIATIONS

1D	1 Dimensional
3D	3 Dimensional
ABS	Acrylonitrile Butadiene Styrene
AFP	Automated Fiber Placement
APA	Anionic Polyamide
ASTM	American Society for Testing and Materials
ATL	Automated Tape Layup
DCPD	Dicyclopentadiene
DMA	Dynamic Mechanical Analysis
FDM	Fused Deposition Modeling
FRC	Fiber Reinforced Composite
NACA	National Advisory Committee for Aeronautics
NREL	National Renewable Energy Laboratory
PMC	Polymer Matrix Composite
PVA	Polyvinyl Alcohol
SH	Self-Healing
UV	Ultra Violet
VARTM	Vacuum Assisted Resin Transfer Molding

NOMENCLATURE

A	Average cross-sectional area, mm^2
b	Width of beam, mm
E'	Elastic/storage modulus, MPa
E''	Loss modulus, MPa
h	Thickness of beam, mm
L	Support span, mm
P_{max}	Maximum applied force, N
T	Specimen temperature, °C
T_g	Glass transition temperature, °C
T_r	Room temperature, °C
η	Healing Efficiency, %
σ_{max}	Stress at the outer surface at mid-span, MPa

ACKNOWLEDGMENTS

I thank Dr. Amano for his support both at a personal level and for carrying out this research project. I thank Dr. Rohatgi for providing valuable insights and feedbacks and allowing me to use his laboratory facilities. I thank Dr. Church for providing vital inputs and also training and allowing me to use his laboratory equipment. I thank Mr. Jie Guo, Mr. Shawn Strong for their extended help throughout the project. I also thank Mr. Jose Rodriguez, Mr. Mathew Rentmeester, Mr. Calvin Falk, Mr. Jeffery Cebe and Mr. Jonathan Christian for their valuable contributions. I thank Mr. Shobhit Misra for his help and guidance. I thank Mr. Rahim Reshadi for his help in carrying out mechanical tests. I thank Dr. Qianyi Zhang and Dr. Steven Hardcastle for their help with SEM and microscopic analysis. I thank Ms. Sulekha Tamvada for proof-reading and supporting this work. Importantly, I thank National Science Foundation (NSF) for funding this project.

I thank my parents and my sister for their invaluable motivation and support.

CHAPTER 1 : INTRODUCTION

Wind Energy currently contributes to 5% of the country's electricity generation making the U. S. rank first in world wind power generation [1]. U. S. Department of Energy (DOE) has reported that wind energy can contribute to 10 percent of the country's electricity by 2020, 20 percent by 2030 and 35 percent by 2050 [2]. It projects that there will be an increase of 86% in the wind energy generated in the U. S. from 2013 to 2020; 273% increase from 2013 to 2030 and a whopping 573% increase from 2013 to 2050 making it potentially, one of the most significant sources of energy. The extensive use of renewable source of energy like the wind energy would avoid more than 12.3 billion tons of carbon pollution cumulatively by 2050 which is equivalent to avoiding one-third of global annual carbon emissions. It can also save approximately 260 billion gallons of water by 2050 by side-stepping the currently water-intensive energy production processes. With this growth, it not only helps prevent air pollutants from burning fossil fuels but also creates 600,000 jobs and saves $108 billion in health care costs and economic damages caused by burning fossil fuels till 2050 [1]. Annual wind turbine blade failures are estimated to be around 3,800 failures worldwide which accounts for 40% of insurance claims, ahead of gearboxes and generators in the wind power industry [3].

The current material used in the industries as a standard for manufacturing wind turbine blades is thermoset polymer matrix composites and hence, is used in this study. Thermoset polymer includes epoxies, vinyl esters, unsaturated polyesters and more. The chemical composition of thermoset polymer consists of a resin and a hardener. Thermoplastic is another candidate material that was sought after in this study for the application in wind turbine blades. With properties such as higher strength, higher impact resistance, it does not turn brittle at low temperatures and most importantly, the material can be fully recycled for use in another wind turbine blade or any other polymer

application. The main drawback with thermoplastics is with its stringent processing requirements (for reactive processing) during the molding process.

The industry standard used currently for the production of wind turbine blades is the Vacuum Assisted Resin Transfer Molding (VARTM) as the standard process. This process essentially infuses resin uniformly through the mold and minimizes entrapped air by using a vacuum to degas and generate suction.

Turbine blades account for 8% of wind turbine failures and are among the most detrimental of failures. Wind turbine blade failures also cause a downtime of 3-4 days and require preventive maintenance programs by the operator [4]. The most significant challenge faced by the leading industries of renewable energy sector i.e. wind farming industry is that the primary cause of accidents in wind turbines is from blade failure [5]. A survey [6] suggests that there have been 317 separate incidences due to wind turbine blade failure from the 70s to May of 2015 and it emphasizes that this could only be a fraction of the actual (no official information) incidences that take place world over. It is reported that in Germany, pieces of blades have gone through the roofs of nearby buildings [6]. The dangers posed by damaged, high speed wind turbines signify the importance of improving safety mechanisms and the need for development and improvement of these blades.

This research brings to light a bio-mimicking technique called self-healing. Self-healing has been one the most studied area regarding an alternative to damage-tolerant design approach, improving the safety and increasing the life span of the materials including polymers, metals, and ceramics. Most notable development has only been made in implementing this unique characteristic in polymers due to its ease of mimicking.

Figure 1: Photograph of a broken turbine blade at the Prairie Breeze wind farm in Nebraska [7].

Figure 1 shows one of the two blades that broke in a span of two weeks at Nebraska wind farm. With polymers and composites being increasingly used in structural applications in aircraft, cars, ships, defense and construction industries, several techniques have been developed and adopted by industries for repairing visible or detectable damages on the polymeric structures. However, these conventional repair methods are not effective for healing invisible micro-cracks within the structure during its service life. In response, the concept of self-healing polymeric materials was proposed in the 1980s as a means to heal invisible micro-cracks to extend the working life and safety of the polymeric components, which is a novel concept that can be used as an alternative to damage-tolerant design and repair the damaged structures [8].

Since 80% of the total world energy is from non-renewable and depleting fossil fuels, there is a great deal of emphasis on improving the existing renewable sources. Wind energy is one of the

prime sources of energy among the renewable sources of energy. Although biomass and hydropower are some of the most widely used renewable energy sources, wind energy has got the most potential due to its inherent advantages.

Usage of thermoplastics can be a lucrative option when compared to thermoset plastics due to reusability. Usage of thermoplastics gives an edge over thermoset plastics which can be used to produce larger and thicker blades. The main advantage of using larger blades is increased power output per turbine and decrease in cost per kWh. These larger blades are especially suitable for off-shore applications where there are higher power output and no noise pollution or aesthetical issues arise due to increased blade size. Larger blades also promote usage of materials with higher specific properties and requirement of the efficient design.

Self-healing or the ability to autonomically heal cracks in polymers has been of significant research interest since 2001 when White et al. [9] Introduced using micro-encapsulated healing agents. Self-healing has been applied to successfully heal and re-heal (multiple healing cycles) polymer materials.

Self-healing materials can be classified broadly into three groups: (a) capsule based (b) vascular, and (c) intrinsic type of self-healing [10]. The blue and orange/red colors in Figure 2 are representing resin and hardener or curing agent respectively. Each approach differs according to the method by which healing functionality is integrated into the bulk material. (a) In capsule-based self-healing materials, the healing agent is stored in capsules until they are ruptured by damage or dissolved. (b) For vascular materials, the healing agent is stored in hollow channels or fibers until damage ruptures the vasculature and releases the healing agent. (c) Intrinsic materials contain a latent functionality that triggers self-healing of damage via thermally reversible reactions, hydrogen bonding, ionomeric arrangements, or molecular diffusion and entanglement [10].

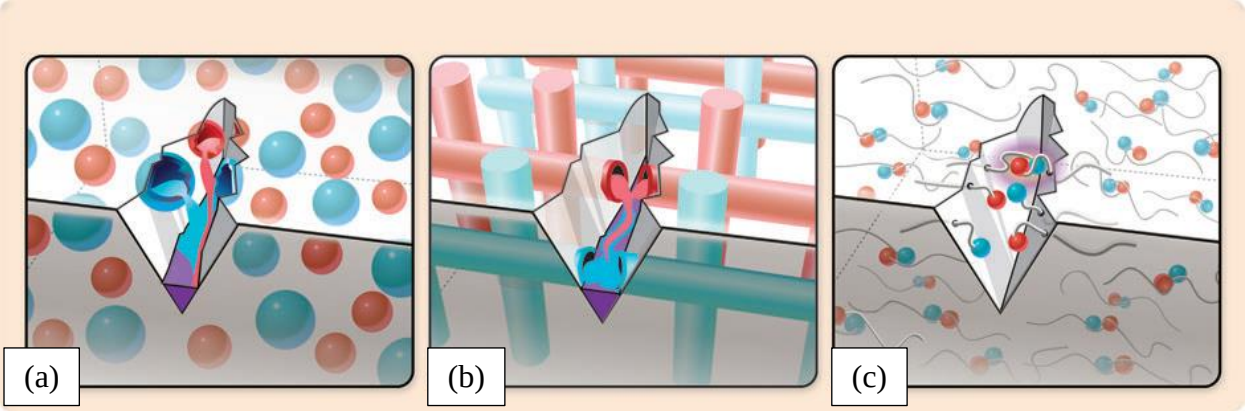

Figure 2: Approaches to self-healing [10]. (a) Capsule based self-healing (b) vascular type of self-healing (c) intrinsic type of self-healing

Ability to automatically and autonomously trigger and heal cracks in a wind turbine blade drives this research at the University of Wisconsin- Milwaukee. This study focuses on the improvement of the current material properties used in the wind turbine blades as a preliminary study. The effect of orientation and the amount of fiber to that of the resin is investigated to suggest improvements to the current turbine blade material. Several materials and configurations are considered to implement self-healing characteristic into fiber reinforced thermoset composite. Variation in tensile properties of the material with and without self-healing configuration is found. The healing performance of self-healing material systems is observed for various arrangements.

CHAPTER 2 : LITERATURE REVIEW

Self-healing in materials is a novel design concept in contrast to the conventional damage tolerance approach. Self-healing materials are a type of smart materials [11] which have a controlled ability to mend thermal and fatigue damages. Cracks in a material start off at a microscopic level, and subsequently propagate and connect causing further damage. A structural material, after regular surface macroscopic maintenance, does not show the same performance standards as the virgin material due to the permanence of internal distortions. The ability to internally fill the crack, delays failure of the material and allows prolonged high-performance standards with low costs in future damage detection and maintenance [12]. As such, these materials promote sustainability in wind turbine energy. Currently, processing of these composite materials is of prime research interest as these novel materials offer potential applicability in various engineering fields.

This approach is inspired by nature where the wounds in mammals are healed by bleeding of the vascular network underneath the skin [13]. Trask et al. made systematic comparisons of the ongoing self-healing mechanisms and categorized the approaches into bio-inspired and biomimetic self-healing [14]. Currently, experiments are in progress to add a strong filling/linking agent within the material to study the healing response to any internal crack. The healing agent could be the polymer itself (i.e., intrinsic self-healing) or pre-embedded agents (i.e., extrinsic self-healing) [15].

White et al. have reported successful autonomic healing (i.e., healing without any human intervention) of structural polymeric materials [9]. Microencapsulated healing agents were introduced into the polymer matrix that released the healing agent upon crack intrusion. Polymerization of the healing agent was then triggered by the catalyst embedded in the matrix material, bonding the crack faces without any human intervention. Kessler and White applied this method to heal glass fiber reinforced composites. They used this method to study the healing of

delamination damage in woven E-glass/epoxy composites and found that, up to 67% of the virgin fracture toughness could be recovered by manually injecting catalyzed monomer into the damaged region, and up to 19% of the virgin fracture toughness could be recovered from self-activated composite samples [16]. Later, Kessler and White reported that as much as 45% of the virgin inter-laminar fracture toughness could be recovered on fiber reinforced structural polymer composite by the use of a microencapsulated healing agent. Comparison of this in situ healing with that of neat epoxy resin was made in the study, and it was found that the presence of these microcapsules did not significantly affect the stiffness of the composite [17]. Although quite successful [18] [19], this method of using microcapsules containing healing agent has limitations in terms of healing efficiency due to the clumping of microcapsules in the interstitial regions within the fiber fabrics that reinforce the composite. More importantly, the healing is limited to a single damage event at a given location with the creation of a void after the healing agent is consumed from the microcapsule [15].

Toohey et al. [20]introduced autonomous healing for multiple cycles. The design was bio-inspired and contained a three-dimensional (3D) network of coating-substrate architecture. The 3D substrate (which was the microvascular structure supplying the healing agent Dicyclopentadiene) was processed using soft lithography technique involving direct-write assembly of a fugitive organic ink. The spacing between the channels was dictated by the visco–elastic properties of the fugitive ink. An epoxy layer was coated on this substrate, and solid catalyst particles (Grubbs' catalyst) were dispersed in the matrix to initiate polymerization. The samples were tested to check the efficiency of healing using four-point bending technique at different percentages by weight of the catalyst to the epoxy coating [20].

Direct-write assembly, by the inherent nature of the process, is not a suitable technique to accommodate the inclusion of glass fibers/carbon fibers to form a composite and hence, the process has not been used to manufacture a glass fiber reinforced composite. The complexity of the healing process is increased by the presence of glass fibers and the consequent increase in the number of damage modes.

The above findings lead to exploring an alternative method to produce the vascular network to supply the necessary healing agent in fiber reinforced composite PMC (Polymer Matrix Composite). As the scope of wind power generation is expanding as a high potential renewable resource, there is a tremendous technological progress regarding design and manufacturing of the wind turbines, with shapes of turbines being regularly updated the world over [21]. Self-healing in wind turbine blades studied in this work, is bound to enhance the reliability of the currently employed fiber reinforced, thermoset composite blades. Also, with the advent of mixed, carbon fiber and glass fiber reinforcements within a blade, the self-healing methodology can be readily extended to carbon fiber reinforcements barring Automated Tape Layup (ATL) or Automated Fiber Placement (AFP) techniques. These techniques use advanced robotics to lay fiber glass layer after layer.

Huang, et al. [22] studied the influence of embedded circular hollow vascules on the structural performance of a fiber reinforced polymer (FRC) composite laminate. The presence of these off-axis vascules caused resin rich regions in the FRC laminates. In-plane and out-of-plane fiber alignment was changed due to the inclusion of these vascules. A proportional correlation between the cross-sectional diameter of vascules to that of the resin-rich region area, the pocket length and the fiber disturbance height was found in their experimental study. The study revealed that the

compressive strength of the FRC composites decreases with the inclusion of vascules and further decreases with the increase in cross-sectional vascule diameter.

Motuku, et al. [23] used hollow glass fibers, Borosilicate glass micro-capillary pipettes (1.15 mm outer diameter), flint glass Pasteur pipettes, copper tubing and aluminum tubing in addition to conventional plain weave fiberglass fabrics in polymer composites to study and choose an optimal material to supply the healing agent for low velocity impact. Borosilicate glass micro-capillary tubes were selected as the best material to supply the healing agent with equivalent impact strength to that of conventional composite material. This concept is supported by the study made by Matt, et al. [24] on hollow Borosilicate tubes (1mm outer diameter) in fiberglass reinforced polymer composites. Equivalent tensile strength was observed in the samples with and without Borosilicate tubes. The tubes were used both as reinforcements and to supply the healing agent.

From this literature review, it was evident that vascular network type of self-heling with the potential to heal multiple cycles is the best match for wind turbine blade application. Also, from the study made by Huang et al. [22] reveals that the decreasing the size of the vascules, decreases resin rich region and therefore, improves the properties of the composite material. Motuku et al. [23] showed that Borosilicate tubes were the best method to supply the healing agent. The project has been carried out with this important lesson from literature in mind.

CHAPTER 3 : METHODOLOGY AND STANDARDS

3.1 Introduction

Fiber glass composites are prominently used in wind turbine blades world over because of their cost, effectiveness and availability. Although wind turbine blade material composition is proprietary information, the core composition is woven fiberglass reinforced thermoset polymer composite at most parts of the blade; most prominently at skin and root end sections of the blade. Hence, the woven fiberglass reinforced thermoset epoxy composite is used in this study. Apart from standards and procedures employed, this chapter also contains details on set-up and optimization of Vacuum Assisted Resin Transfer Molding (VARTM) process.

3.2 Materials used

The details of important materials used in this work are as follows

3.2.1 Resin

Marine Epoxy supplied by fiberglasssite.com website was used for molding all the composites in this work. The details of the chemical name and their weight percentage are mentioned in Table 1,

Table 1: Marine Epoxy chemical name

Material	Chemical Name	Weight %
Resin	Phenol, polymer with formaldehyde, glycidyl ether	>95%
Curing agent	Polyethylene Polyamine	<10%
	Propoxylated Polyethylene Polyamines	<90%

3.2.2 Fiber

Plain weave, woven Fiberglass fabric: 0.254 kg/m^2, 02794mm thick (Ends × Picks per inch = 16 X 14) supplied by Fiberglast.com website.

3.2.3 Healing agent

Dicyclopentadiene was used as the healing agent that was sourced from 'Sigma-Aldrich Co. LLC.' company with a chemical formula of $C_{10}H_{12}$. The chemical is heated in about 150°C for about 5 min to completely liquefy the compound [25] and fill them into the tubes.

3.2.4 Catalyst

Grubb's 1st generation catalyst was used as the catalyst to mix and disperse in the composite matrix (resin). The chemical was sourced from 'Sigma-Aldrich Co. LLC.' company with an empirical formula as $C_{43}H_{72}Cl_2P_2Ru$ as mentioned by the manufacturer.

3.2.5 Tubes

Borosilicate tubes of 500µm outer diameter, 250µm inner diameter and 100mm in length were sourced from 'FHC Co.' company. Similar, Borosilicate tubes of 1mm outer diameter and 0.5mm inner diameter and 100mm length are also sourced from the same manufacturer for initial trails.

3.3 Vacuum Assisted Resin Transfer Molding (VARTM)

Vacuum Assisted Resin Transfer Molding (VARTM) is the industry standard for molding wind turbine blades and schematic of the process is shown in Figure 3. The vacuum infusion process uses vacuum infusion to eliminate or minimize entrapped air and reduce resin volume in the composite. Commercial grade marine epoxy resin and medium cure hardener were used for this study. VARTM process involved placing six layers of glass fibers over wax coated die/base plate.

Over these, a layer of peel ply and breather material was laid and they were then covered and sealed by a vacuum bag which has provisions for resin-hardener mixture inlet and outlet (for vacuum connection and resin overflow). The setup was checked for vacuum leakages and the gaps were sealed

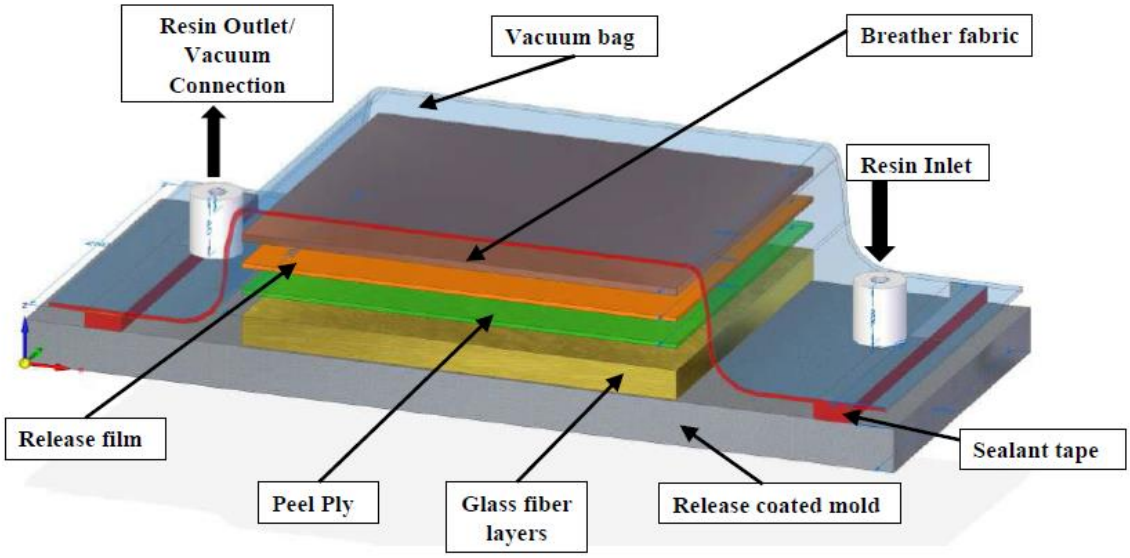

Figure 3: Schematic of the Vacuum Assisted Resin Transfer Molding (VARTM) process (section view)

The resin and the hardener were mixed in 3:1 ratio by volume. Using a vacuum pump, a suction pressure of about -80 kPa was generated to infuse the resin into the glass fiber layers. The mold was left to cure (exothermic reaction) at room temperature for 24 hr. Wax or mold release spray is used over the die before molding for ease of removal of the mold.

3.4 Tensile testing standards

Tensile samples were prepared and tested by ASTM D3039 “Standard Test Method for Tensile Properties of Polymer Matrix Composite Materials” [26]. Tensile tests were performed using Instron Tensile Testing Machine. Extension rate of 0.05 in/min (1.27 mm/min) was used. The samples had ½ in. width. Gage length of 2 in. (5.08mm) was used.

Maximum tensile stress was calculated using

$$\sigma_{max} = \frac{P^{max}}{A}$$

Equation 1. Maximum Tensile Stress (MPa) equation

Where: σ_{max} = maximum tensile stress, MPa

P_{max} = maximum force, N

A = average cross-sectional area, mm^2

3.5 Three-point bend testing standards

Three-point bend test samples were prepared and tested in accordance with ASTM D7264 "Standard Test Method for Flexural Properties of Polymer Matrix Composite Materials" [27]. Flexural tests were performed using 'Instron Corporation' tensile testing machine. Cross-head rate of 0.05 in/min (0.127 mm/min) was used and samples had ½ in. width. A span to thickness ration of 32:1 was used and a fixed span length of 64.23 mm (2.5 in.) was used.

Maximum flexural stress was obtained using

$$\sigma_{max} = \frac{3P_{max}L}{2bh^2}$$

Equation 2: Maximum Flexural Stress (MPa) equation

Where: σ_{max} = stress at the outer surface at mid-span, MPa

P_{max} = Maximum applied force, N

L = support span, mm

b = width of the beam, mm

h = thickness of beam, mm

3.6 Healing Efficiency

Since the specimen geometry remains the same for a particular sample, healing efficiency can be given as

$$\eta = \frac{P_{max}^{Healed}}{P_{max}^{Virgin}}$$

Equation 3: Healing efficiency equation for a self-healed sample under three-point bending

Where: P_{max} = Maximum applied force, N

3.7 Dynamic Mechanical Analysis (DMA) under flexure

Molded samples were subjected to DMA under flexural three-point bend (ASTM standard test method for Plastics to obtain dynamic mechanical properties in flexure) (three-point bending) [28]. The equipment used was "TA instruments," Q800 DMA [29]. Oscillation amplitude of 20 µm and 1Hz frequency was used for the analysis.

3.8 Polishing and microscopy

Molded samples were cut using a tungsten carbide cutting tool (Dremel™). For optical examination, the samples were polished using 240, 320, 400, 600, 800, and 1000 grit silicon carbide emery papers progressively. Micron range alumina slurry on a fine cloth was used for final polishing of the samples. The macrographs were taken using 'Carl Zeiss AG' stereo microscope.

CHAPTER 4 : THERMOSET COMPOSITE EXPERIMENTAL DETAILS

4.1 Introduction

The study involves optimization of fiber layup and orientation. Dynamic flexural analysis of the neat composite material to obtain storage modulus and glass transition temperature. Development of vascular channels through the composite to supply the healing agent and hence, to implement self-healing characteristic into the composite material.

4.2 Effect of fiber orientation and vacuum infusion process

To study the effect of orientation of the glass fibers on the tensile strength of the composites, the weave directions of the glass fiber layers are varied, and the comparison is made with the ones that are kept constant. Three samples were molded with variation of fiber layout and variation in molding processes to compare their tensile properties. The mold used to prepare Sample I for tensile testing had glass fibers oriented at 45° to each other between layers i.e., the weave direction of the bottom most glass fiber layer would be at 45° angle to the weave direction of the 2^{nd} layer from the bottom and so on up to 6 glass fiber layers. Similarly, the mold used to prepare Sample II for tensile testing had glass fibers oriented parallel to each other between the layers i.e., the weave directions of all the glass fiber layers used to prepare the composite had the same orientation. To study the effect of vacuum infusion process, a glass fiber polymer matrix composite mold used to mold Sample III was molded using simple hand layup process where in resin-hardener mixture is manually poured on to six layers of glass fibers on a flat die/ base plate. The

orientation of the weave in the woven roving glass fiber layers are aligned in the same direction between the layers. Analysis and results of the samples are discussed in the results section.

4.3 Dynamic Mechanical Analysis (DMA) sample preparation

A conventional PMC was molded using this process and three samples “A,” “B,” and “C” each measuring 20mm × 13mm × 2.2mm were cut from the main sample at equal intervals. All three samples were tested to assure consistency in the results obtained.

4.4 Developing a novel method to mold hollow vasculatures

Wind turbine blades undergo fatigue and their performance depletes as time progresses due to the formation of internal cracks that hamper the performance of the wind turbine blade. Self-healing in polymers is a novel technique used to heal the cracks autonomously as they form. In this study, new methods are tried as explained in section 4.4.1 through 4.4.6and a method is demonstrated to supply the monomer through the composite that is quintessential for the healing process.

4.4.1 Commercial Borosilicate tubes- larger size (1mm outer diameter)

Commercial tubes were used to produce a 2-D planar network between glass fiber layers to increase the accessibility of the healing agent. The tube orientations were varied and their effect on the composite structure is observed.

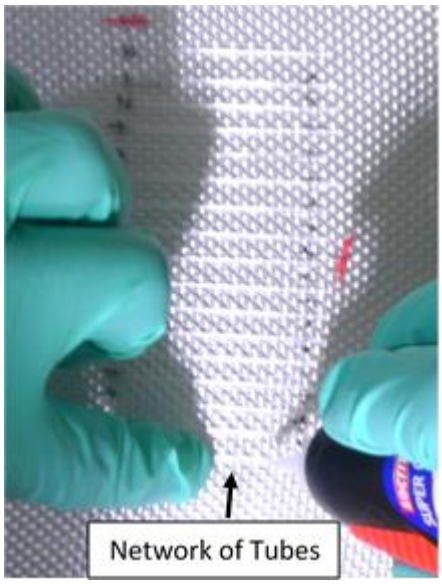

Figure 4: Photograph of the tubes being placed with small drops of glue to hold them in place

The microtubes in the mold used to obtain sample "D" were placed in between the layers of glass fiber fabrics as seen in Figure 4. The layout of microtubes was oriented perpendicular to each other between the layers, i.e., the direction of the tubes between layers was 90° to each other through the thickness. The tubes were parallel and placed equidistant at approximately 6 mm apart from each other within a layer. Therefore, sample D, in essence, contained three layers of micro-tubes along the resin-hardener flow direction during the resin infusion process and two layers of micro-tubes perpendicular to the direction of the flow. The ends of the microtubes were sealed with commercial glue to avoid resin penetration

Figure 5. Photograph during the molding process of sample D. Resin-hardener mixture is flowing from right to left.

A similar process was used for the preparation of the mold used to obtain sample "E," the only difference being the orientation of microtubes.

The microtubes were placed along the resin-hardener flow direction i.e., all the tubes within and between the layers were all parallel to the resin flow direction during the resin infusion process. Flow of resin during the vacuum infusion process is shown in Figure 5. The tubes were all 6mm apart within any particular layer. Mold analysis and tensile test results of samples with large tubes are discussed in the results section.

4.4.2 Floral stem wire pull-out

The second trial was conducted using floral stem which are used in gardening to vertically straighten and support the growth of a plant. Floral stem wires were used so that they could be pulled out of the cured sample. This trial had similar layup as the first trial; six layers of fiberglass with a layer of 1 mm diameter, floral stem wires in the middle of the composite. The stem wires were placed 6 mm apart and coated with wax before conducting the VARTM process. After the curing process as seen in Figure 6, it was found that, although the resin did not bond with the wires, a large amount of friction between the cured resin and wires was present. The process of pulling out the wire from the cured composite damaged the sample due to high friction between the wires and the polymer matrix making the method non-viable for practical applications.

Figure 6: Photograph of the as-molded sample with floral stem wires embedded in it.

4.4.3 Soldering wire pull-out

The third trial was conducted using smooth wires during the molding process. This test was to determine the effect caused by weaving the wires through the fiberglass fabric and without the

weave arrangement to check for the roughness effect in comparison with floral stem wire. The two types of wire arrangements are:

1. With a layout similar to the previous two trials, i.e., a central layer of floral wires without being weaved into the fiberglass layers.
2. A central layer of smooth wires was fabricated into the fiberglass layer beneath it. The weaves had an approximate interval of 5 mm (2 in) between them.

The sample was molded using the VARTM process and allowed to cure, similar to the other trials. Figure 7 shows molded composite photograph. The process of pulling out the smooth wires from the cured, weaved arrangement sample revealed that there was higher friction between the wires and the composite. The process of pulling out smooth wires, without weave arrangement, did not ease the process as friction between the wires and the composite was high enough to twist the wires or damage the composite during the pulling out process. This method of pulling out coated wires was not pursued.

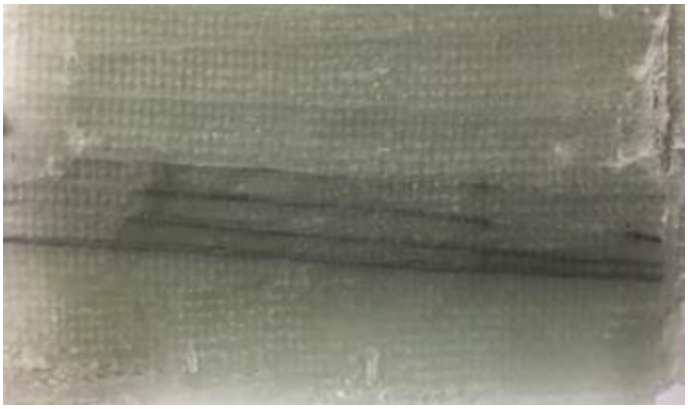

Figure 7: Photograph showing inter-weaved wires resulted in stronger adhesion with the matrix and failing to be pulled out

4.4.4 Polyvinyl Alcohol (PVA) threads

The fourth trial conducted was with the use of polyvinyl alcohol threads. This method was used as an alternative to the wire method, as the pulling out process damaged the composite. When placed in water, polyvinyl alcohol dissolves, creating channels within the sample without destroying it. However, completing the VARTM process and immersing the sample in water for extended periods was unsuccessful to dissolve PVA threads.

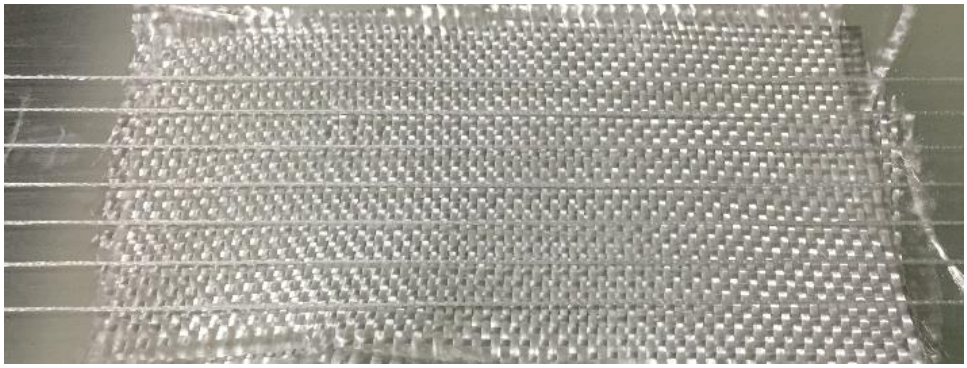

Figure 8: Arrangement of the PVA threads in the middle of fiber glass layers. The threads were glued to the vacuum tape to retain its shape

The PVA threads although having 1mm diameter collectively, contained several thin threads screw threaded together as seen in Figure 8. Hence, the resin during the vacuum infusion process penetrated the interstitial regions between the individual threads.

Figure 9: Photograph of the mold with a layer of PVA strings as central layer

After the VARTM process, the sample was immersed in water for more than 24 hours and because of the small diameter of individual strands in the PVA thread, water did not seep through the mold. As a result, the PVA threads did not dissolve.

Figure 10: Photograph of PVA strings with sugar syrup coat (red dye used to check hollowness)

To overcome the problem, an attempt was made to coat or infuse the strands with sugar syrup. The syrup when dried forms a PVA strand that is impermeable to resin mixture during the vacuum infusion process as shown in Figure 10. The mold was immersed in hot water for about an hour and a red dye was used to check the formation of the channel. Although the method showed positive results in obtaining a hollow cavity, the cavity was inconsistent, the size of the cavity was significantly larger and wider due to the softness of the sugar syrup- PVA thread combination.

4.4.5 Petroleum jelly with wax

The fifth trial conducted was with the use of wax and petroleum jelly mixture. The wax could be melted out of the cured sample without mechanical force. The melting temperature of the wax mixture is lower than the glass transition temperature of the polymer matrix. The mixture consisted of 40% by weight, wax and 60% by weight, petroleum jelly, which was chosen from the study conducted by K S Toohey et. al. [20]. The process was carried out in a hot bath to decrease the viscosity and ease the mixing process. The mixture was then dispensed using a syringe, in rows (approximately 1mm in diameter) as a layer onto the fiberglass. However, this method of

distributing the mixture proved difficult due to the higher viscosity of the mixture as shown in Figure 11. The main concern with this process was with the softness of the mixture for the vacuum infusion process. The wax mixture was squashed under the high vacuum pressures generated during the vacuum infusion process.

Figure 11: Distribution of the mixture proved difficult due to the high viscosity of the material

To overcome this issue, an attempt was made to enclose the wax mixture strands with cured resin before the vacuum infusion process, making it a two-step molding process. Using a thin brush, the resin was brushed onto the wax strands and was allowed to cure as shown in Figure 12. The method proved unsuccessful to form a hard polymer layer around the wax strands as the resin slid down the slippery wax strands, leaving behind a soft, uncovered portion of wax exposed, on the top surface of the wax strands.

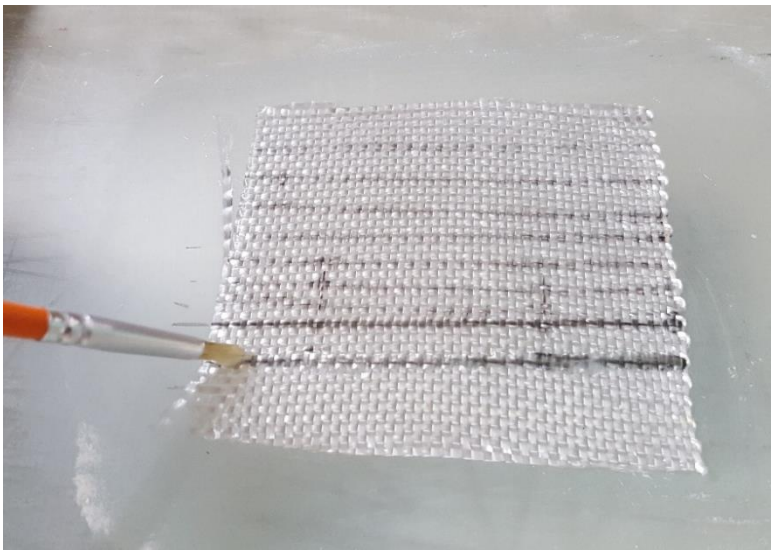

Figure 12: Application of resin on fiberglass using a brush

4.4.6 Commercial Borosilicate tubes- smaller size (500µm outer diameter)

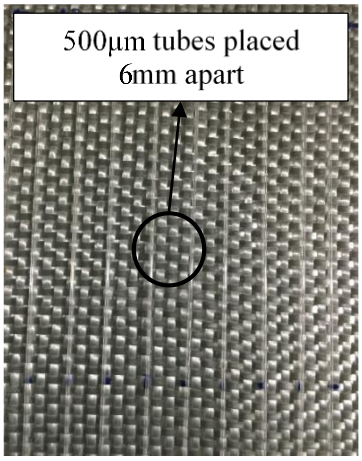

Figure 13. Photograph of hollow Borosilicate tubes arranged approximately 6mm apart

Commercially available hollow, thin walled (250µm thick) Borosilicate tubes were used to study their feasibility to store and supply the healing agent. Vacuum Assisted Resin Transfer Molding (VARTM) process is used to mold the samples to comply with industry standards. The tubes are spaced approximately 6 mm apart and are laid along the direction of resin flow during the vacuum infusion process. Photograph of the arrangement of the tubes is shown in Figure 13. The samples contained a single, central layer of tubes placed at the center of the reinforcing fiberglass fabric layers of the composite material (tubes placed above the 3rd fiberglass fabric from bottom). Sample thickness obtained was about 2 mm thick. Part of the molded composite was cut to 25mm in length and mounted in an acrylic mounting mixture and polished using standard metallographic techniques.

Figure 14. Fiberglass reinforced polymer composite with a central layer of hollow Borosilicate tubes

The combination of Dicyclopentadiene and Grubb's 2nd Generation catalyst was chosen to achieve self-healing. Commercially available Dicyclopentadiene was sourced (from Sigma-Aldrich Co LLC) and heated to around 150°C to liquefy. At this temperature, Dicyclopentadiene undergoes Retro-Diels-Alder reaction to yield Cyclopentadiene. The reaction is reversible and at room temperature, Cyclopentadiene slowly dimerizes to reform Dicyclopentadiene [25]. Dicyclopentadiene and Grubbs 2nd generation catalyst react using ring-opening metathesis polymerization forming the homopolymer polydicyclopentadiene. Liquefied Dicyclopentadiene was filled into the smaller diameter tubes using suction pressure from the vacuum pump while in the liquid state. The process of heating the monomer to around 150°C was repeated as the monomer solidified during the filling process. Figure 15 shows the photograph of 500µm size Borosilicate tubes filled with a healing agent.

Figure 15. 500µm outer diameter Borosilicate tubes filled with Dicyclopentadiene/healing agent

These tubes were chosen for further testing due to their ideal size combined with reinforcing strength.

4.5 Comparison of tensile and flexural strength between conventional (without tubes) and with -tubes composite- sampling

Small Borosilicate tubes were chosen to supply the healing agent, and the reasons are discussed in the results section. 21 specimens were prepared to compare the tensile and flexural strength between conventional (with-out tubes) composite to that of without tubes composite.

4.5.1 Conventional (without-tubes) composite samples

Sample 1 and Sample 2 both contained six layers of glass fibers vacuum infused with epoxy resin.

4.5.1.1 Three-point bending samples

Six three-point bending specimens were cut and finished for testing:

1. Three specimens from sample 1 – S1B1, S1B2, S1B3
2. Three specimens from sample 2 – S2B1, S2B2, S2B3

4.5.1.2 Tensile testing samples

Five tensile test samples were cut and finished for testing:

1. Three specimens from sample 1 – S1T1, S1T2, S1T3
2. Two specimens from sample 2 – S2T2, S2T3

4.5.2 With-tubes composite samples

Sample 3 contained six layers of glass fibers with a central layer of Borosilicate tubes filled with DCPD (Dicyclopentadiene). Sample 4 contained six layers of glass fibers with a central layer of Borosilicate tubes filled with DCPD mixed with 2% by volume a UV (Ultra Violet) reflective dye. Both samples had tubes placed equidistant at around 6mm apart Double sided tape was used to align the tubes.

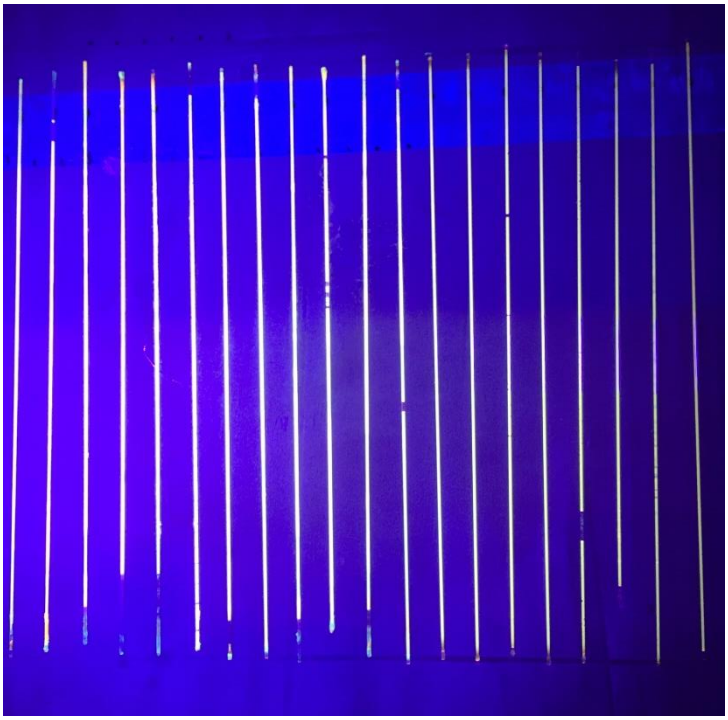

Figure 16: Arrangement of Borosilicate tubes filled with DCPD mixed with UV reflective dye that are 6mm apart

4.5.2.1 Three-point bending samples

Five three-point bending specimens were cut and finished for testing

1. Two specimens from Sample 3 – S3B1, S3B2
2. Three specimens from Sample 4 – S4B1, S4B2, S4B3

4.5.2.2 Tensile testing samples

Five tensile test samples were cut and finished for testing

1. Two specimens from Sample 3 – S3T1, S3T2
2. Three specimens from Sample 4 – S4T1, S4T2, S4T3

4.6 Self-healing of thermoset polymer composites- sampling

The similar procedure used to prepare with-tubes samples (Sample 3 and Sample 4) was used to mold self-healing composites with the inclusion of around 2% by weight catalyst (weight of the uncured resin-hardener mixture). One gram of Grubb's 1st generation catalyst was used for 120ml of resin-hardener mixture).

4.6.1 Self-healing samples with a central layer of tubes

Sample 6 contained six layers of glass fibers with a central layer (above the 3rd layer of glass fiber from bottom) of Borosilicate tubes filled with DCPD mixed with 2% by volume a UV reflective dye. Tubes were placed equidistant at around 6mm apart.

4.6.1.1 Three-point bending samples (self-healing with central layer tubes)

Two specimens from Sample 6 – S6B2, and S6B3 was used for testing. S6B1 had fiber breakage during the neat test (unhealed) and hence, has been eliminated from list

4.6.2 Self-healing samples with tubes as the last layer of composite

Sample 7 was prepared similarly to Sample 6 except that the tubes were places as the final layer i.e. below the 6 layers of glass fiber fabrics (from top).

4.6.2.1 Three-point bending samples (self-healing with tubes as the last layer)

Five specimens from Sample 7 – S7B1, S7B2, S7B3, S7B4, S7B6 was used for testing. Specimens S7B5, S7B7 had fiber breakage during the neat test (unhealed) and hence, has been eliminated from the list.

4.6.3 Self-healing samples with tubes as the penultimate layer

Sample 9 was prepared similarly to Sample 6 except that the tubes were placed above the last layer of glass fiber fabric (from top)

4.6.3.1 Three-point bending samples (self-healing with tubes as the penultimate layer)

Four specimens from Sample 9 – S9B2, S9B3, S9B5 and S9B7 was used for testing. Specimens S9B1, S9B4, S9B6 had fiber breakage during the neat test (unhealed) and hence, have been eliminated from the list.

4.7 List of samples used in this study

Table 2: List of samples used in this study

Sample number	With-tubes/without tubes composite	Use of Catalyst/ no catalyst/ NA (Not Applicable)	Uniqueness in composition of sample
Sample I	Without tubes	NA	Fiber fabrics perpendicular between layers
Sample II	Without tubes	NA	Fiber fabrics parallel between layers (control sample)
Sample III	Without tubes	NA	No VARTM process employed
Sample D	With tubes	No catalyst	Tubes are perpendicular between layers
Sample E	With tubes	No catalyst	Tubes are parallel between layers

Sample 1	Without tubes	NA	Control sample; fiber fabrics parallel between layers
Sample 2	Without tubes	NA	Same as Sample 1
Sample 3	With tubes	No catalyst	Tubes along the resin flow direction in VARTM process (used as a standard in this study)
Sample 4	With tubes	No catalyst	Same as Sample 3
Sample 6	With tubes	Catalyst	Tubes as a central layer
Sample 7	With tubes	Catalyst	Tubes as the last layer
Sample 8	Without tubes	Catalyst	Conventional Thermoplastic composite
Sample 9	With tubes	Catalyst	Tubes as the penultimate layer

CHAPTER 5 : THERMOPLASTIC COMPOSITE

The initial stage of the project was on Thermoplastic wind turbine blades in contrast to the now used, industry standard Thermoset polymer matrix composite. The lead towards thermoplastics was based on the work at TU Delft, Netherlands, [30] which showed detailed feasibility studies on thermoplastic composite wind turbine blades. Because intrinsic self-healing of thermoplastic material could be implemented in wind turbine blades, purchase of Glove Box and Anionic Polyamide (APA) 6 was made. APA 6 with initiator and activator was from Bruggemann Chemicals.

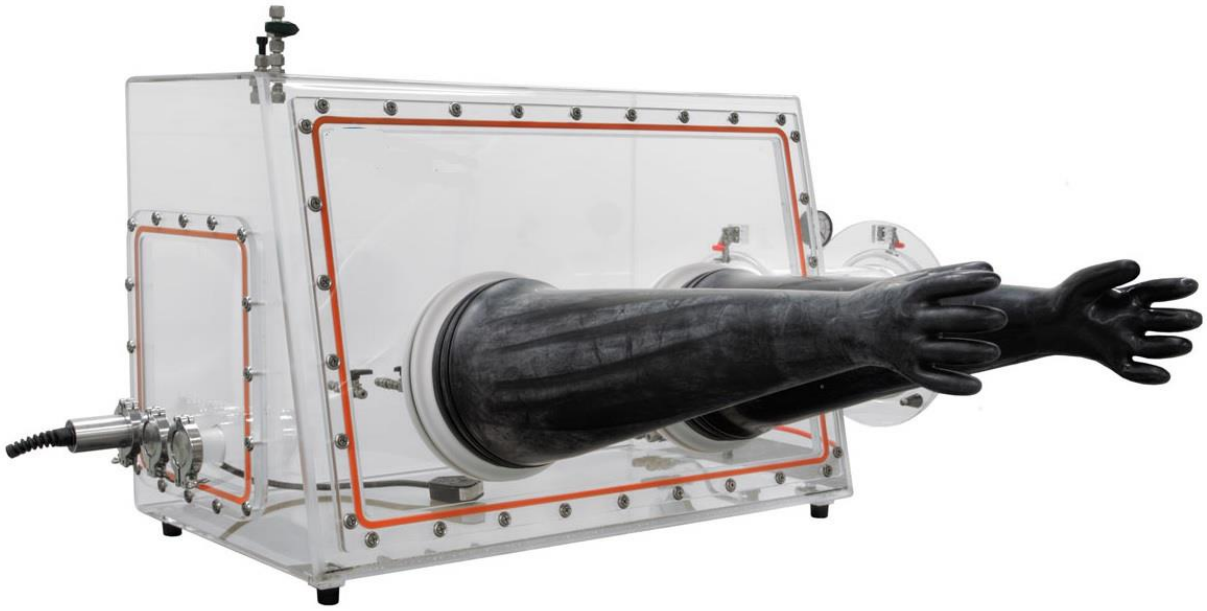

Figure 17: Photograph of the Acrylic glovebox [Photo courtesy- Innovative Technology]

Thermoplastics can be processed by the conventional Melt processing or by newer reactive processing. Reactive processing gives better properties when compared to melt processing. The disadvantages of melt processing are: 1) Poor fatigue performance due to poor fiber-to-matrix bond; 2) Requires introduction of new and expensive technology 3) High material costs due to the

need for intermediate processing steps; 4) High processing temperatures (>200°C); 5) Melt processing limits achievable part size and thickness. For comparison, the advantages of Reactive processing can bring better impact properties and do not turn brittle at low temperatures. Also, it has unlimited shelf-life of raw material and environmental & economic benefits from fully recyclable blades. These advantages over Thermoset plastics motivated us to study on Thermoplastic Wind turbine blades.

As found by Kjelt van Rijswijk in their work [30], APA 6 is extremely susceptible to moisture and required lower than 200ppm of moisture even to open the package. The Acrylic purge box required house inert gas supply as the moisture levels never dropped below 400ppm. The acrylic purge box could not sustain the low moisture levels as it needed a house inert gas supply. Several trials were made to reduce the moisture levels:

1. Silica gel was used
2. Anhydrous Calcium Chloride
3. 99.99% pure Nitrogen as purge gas
4. 99.99% pure Argon gas

None of the above attempts yielded in the drop of the moisture levels in the glove box.

It was evident from these trials that the implementation of Thermoplastic materials into industries was not a practical route to improving the wind turbine blades as the complexity was shown in their feasibility study of Kjelt van Rijswijk [30]. Sample 8 was molded at ambient conditions despite higher moisture levels with 6 layers of fiber glass fabrics parallel between the layers using VARTM process. A combination of Caprolactam, activator and initiator from Bruggemann

Chemical Company was used by melting their original form to liquid at 180°C as per study made by Kjelt van Rijswijk.

5.1 Tensile strength of moisture inhibited thermoplastic composite

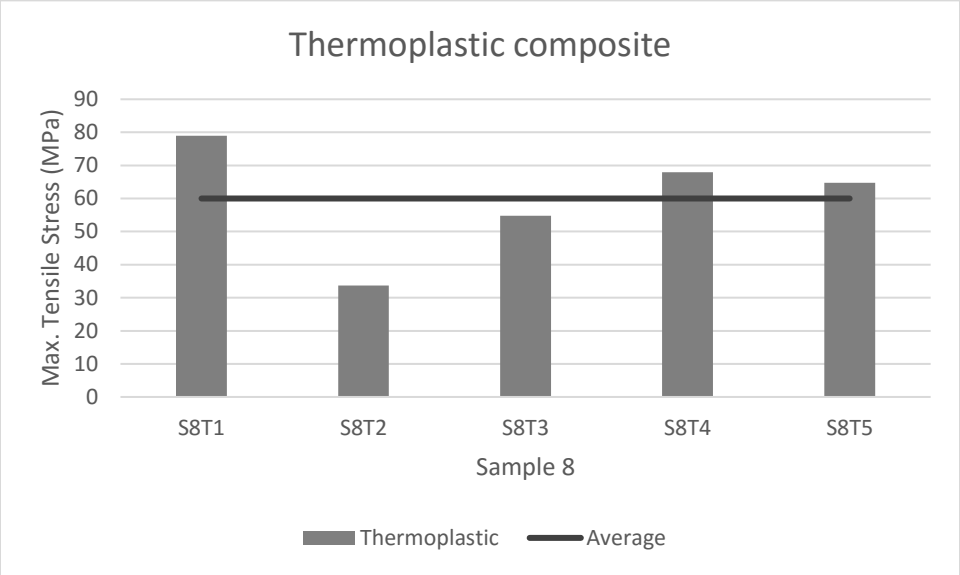

Figure 18: Mas. Tensile Stress (MPa) of moisture inhibited thermoplastic composite

The average maximum tensile stress of the thermoplastic composite was 60 MPa. The tensile strength was about 71.52% decrease in strength as compared to conventional thermoset composite.

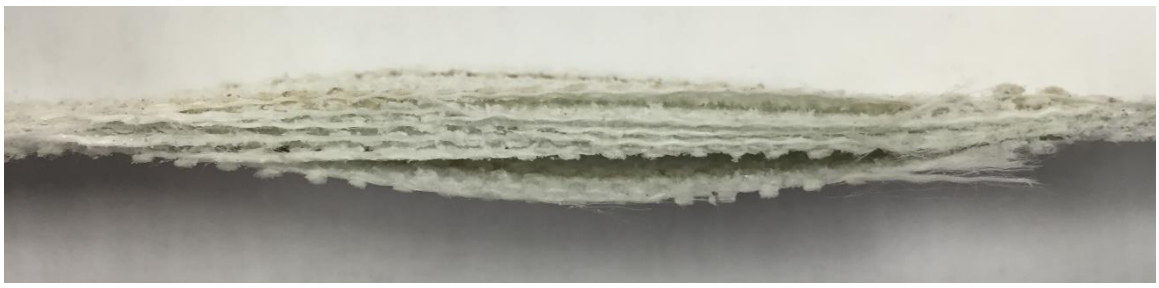

Figure 19: Photograph of reactive processed thermoplastic sample after tensile test exhibiting delamination.

Incomplete polymerization due to higher moisture content weakened the composite drastically its tensile strength. Figure 19: Photograph of reactive processed thermoplastic sample after tensile

test exhibiting delamination. Figure 19 showing complete delamination of the thermoplastic sample after tensile test.

CHAPTER 6 : RESULTS AND DISCUSSION

6.1 Effect of fiber orientation and vacuum infusion process

6.1.1 Advantage of using vacuum infusion process

The molds prepared using VARTM process were around 60% thinner than the mold prepared by using basic hand layup process. The mold due to hand layup process was 5mm thick as compared to 2mm thick molds processed by VARTM process. The VARTM process proved useful in processing the polymer matrix composites. The vacuum assists in the uniform distribution of the resin throughout the fibers producing a composite with uniform thickness. The vacuum also assists in the penetration of the epoxy mixture in between the fiber layers there by obtaining an overall sound matrix-fiber bonding. The hand layup process on the other hand, gives non-uniform thicknesses in the mold and bonding between the glass fibers and resin infusion is limited to just the outer layers of the glass fibers.

6.1.2 Effect of fiber orientation and volume fraction of fibers

The effect of glass fiber orientation was studied by varying the angles of the fibers between each other between the layers using the VARTM process. The tensile strength of composite with glass fiber layers oriented at 45º to each other (Sample I) was compared to composite with glass fiber layers oriented in the same direction (Sample II). The effect of volume fraction of fibers was studied by testing composite molded using the hand layup process (Sample III) similar to the samples molded using the VARTM process. The sample molded using the hand layup process quite clearly had lower fiber to resin volume fraction in comparison to the samples molded using the VARTM process. The tensile strengths and percentage elongation of the individual samples are given in Table 1.

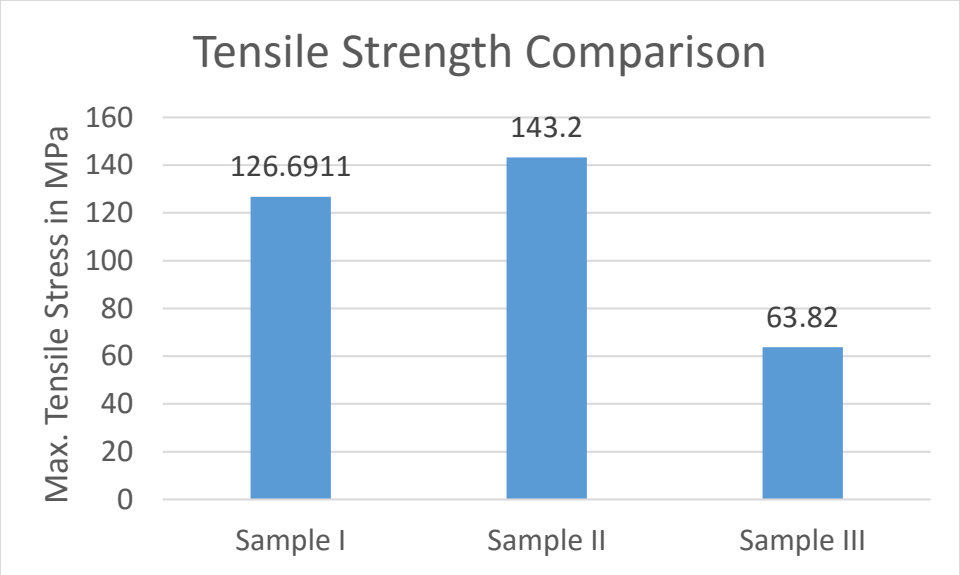

Figure 20: Tensile strength comparison. Sample I and II have varying fiber orientation and Sample II and Sample III are molded using different molding processes

The tensile tests reveal that Sample II has the highest tensile strength followed by Sample I and III in the descending order of strength. This high strength can be attributed to the composite constituents and their orientations. Sample II has the highest load bearing capability as all the glass fiber layers reinforcing the composite are oriented along the same direction, and one of the two weave directions is parallel to the loading direction during the tensile test thereby increasing the strength. The high value of elongation can also be attributed to this fact as more number of fibers are available along the direction of the applied load and so maximum elongation. The small decrease in strength of Sample I as compared to Sample II is due to the variation in the orientation of the glass fiber layers. Three of the six glass fiber layers constituting the composite reinforcement are at 45^{o} to the direction of the applied load during the tensile test thereby reducing the load bearing capability along that direction. Although, there is a small reduction in strength, Sample I has its advantage as it would hold this value of strength nearly independent of the direction of the applied load in that plane.

Sample I and II processed by VARTM process, shows good load bearing capability as compared to Sample III which is processed by basic Hand layup process. Sample III shows least load bearing capability due to lower volume percentage of fiber in the composite. The sample also has the least percentage elongation making it the most brittle of the three composites.

6.1.3 Morphological analysis of the fracture surface

The Scanning Electron Microscope (SEM) examination of the fracture surface of the composite support the tensile test data. The morphological study of the fracture surface of the tensile Sample I reveal that there is a considerable elongation of fibers before fracture in the composite with varying fiber angles by the tensile test data. The elongation in Sample II composite with fibers oriented in the same direction was found to be much higher than that of composite with varying fiber orientation between layers (Sample I).

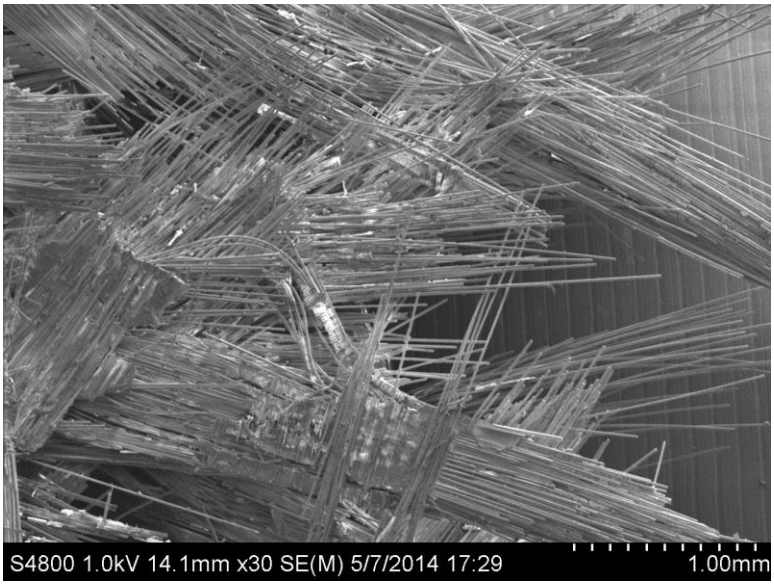

Figure 21. Scanning Electron Microscope image of the fracture surface of the composite with varying fiber orientation between layers and molded by VARTM process (Sample I)

The decrease in strength and elongation in Sample I as compared to Sample II, as seen in (Figure 21), is due to reduced number of fibers oriented in the loading direction unlike in Sample I (Figure 22).

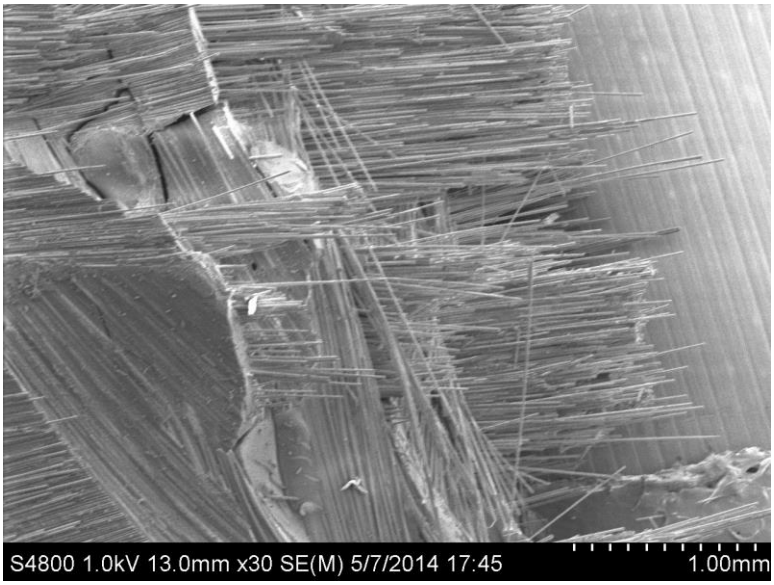

Figure 22. Scanning Electron Microscope image of the fracture surface of the composite with uniform fiber orientation between layers and molded by VARTM process (Sample II)

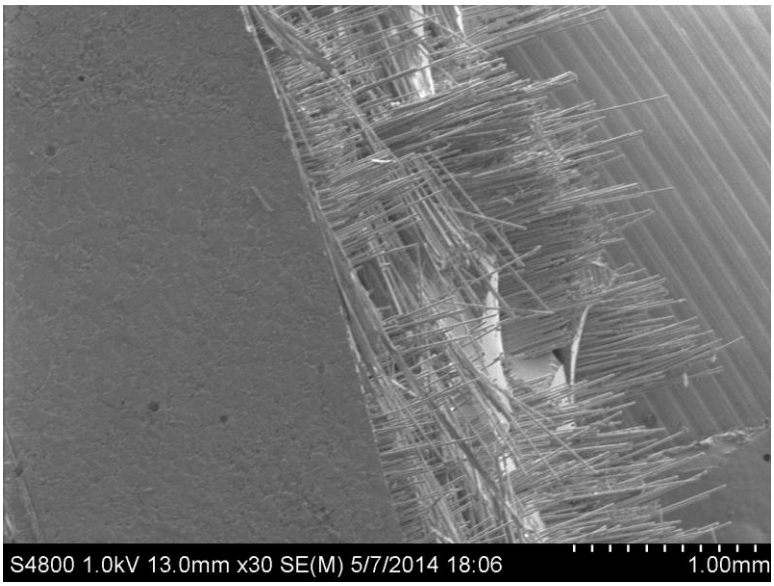

Figure 23. Scanning Electron Microscope image of the fracture surface of the composite with uniform fiber orientation between layers and molded by Hand layup process (Sample III)

With reduced volume fraction of fibers in Sample III (Figure 23), the type of fracture is dominated by the resin in the composite and hence, a brittle type of fracture can be observed with minimum elongation. This kind of failure is considered the most detrimental of all the type of failures as the component does not provide any signs of failure like yielding but fails suddenly without warning. Hence, such materials must be avoided for engineering applications.

6.2 Dynamic Mechanical Analysis (DMA) results

The DMA in flexure were carried out for samples A, B, and C (the conventional PMC mold) by using ASTM standards as mentioned in Section 4.3. All the conventional composite samples showed consistent results. The plot of (a) storage modulus, (b) loss modulus, and (c) tan -delta as a function of temperature for one of the three samples is shown in Figure 24 (corresponding to sample 1).

In Figure 24, (for specimen "A") the curves show the variation of storage modulus, Loss modulus and tan -delta of the sample against temperature. The specimen's elastic (storage) modulus is constant at around E' =13,750 MPa, right at room temperature (Tr =23°C) till it reaches the glass transition temperature. The modulus onset at E' onset ≈57°C. This temperature relates to the mechanical failure of the material during which it softens due to the onset of cross-linked polymer chain movement of the cured epoxy material. This in turn, decreases the modulus significantly to E' =500 MPa at T =75°C in a linear manner. The loss modulus plot peaks at Tg by E'' Peak= 62.5°C and is related to the physical property changes attributed to the glass transition. The tan -delta peak gives the conventional value of glass transition temperature historically found in the literature. The peak represents a good approximation of glass transition temperature from the midpoint between glassy and rubbery states of a polymer. The peak in sample A was found to be at Tg by tan-delta peak =67°C. Samples B and C also showed close similarities in variation as sample A. The glass

transition temperature of tan -delta peak was consistent at approximately 67°C substantiating that the results were consistent.

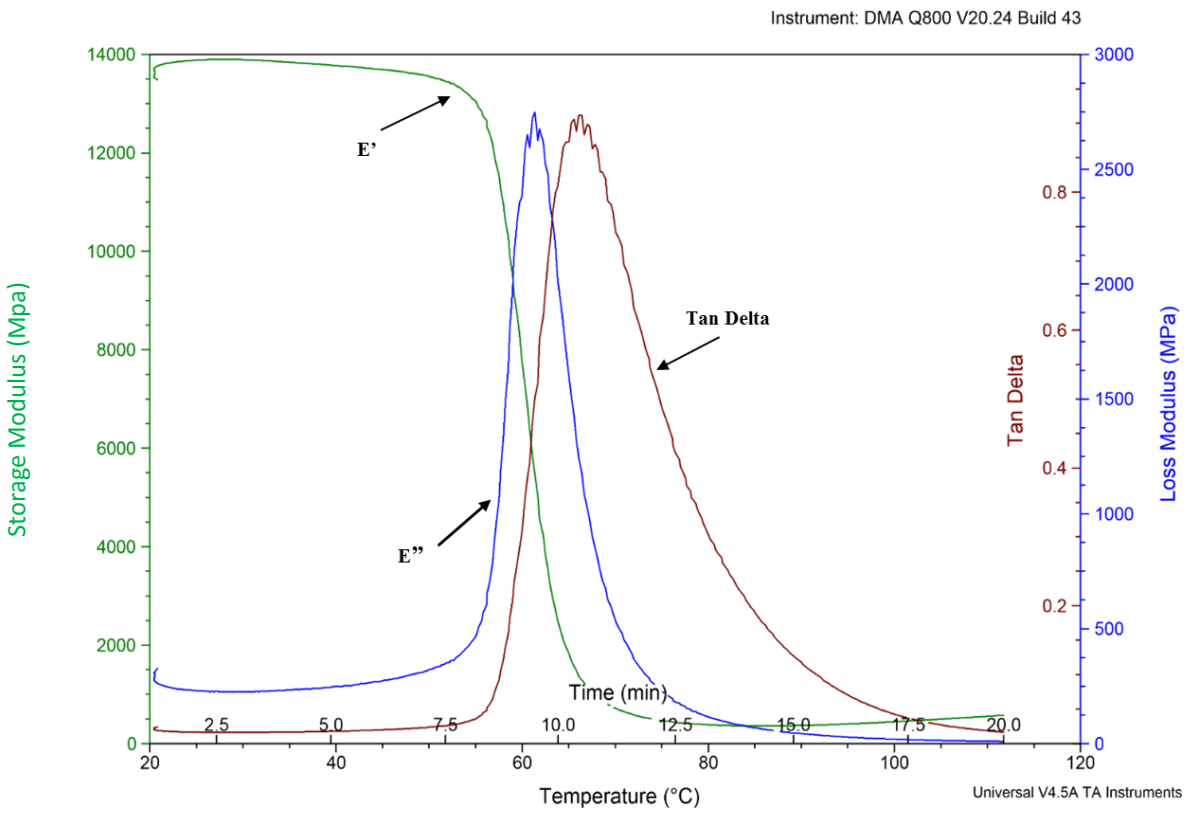

Figure 24: Dynamic Mechanical Properties in three-point bending for sample 'A'

6.3 Developing a novel method to mold hollow vasculatures

The process of pulling out the floral wires from the composite caused delamination of the composite at the junction where the wires were layered. This delamination damage can be of significant concern in wind turbine composite structure if large channels to supply the healing agent are used. This delamination damage can be attributed to the large diameter (1mm) of the wires and the bend in them. Delamination damage is of significant concern for implementing self-healing channels in the wind turbine composite material and the trials signified that further improvements must be made to decrease the size of these channels. The first test, with a layer of

Borosilicate tubes, showed promising results by retaining the tensile strength of the composite material. Self-healing trails with the Borosilicate tubes containing the healing agent (Dicyclopentadiene) as a part of the future study, shows promising potential to help safeguard the wind turbine blades against bird strikes and other high impact damages.

6.4 Commercial Borosilicate tubes- larger size (1mm outer diameter)

The microtubes were well distributed in the composite matrix which retained their pre-molding positions through the molding and curing processes. The glue used to close the ends of the micro tubes served their purpose and the micro tubes remained free from resin. The tubes were sufficiently strong to withstand the forces under vacuum during vacuum infusion process.

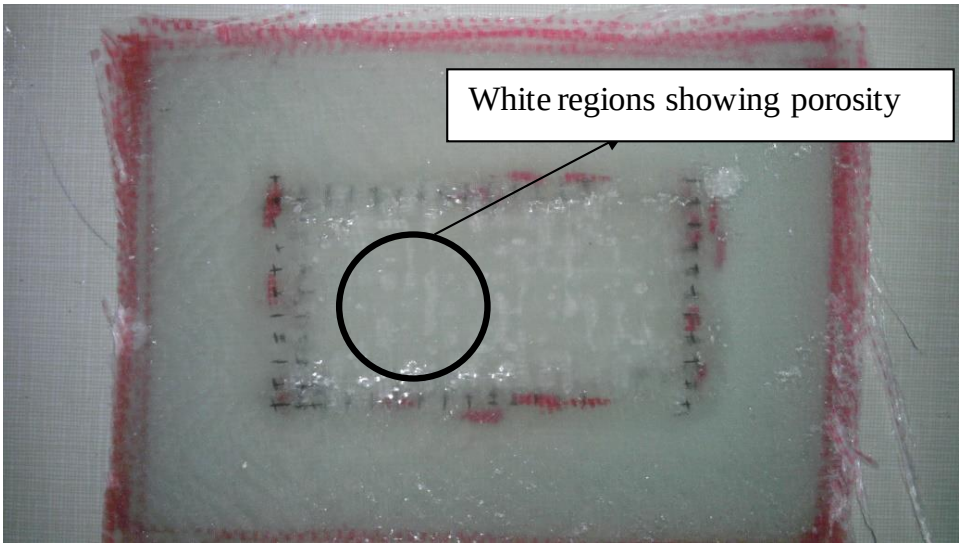

Figure 25. Photograph of the Polymer Matrix Composite with micro-tubes aligned parallel and perpendicular to the resin flow direction during vacuum infusion process (Sample 'D'). Only the rectangular portion contains micro-tubes

Sample D with two layers of microtubes oriented in perpendicular directions between the layers showed higher porosity (Figure 25). The optical images of the sample (Figure 26) show high porosity within the composite sample.

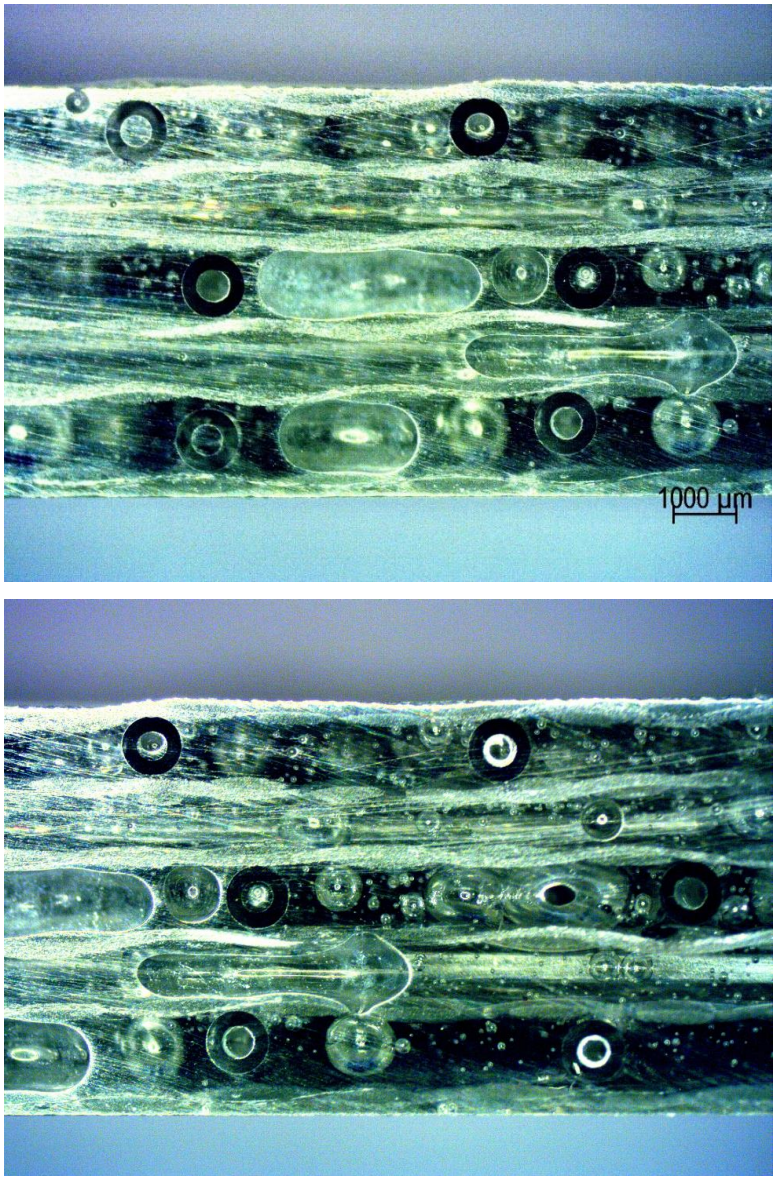

(a)

(b)

Figure 26: Photographs of the transverse section of sample 'D' perpendicular to the direction of flow of the resin during the vacuum infusion process

This could be because two layers of microtubes were placed perpendicular to the flow direction of the resin during vacuum infusion process. The increased porosity in the mold can, therefore, be attributed to the obstruction caused by these tubes to the flow of the resin during the molding process. Sample E which had all tube oriented in the direction of the flow, on the other hand, showed no significant porosity issues or any other visible damage (Figure 27).

(a)

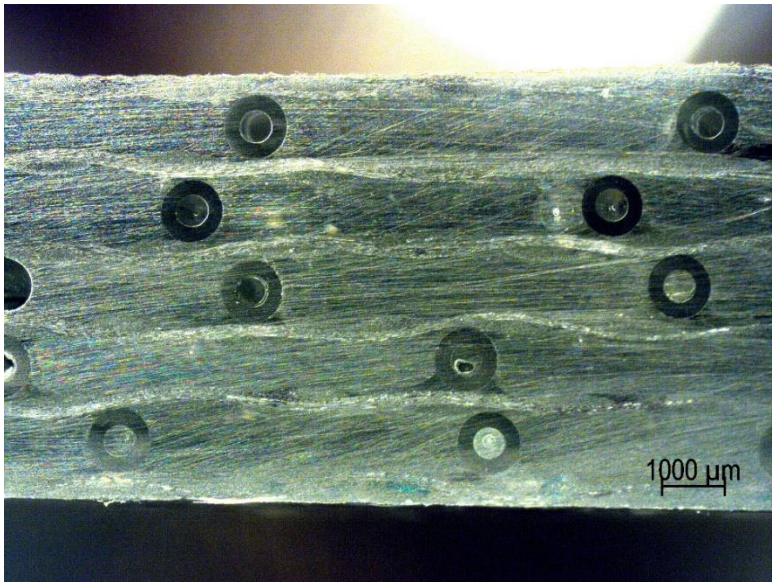

(b)

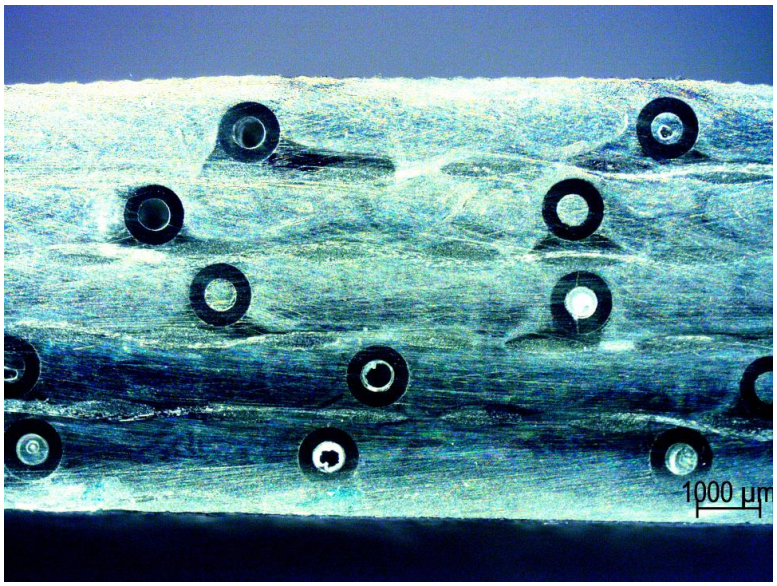

Figure 27: Photographs of the transverse section of sample 'E' perpendicular to the direction of flow of the resin during the vacuum infusion process

Hence, this can be suggested as the most appropriate tubing arrangement for the implementation of a vascular network type of self-healing capability into fiber reinforced PMC.

6.4.1 Tensile Strength of the composite with larger Borosilicate tubes

Tensile tests were performed on Sample E i.e. sample containing 5 layers of tubes all oriented in along the direction of flow of resin during the vacuum infusion process. The test was by ASTM standards mentioned at the start of this document.

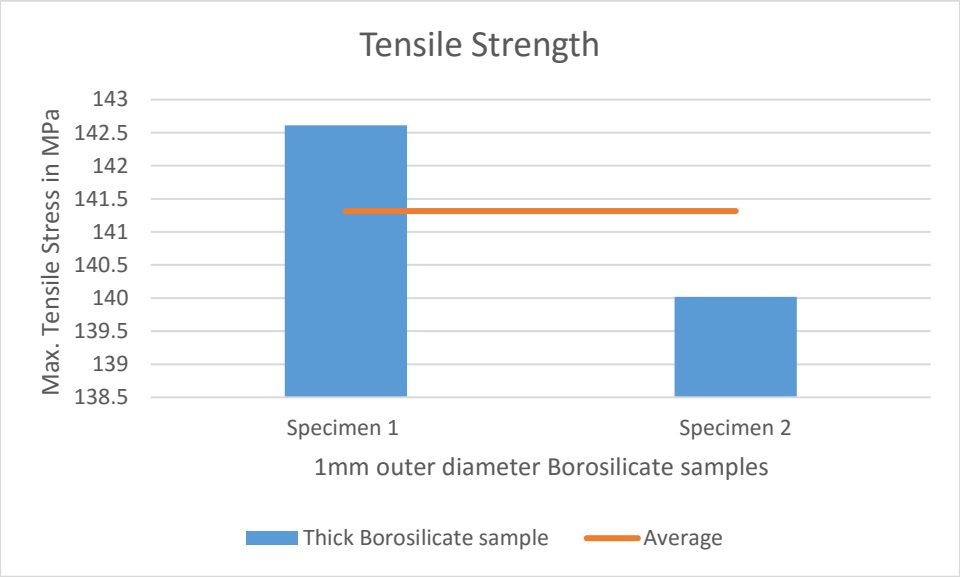

Figure 28: Tensile strength of sample E containing 5 layers of Borosilicate tubes all aligned along the direction of flow of resin during the vacuum infusion processes

The average tensile strength (2 specimens) of Sample E with tubes all aligned along the direction of resin flow during the vacuum infusion process was found to be 141.32 MPa. This about 32% lower than the average tensile strength of conventional composite material (210.67MPa) as shown in Figure 28.

The major downside to using larger diameter tubes was their strength. Although their strength reinforced the composite, the tubes were much stronger than the matrix material for cracking and consequent self-healing. As per the study made by Huang et al. [22], reducing the size of the tubes would decrease the resin rich region and hence, smaller Borosilicate tubes were procured and studied.

6.5 Commercial Borosilicate tube- smaller size (500µm tubes)

Due to the improvements in material properties, smaller size Borosilicate tubes were used to demonstrate self-healing methodology in polymer composite materials.

6.5.1 Microscopic analysis

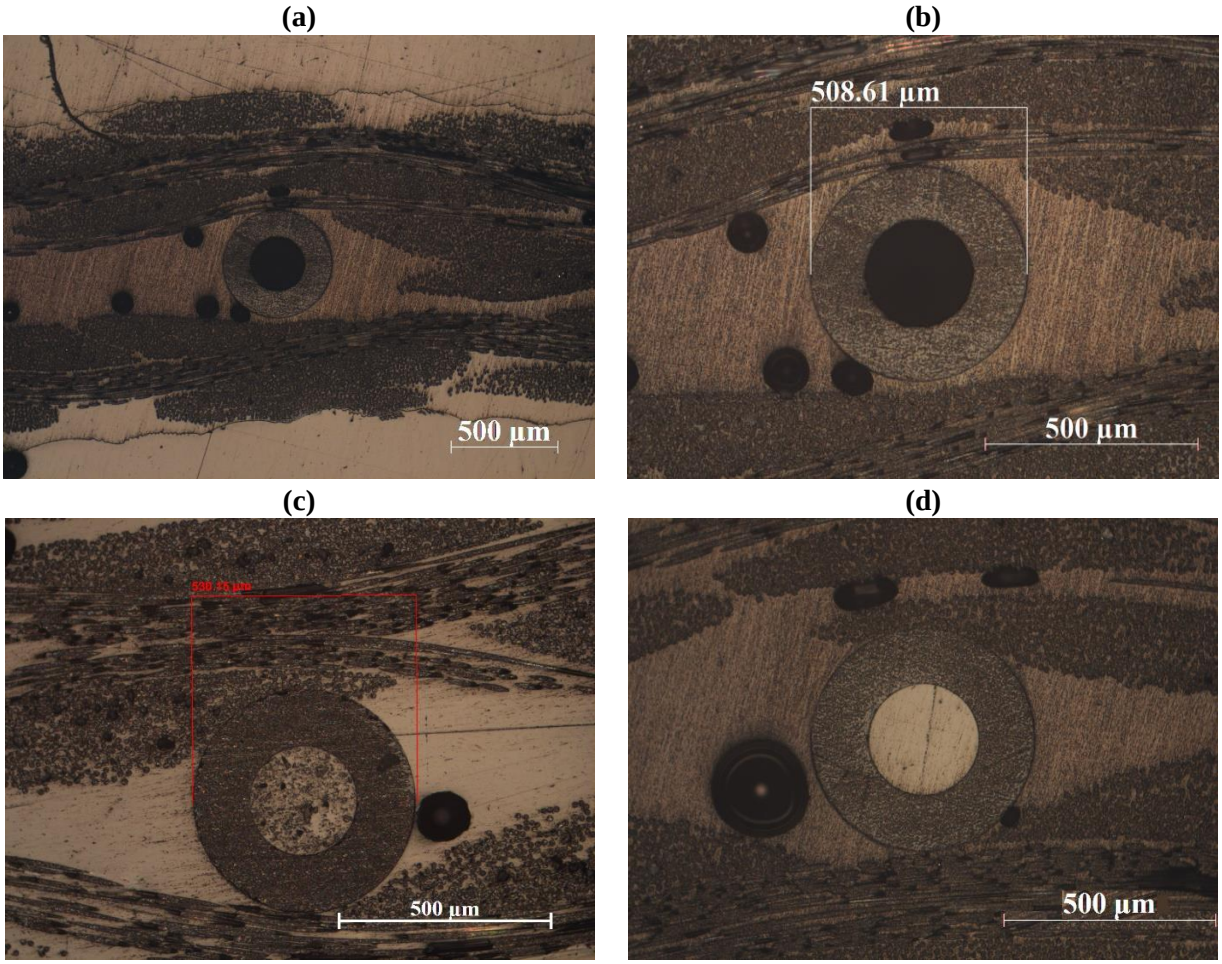

Figure 29. Cross-sectional images (a),(b),(c),d) of molded composite with 500µm tubes showing void distribution around the tubes

Embedded Borosilicate tubes in the molded composite caused a disturbance in the woven fiberglass alignment causing ridges on the surface of the composite at the location of tubes underneath the surface. Samples polished using standard polishing methods revealed good bonding between the tube surface and polymer matrix. A large number of porous spots were present around

the tubes in the polymer matrix. Figure 29 shows cross-sectional images of the area of the tubes in the molded PMC which show a higher void content around the tubes. Figure 29(a) is the only image with lower magnification and magnified image of it is shown in Figure 29(b). Figure 29(c) and Figure 29(d) shows cross sectional images of other Borosilicate tubes embedded in the composite material. The size of the tubes remained unchanged as expected due to room temperature curing (reaction is exothermic) of the resin-hardener mixture.

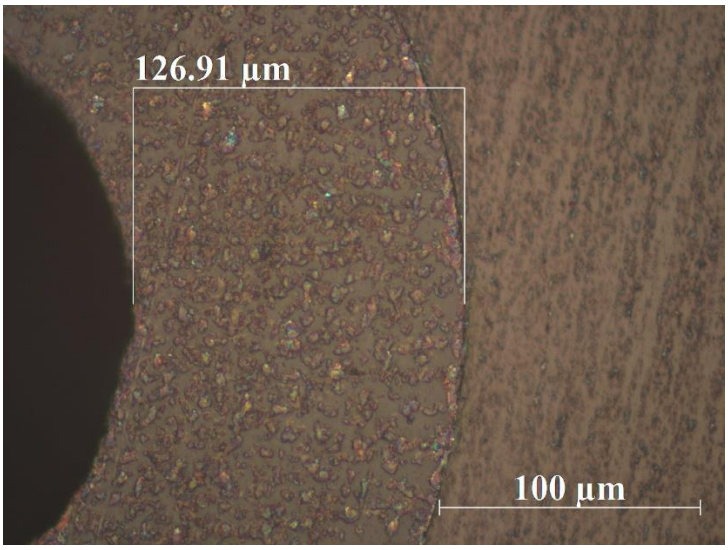

Figure 30. Magnified image through the cross section of the tube showing good wetting between tube and resin matrix

In support of the study made by Huang, et al. [22], woven fiberglass composite samples with embedded tubes showed resin rich regions around the tubes due to the change in the In-plane and out-of-plane fiber alignment in the composite. Huang, et al. also found that the size of the resin-rich region decreased proportionally as the diameter of the circular vasculature used, decreased. Accordingly, the size of the resin-rich region proportionally decreased from using smaller diameter (500µm) Borosilicate tubes as compared to larger diameter Borosilicate tubes (1mm) from the study made by Matt, et al [24]. Figure 30 shows good wetting between Borosilicate tube material and the resin matrix. A small number of regions in the polished samples showed much larger voids

around the tubes. Higher magnification images showed good wetting around the outer diameter of the tube surface. The reason for this good bonding can be due to possible local melting and mixing of the borosilicate tube material with the polymer matrix at the outermost surface of the tubes due to exothermic curing process of the epoxy. The dimensions of the tubes remained unchanged through the Vacuum Assisted Resin Transfer Molding (VARTM) process.

6.6 Comparison of tensile strength between conventional (without tubes) and with -tubes composite

Tensile and flexural strength between samples without tubes and with tubes are made to quantify the loss in mechanical properties with the addition of tubes into the sample. The differences between the samples are mentioned in section 4.5 of this document.

6.6.1 Conventional (without-tubes) composite results

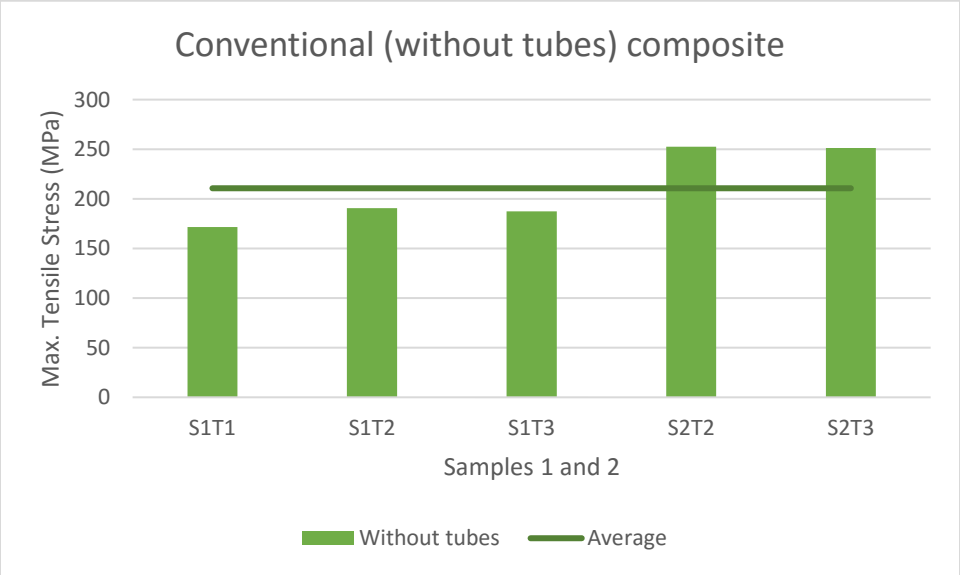

Figure 31. Max. Tensile Stress (MPa) of conventional (without tubes) composite

The average maximum tensile strength of the specimens were 210.67 MPa as shown by the line in Figure 31. A standard deviation of 34.31 MPa was obtained for the samples from the tensile test

Tensile strength of thermoset composite is significantly higher (by 71%) than the tensile strength of thermoplastic samples molded under ambient conditions with same fiber layout.

6.6.2 With-tubes composite results

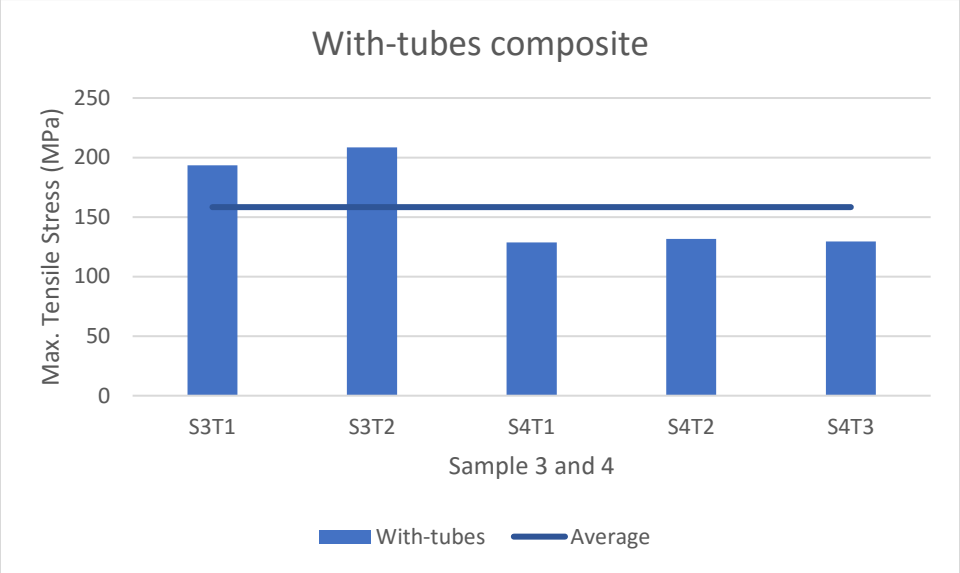

Figure 32: Max. Tensile Stress (MPa) of with-tubes composite

The average maximum tensile strength of the specimens was 158.36 MPa as shown by the line in Figure 32. The decrease in Tensile strength with the use of tubes was found to be 24.83% from that of conventional (without tubes) composite. A decrease of 52.30 MPa was observed in the average maximum tensile strength. A standard deviation of 35.19 MPa was obtained for the samples.

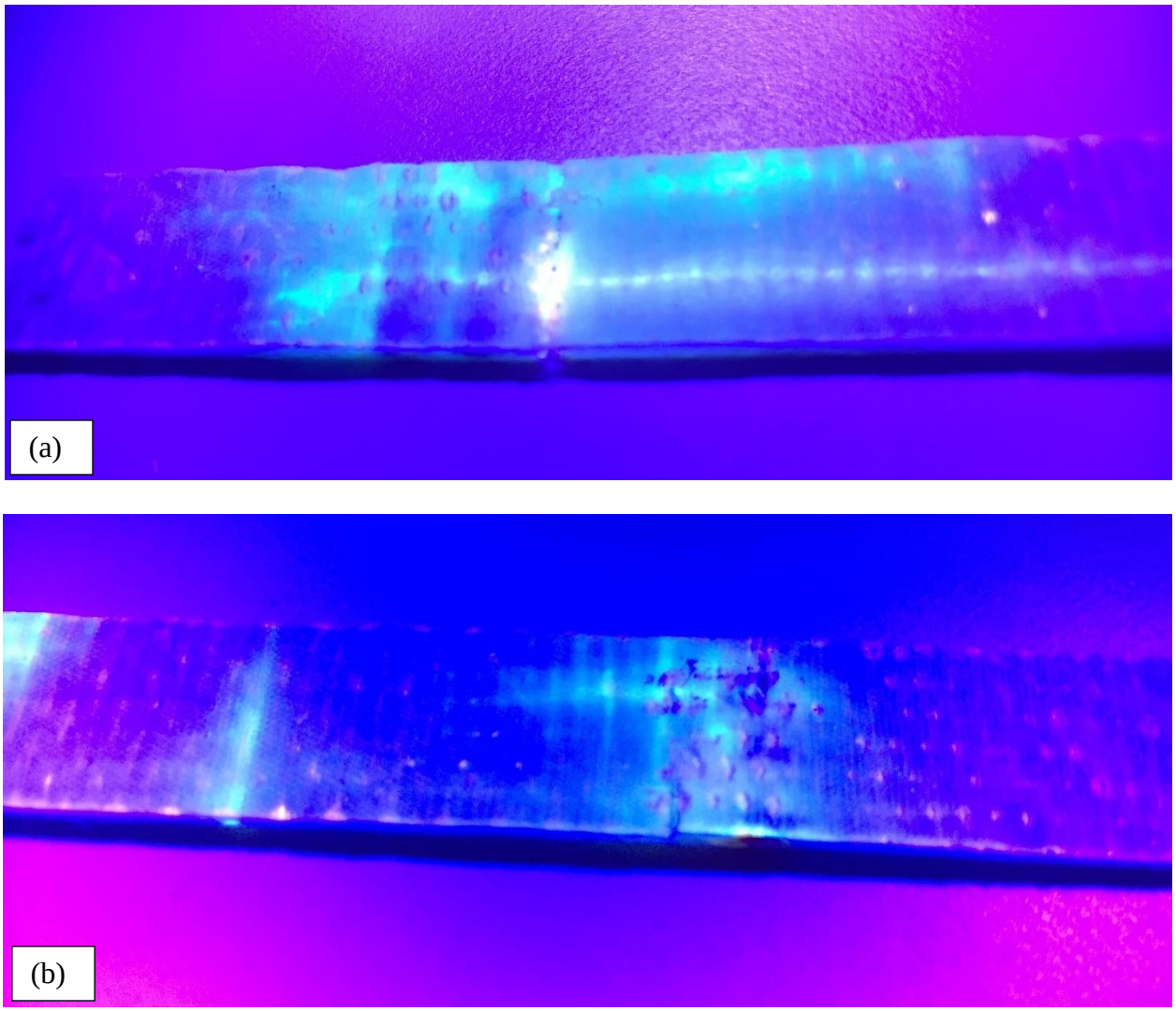

Figure 33: Photographs of two specimens are shown in (a) and (b) after completion of tensile testing of the two specimens' with-tubes showing bleeding of healing agent (glowing liquid) at their damage locations

Tensile testing of Sample 4 with tubes filled with DCPD and UV reflective dye revealed the breakage of tubes at damage locations due to the destructive test (tensile test) on the specimens. Figure 33(a) shows damage of a specimen in sample 4 and flow of healing agent (glowing liquid in the image) within the gauge length of the specimen. Figure 33(b) shows damage of a specimen in sample 4 at gripping end and dispersion of the healing agent at the site. Dispersion of UV reflective dye around the damaged regions reveal tube breakage and bleeding of DCPD (glowing liquid in Figure 33(a) and (b)) into the composite around the damage.

6.7 Comparison of flexural strength between conventional (without tubes) and with -tubes composites

Comparison between the flexural strength of conventional (with-out tubes) composite to that of with-tubes composite was made to observe the loss or gain in flexural strength with the implementation of Borosilicate tubes in the composite material.

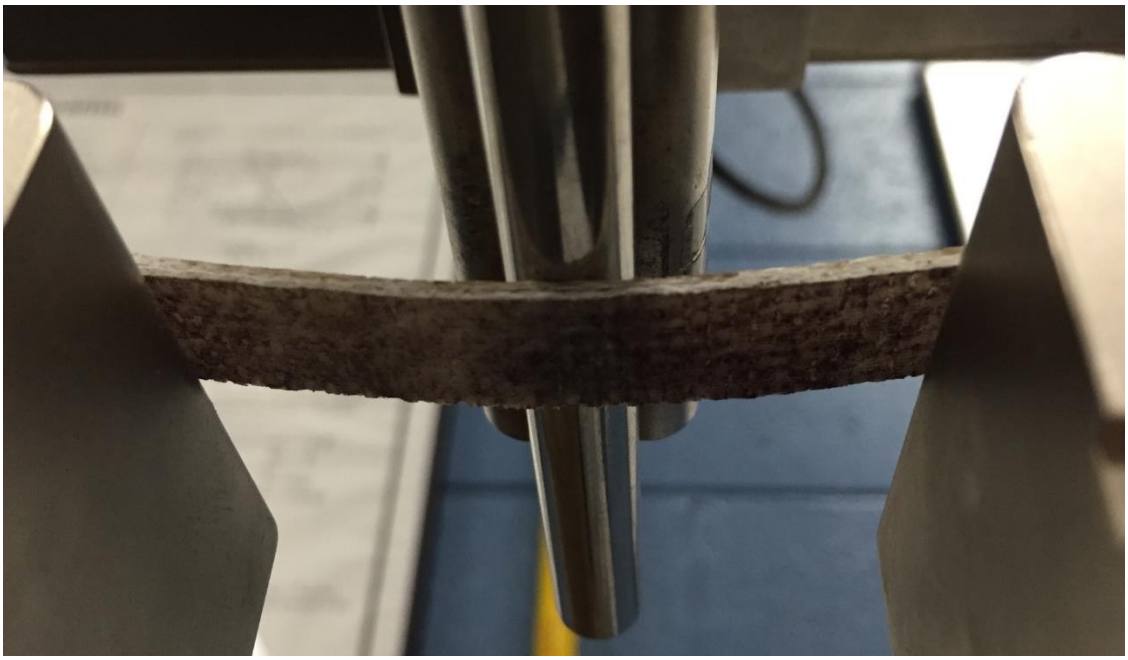

Figure 34: Photograph of the underside of the loading arm. Wedges on left and right are simply supporting, and the cylindrical rod in the center is the loading arm

Figure 34 shows the bottom side of the specimen underneath the loading arm. This camera perspective is used with the UV light to check the flow of healing agent within the composite sample during three-point bending in the sections below. It can be observed that the thickness on one side of the width of the specimen can be seen in Figure 34 and is important to understand the images in Figure 41.

6.7.1 Conventional (without-tubes) composite results

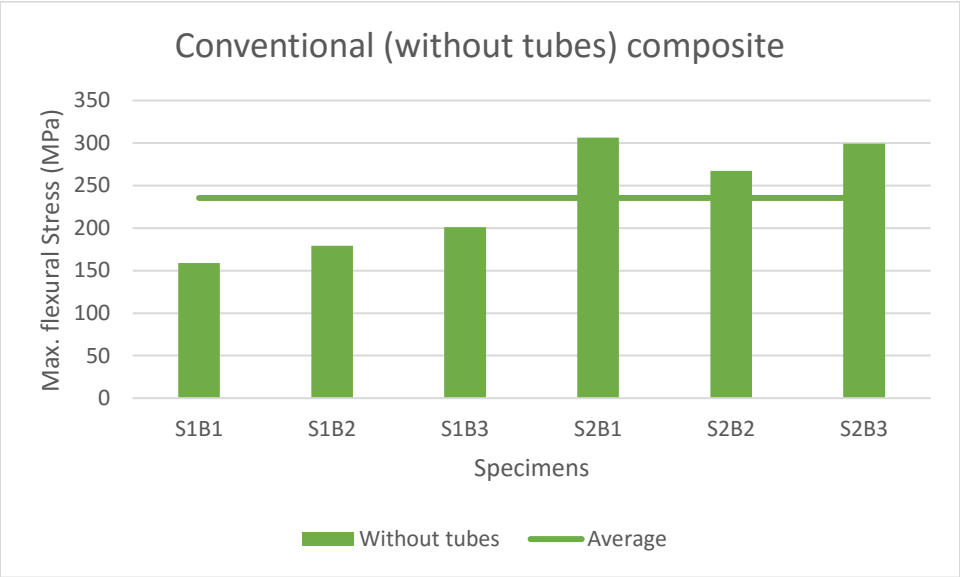

Figure 35: Max. Flexural stress (MPa) of conventional (without tubes) composite

The average maximum flexural stress of the specimens was 235.41 MPa. A standard deviation of 58.26MPa was observed in the samples.

6.7.2 With-tubes composite results

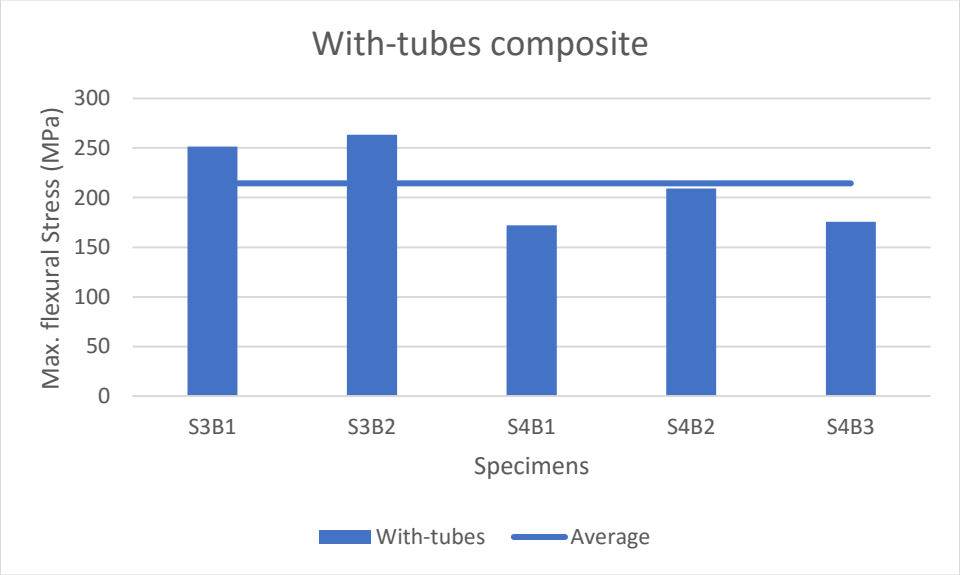

Figure 36: Max. Flexural stress (MPa) of with-tubes composite

The average maximum flexural stress of the specimens was 214.39 MPa which is 21.03MPa lesser than Average maximum flexural stress of the conventional composite. A standard deviation of 37.61MPa was observed in the samples. The depletion in flexural strength with embedded tubes is lesser than reduction in tensile strength.

6.8 Self-Healing results of samples with-tubes as a central layer

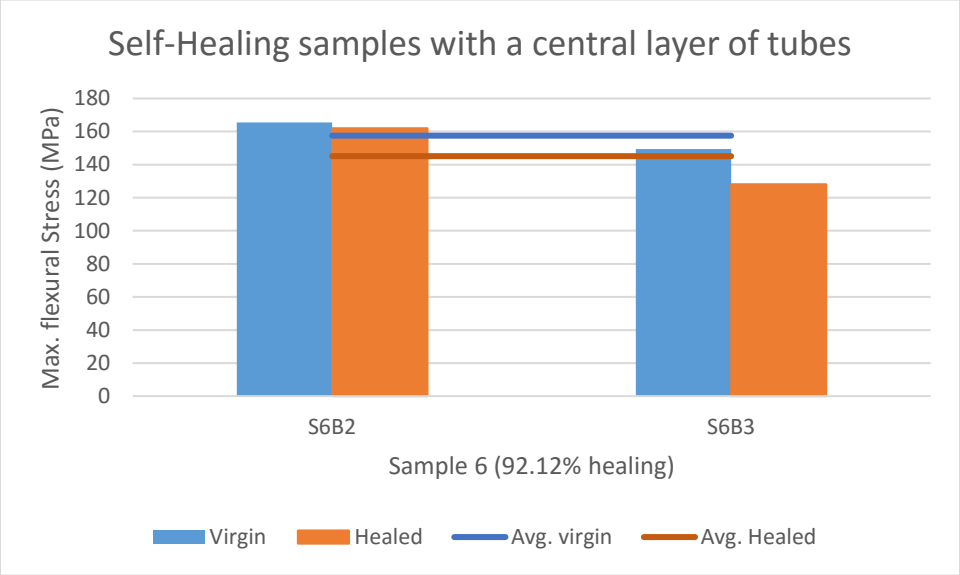

Figure 37: Max. Flexural stresses (MPa) of self-healing samples with tubes as a central layer

The average maximum flexural stress of the virgin specimens was 157.52MPa and Average maximum flexural stress of the healed specimens was 145.11 MPa accounting for 92.12% percent healing of flexural strength with a loss of 12.41MPa. Specimen and sample details are provided in section 4.6.1 and plots of each of the specimen is provided in Appendix A of this document.

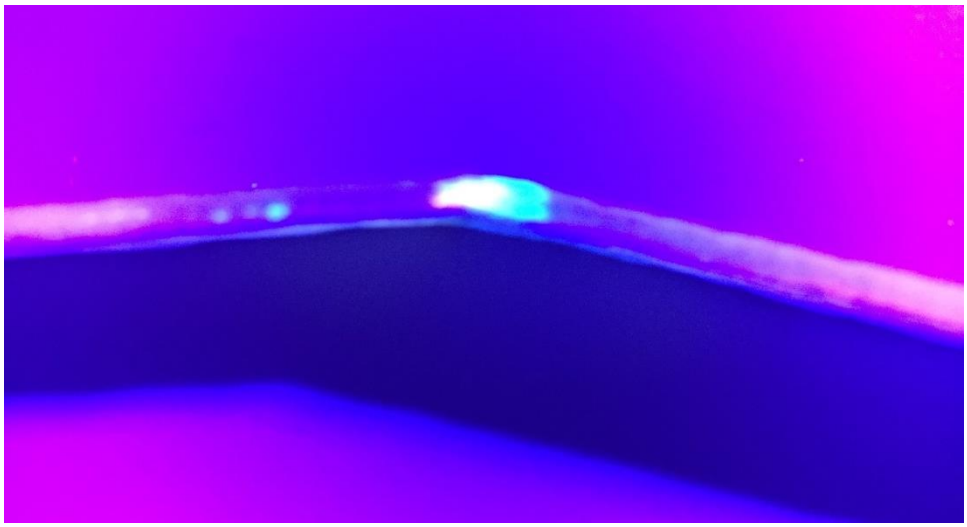

Figure 38: Photograph of a side of one of the specimens from sample 3 showing bleeding of tubes along the line of flexural load

Side view photograph of one of the specimens from sample 3 after the flexural test revealed the discharge of healing agent at the bending plane. Figure 38 shows the bright region filled with DCPD and UV reflective dye mixture that bled after the flexural test.

6.9 Self-healing results of samples with tubes as the last layer

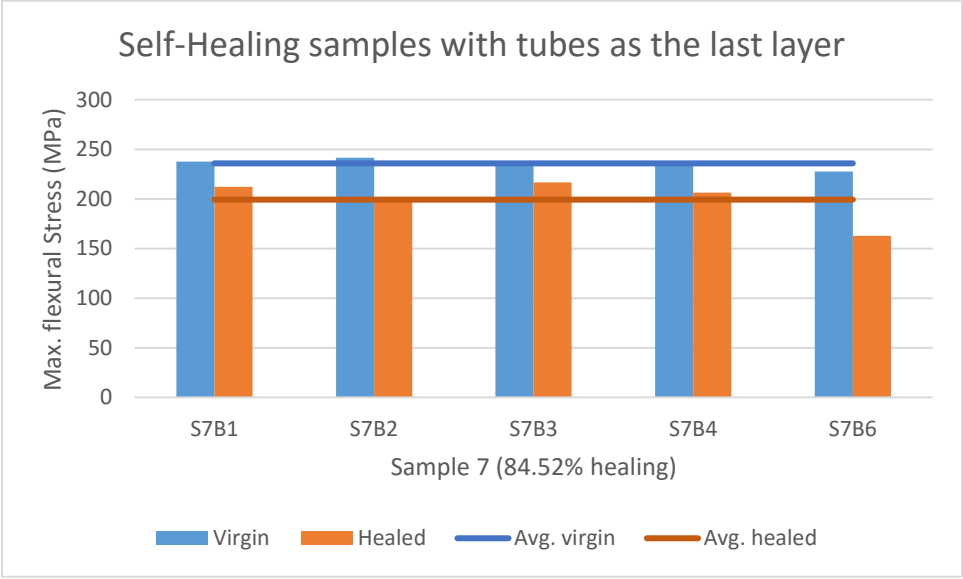

Figure 39: Max. Flexural stresses (MPa) of self-healing samples with tubes as the last layer (from top)

The average maximum flexural stress of the virgin specimens was 235.77 MPa and Average maximum flexural stress of the healed specimens was 199.27 MPa accounting for 84.52% percent healing of flexural strength with a loss of 36.50 MPa. Specimen and sample details are provided in section 4.6.1 and plots of each of the specimen is provided in Appendix A of this document.

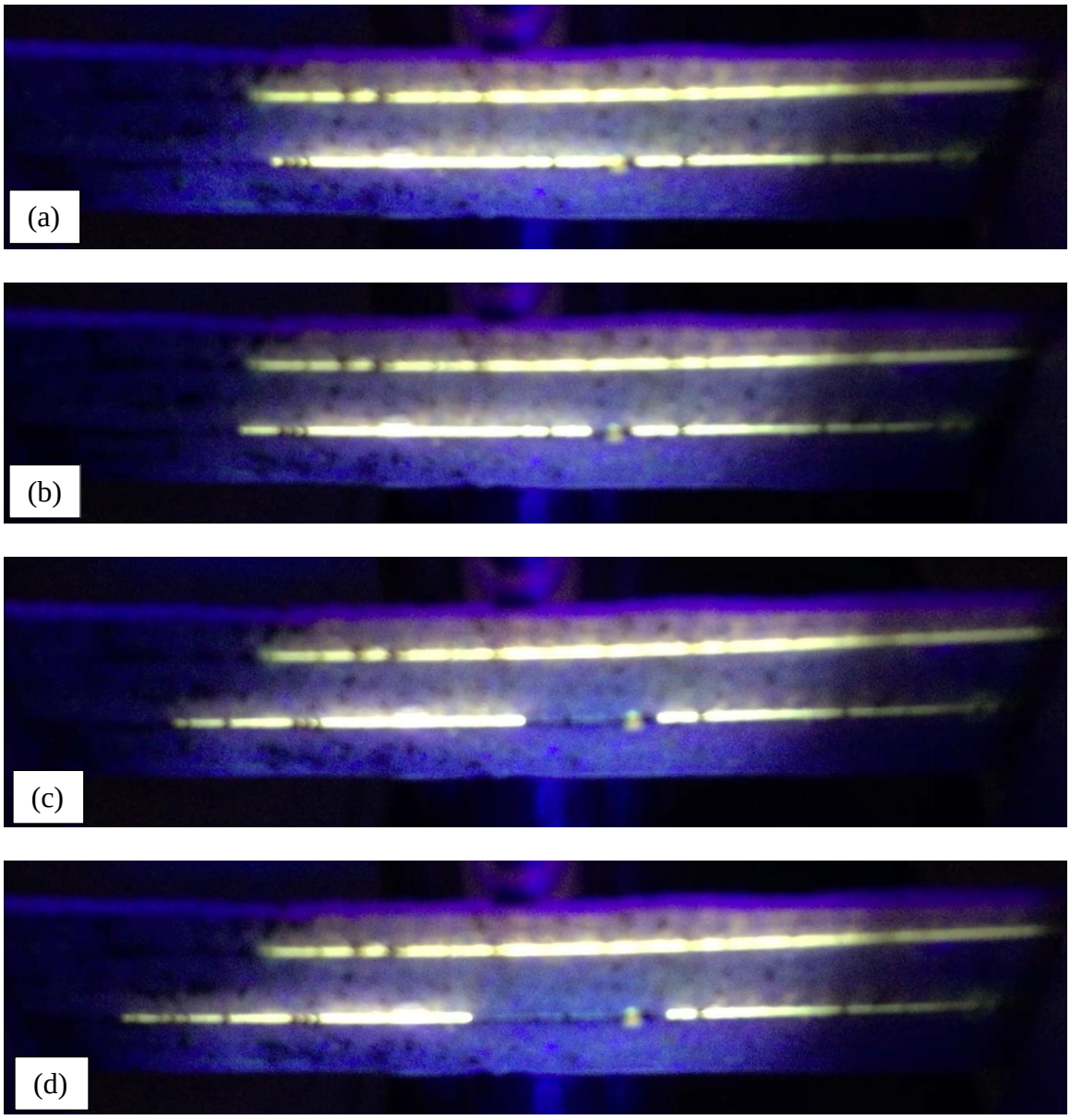

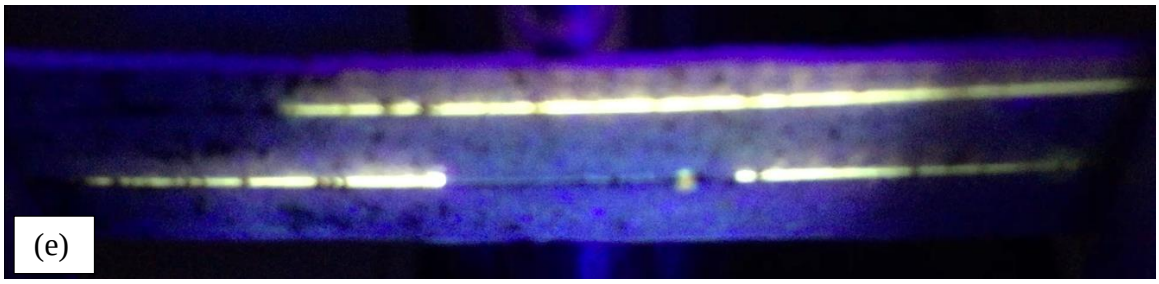

(e)

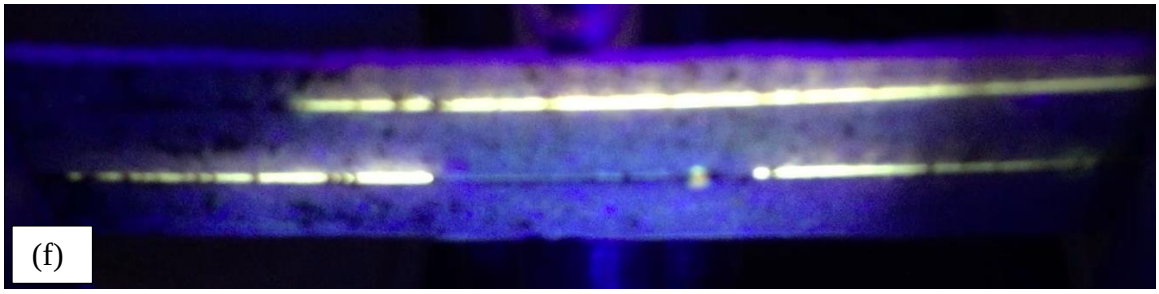

(f)

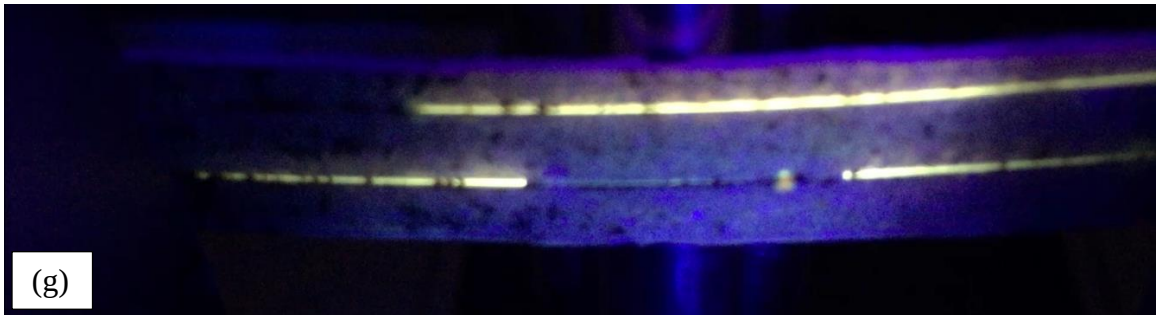

(g)

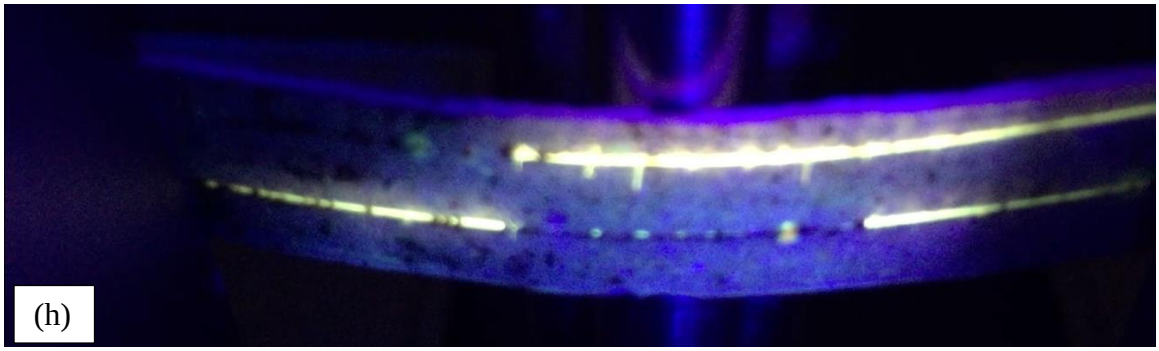

(h)

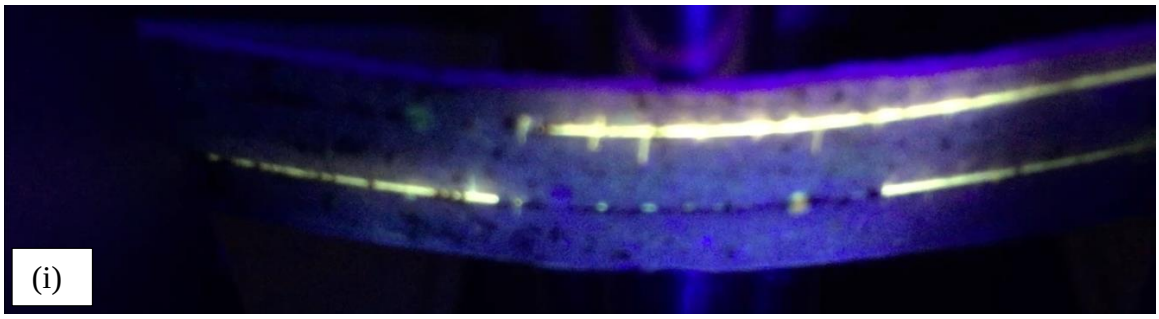

(i)

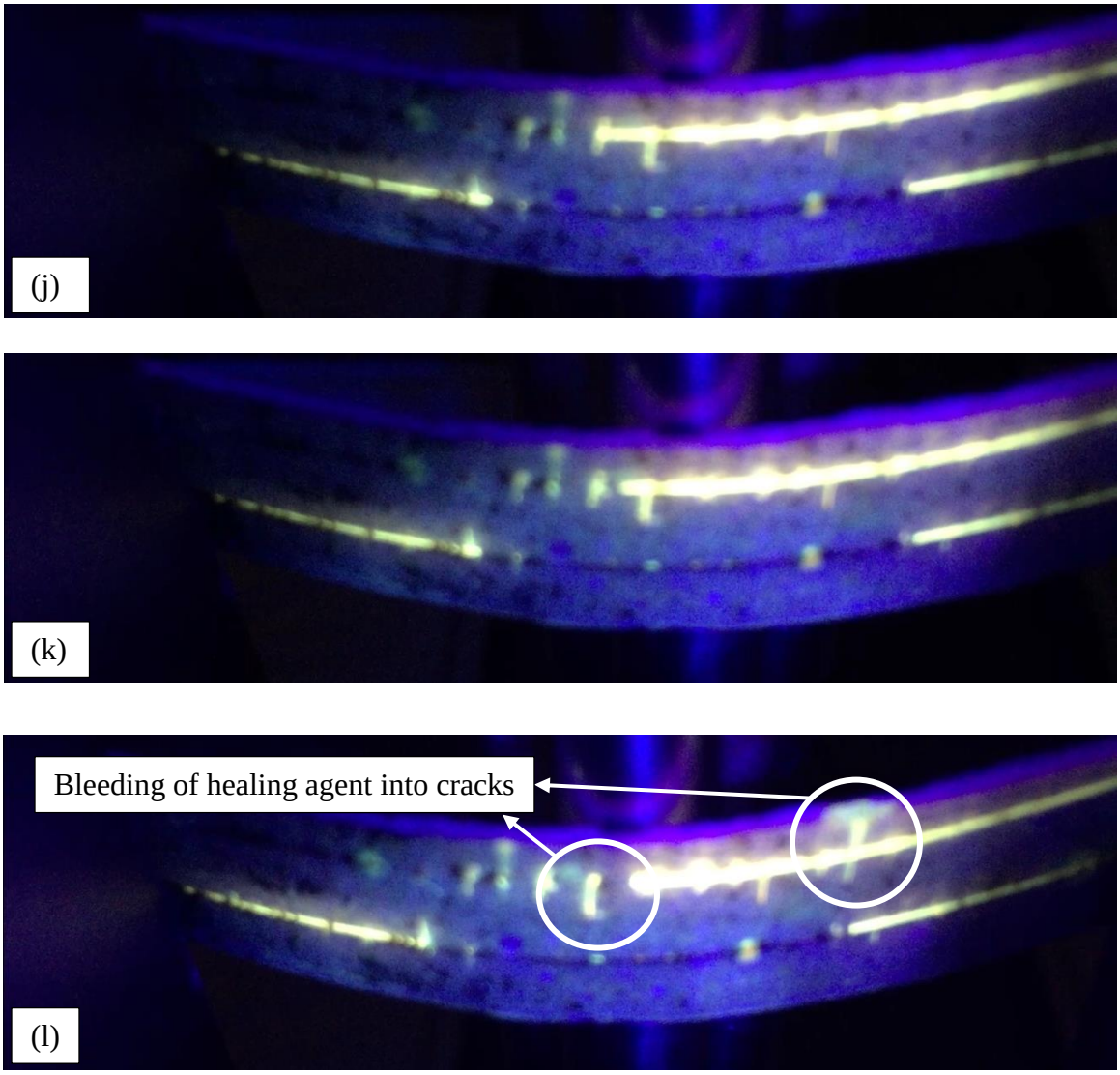

Figure 40: Photographs during three-point bending test showing evident signs of breakage and bleeding (glowing liquid) of the tubes. Image (a) is the earliest photograph and (l) is the latest photograph during the test. (a) through (f) have 15s interval between the images in the second minute of the test and (g) through (l) have same interval to the end of the test. (Specimen is S7B2)

Figure 40 shows photographs during three-point bending test with the photograph on the top being the earliest. The collection of photographs show clear signs of cracks; tube breakage and dispersion of healing material into the cracks. The time step between the photograph are unevenly distributed with first six photograph from (a) to (e) in Figure 40 have an time interval of around 10 seconds within the second minute through the bend test and the rest of the photographs about 15 seconds

time interval in the fifth minute through the test. The tube on the lower side of the sample in the photographs is consumed within two minute of starting the bend test and the tube on the upper side of each the photographs cracks with the cracking composite around it, bleeding into the cracks towards the end of the test substantiating the claim of autonomous self-healing in the composite.

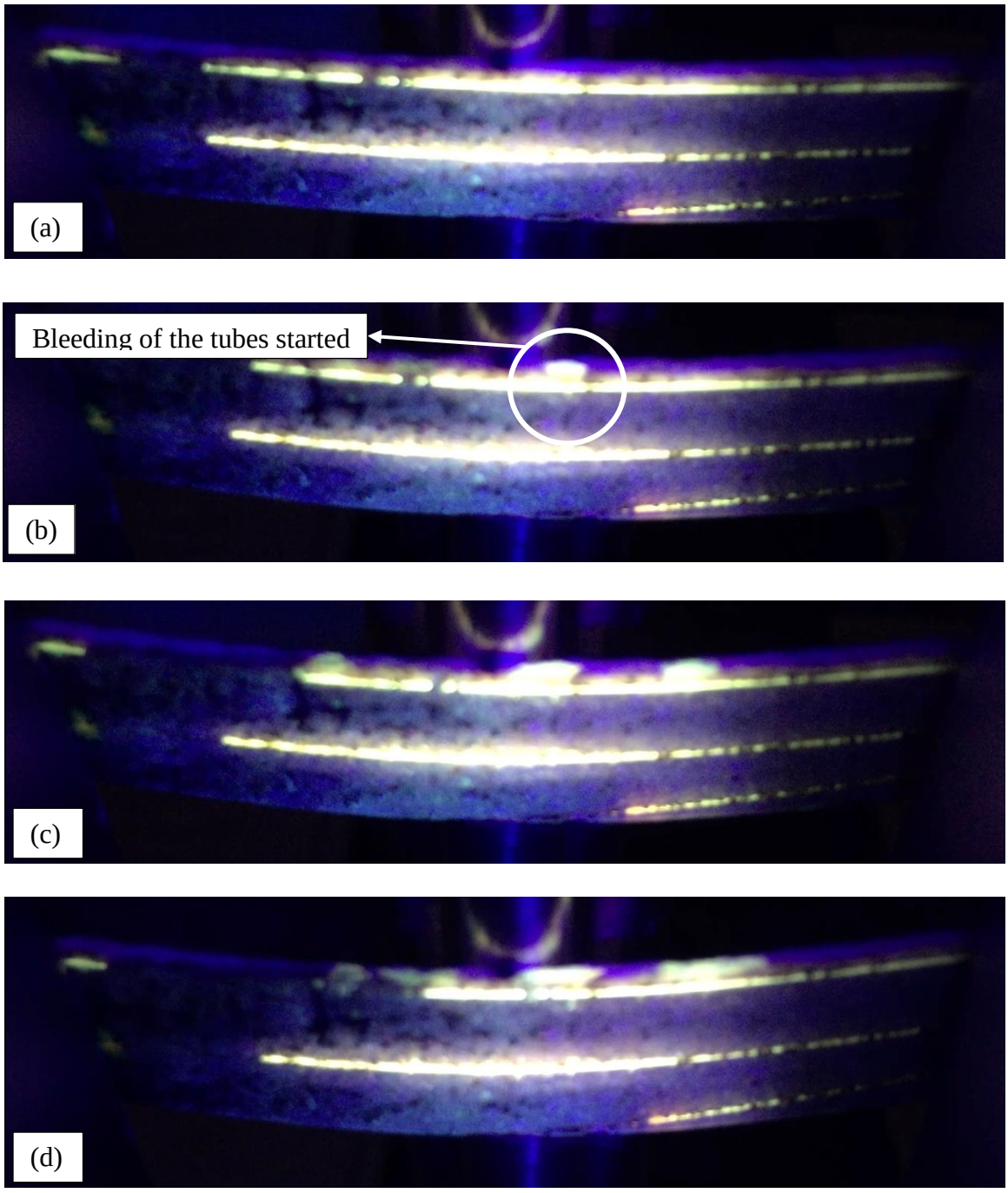

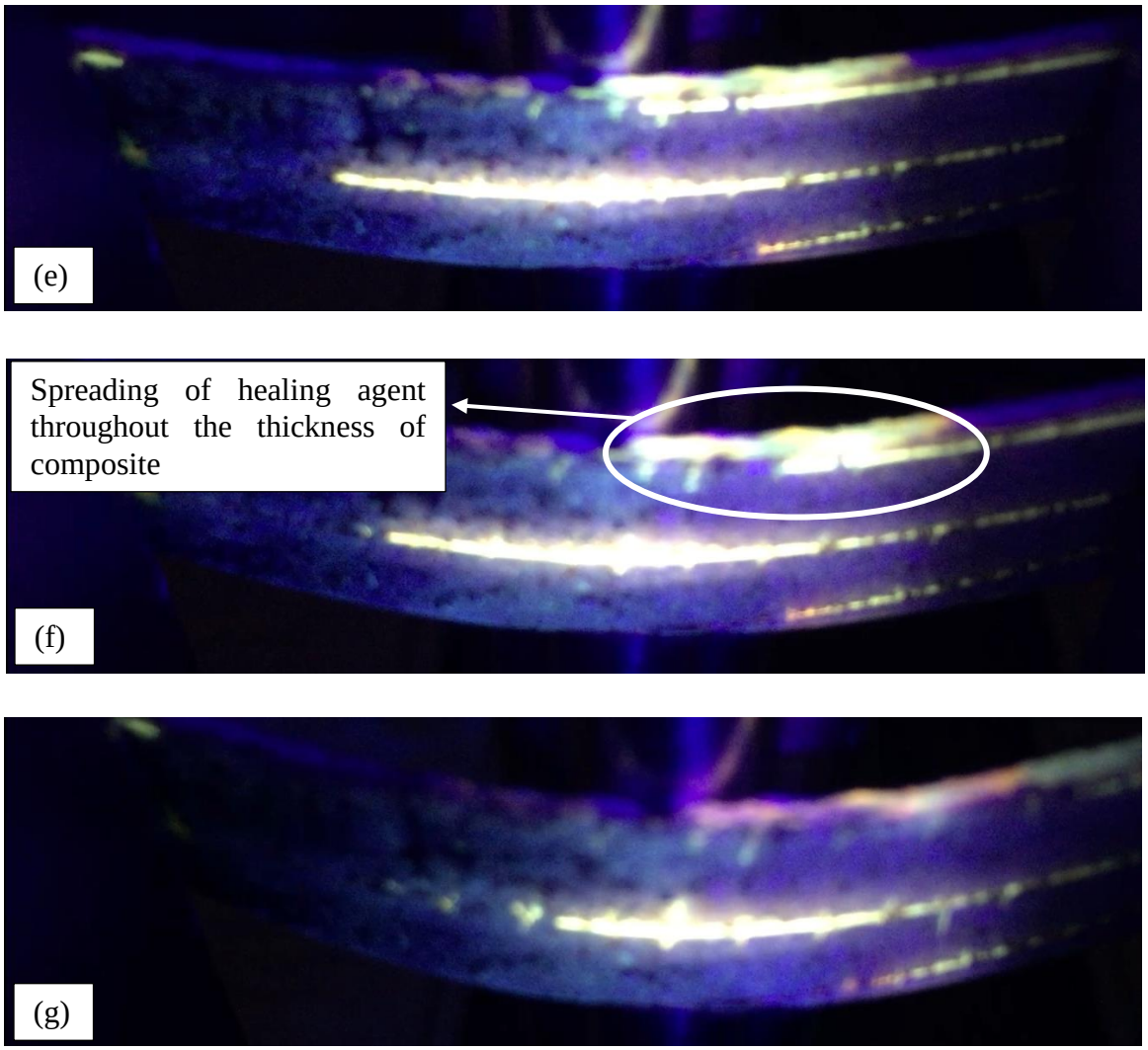

Figure 41: Photographs (a) to (g) of a specimen during three-point bending test showing evident signs of breakage, bleeding of the tubes and spreading of healing agent (glowing liquid) through the thickness of the composite. (a) being earliest and (g) being latest photograph. Image (a) is at the start of the test and (b) through (g) have 15s interval between the images to the end of the test (Specimen is S7B4)

Figure 41 shows clear signs of bleeding of the healing agent from the tubes and spreading of the healing agent throughout the thickness of the composite material. Camera perspective used in section 6.7 is useful in understanding the images in Figure 41. The top most tube in each photograph of Figure 41 shows cracking and bleeding starting from photograph (b) to (g). The liquid content inside that tube depletes as the test continues and clearly exhibit spreading of the healing agent throughout the thickness of the specimen. Figure 41(b) to Figure 41(g) confirms the

flow of healing agent between glass fiber fabrics by spreading from the last layer to the first layer through the specimen thickness. The tube in the center of the width of the specimen shows apparent filling of a major crack underneath the loading arm with the healing agent, towards the end of the test Figure 41(g). Figure 34 can be used to get a clearer understanding of the camera view of these images.

6.10 Self-healing results of samples with tubes as the penultimate layer

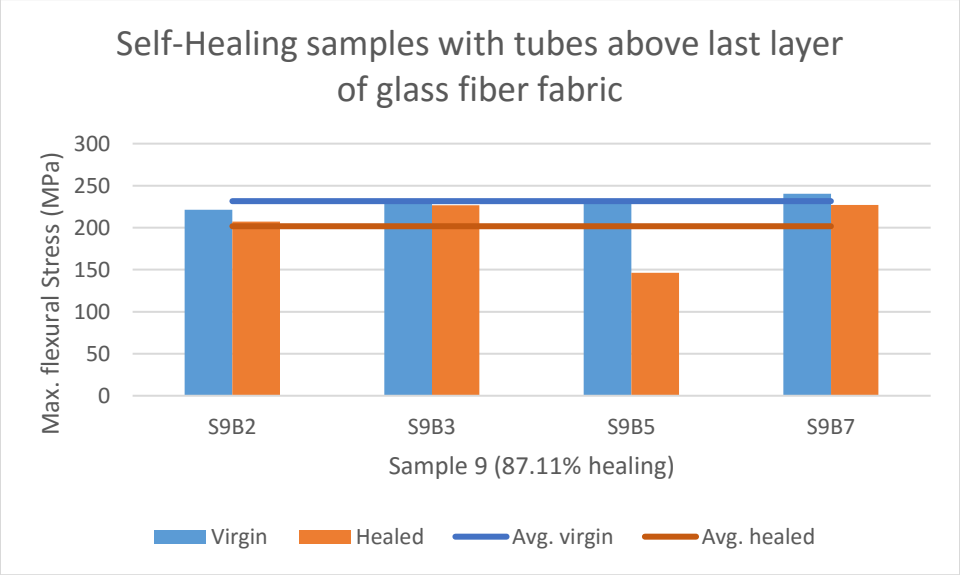

Figure 42: Max. Flexural stress (MPa) of self-healing samples with tubes as the penultimate layer (from top)

The average maximum flexural stress of the virgin specimens was 231.58 MPa and Average maximum flexural stress of the healed specimens was 201.72 MPa accounting for 87.11% percent healing of flexural strength with a loss of 29.86 MPa. Specimen and sample details are provided in section 4.6.3 and plots of each of the specimen is provided in Appendix A of this document.

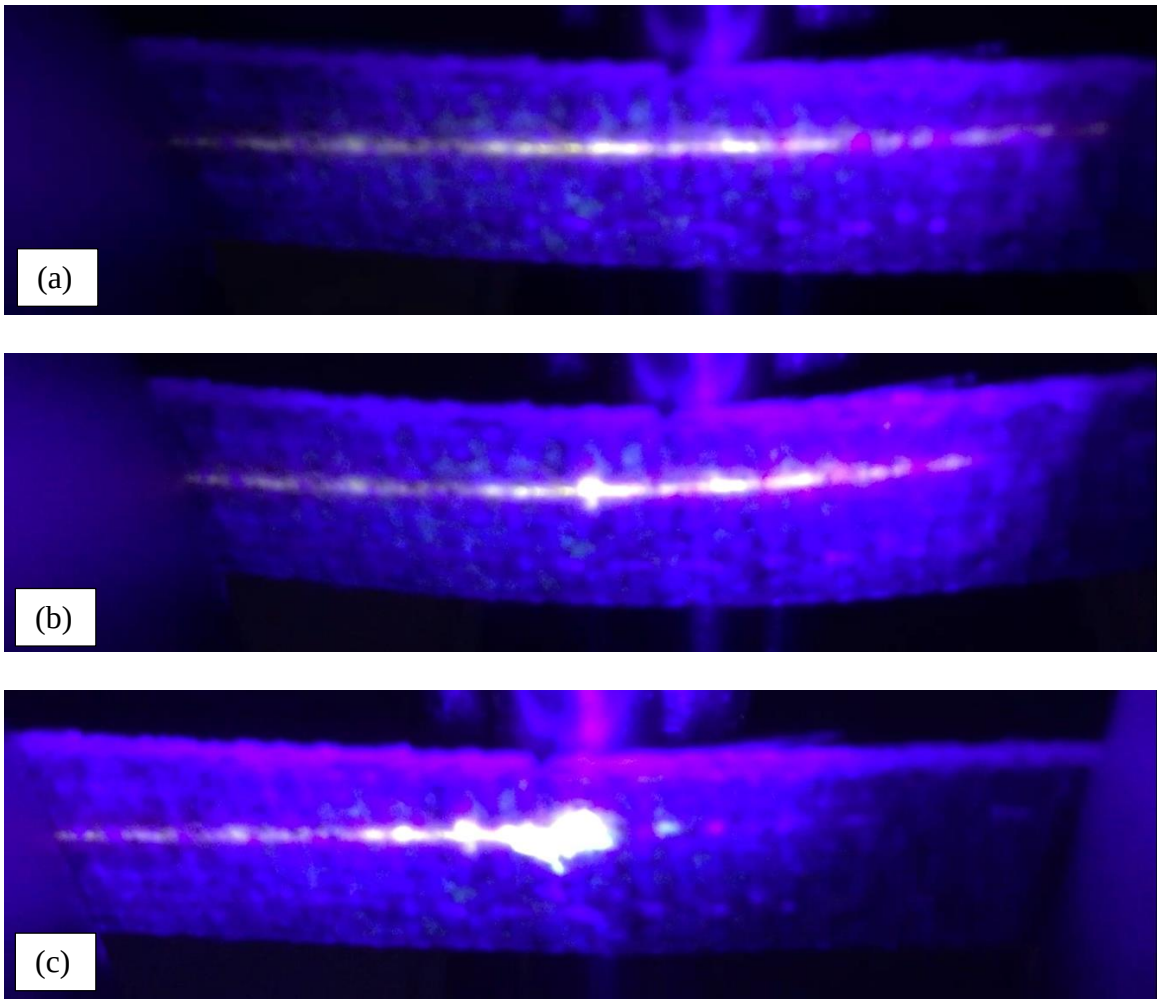

Figure 43: Photographs (a) to (c) of a specimen from sample 9 during three-point bending test showing evident signs of bleeding and spreading of healing agent (glowing liquid) underneath the loading arm. Image (a) is at the start of the test and (b) and (c) is to the end of the test. (Specimen is S9B7)

Figure 43 shows photographs of a specimen form sample 9 during bend testing showing bleeding of tubes underneath the loading arm where tensile stress concentration would be the highest. Since the layer of tubes are underneath a layer of fiberglass fabric, there is reduced clarity of the bleeding. Photograph (b) shows initiation of crack and photograph (c) shows complete spreading of healing agent at the damage site.

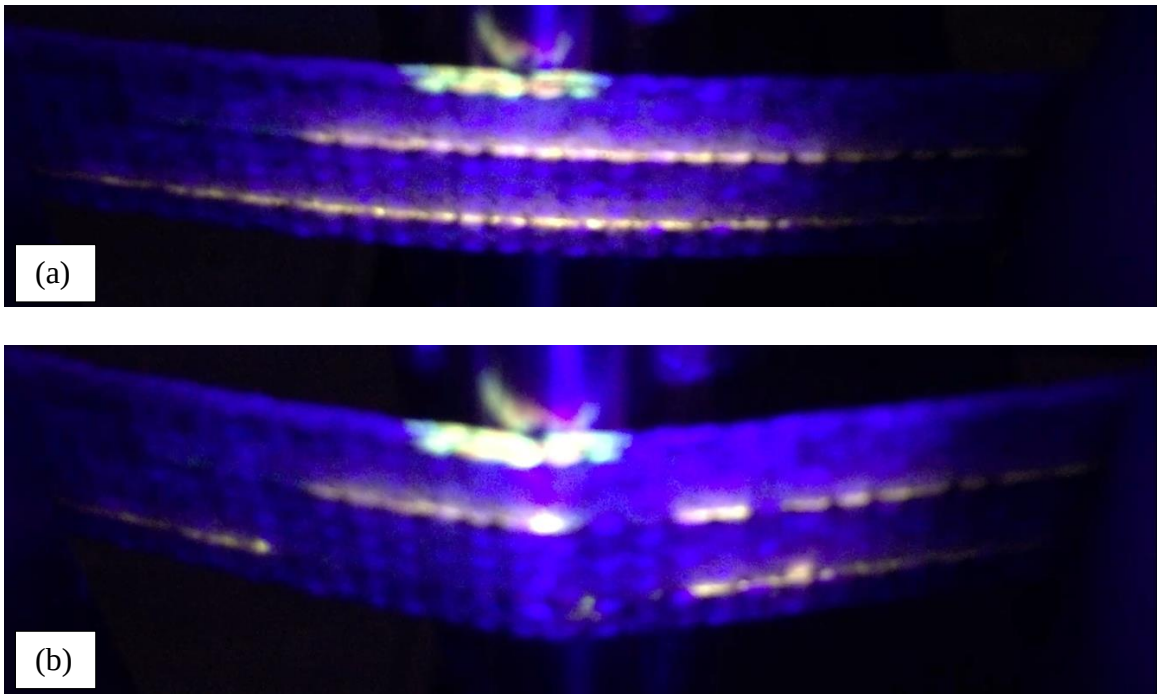

Figure 44: Photographs (a) and (b) of a specimen from sample 9 during three-point bending test showing evident signs of bleeding and spreading of healing agent (glowing liquid) underneath the loading arm. Image (a) is at the start of the test and (b) is to the end of the test. (Specimen is S9B5)

Figure 45 shows photographs of another specimen from sample 9 during flexural test demonstrating depletion of healing agent from the tubes at random crack locations which are more prevalent underneath the loading arm and spreading of healing agent through the thickness of the material. Both the tubes in the photograph (b) show depleted healing agent within the tubes.

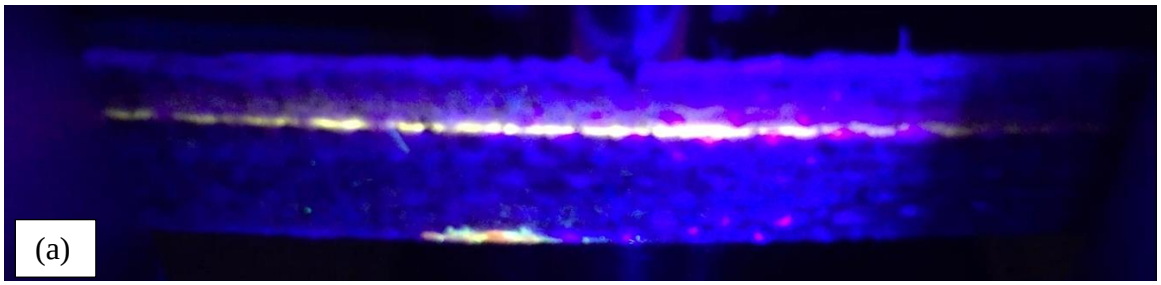

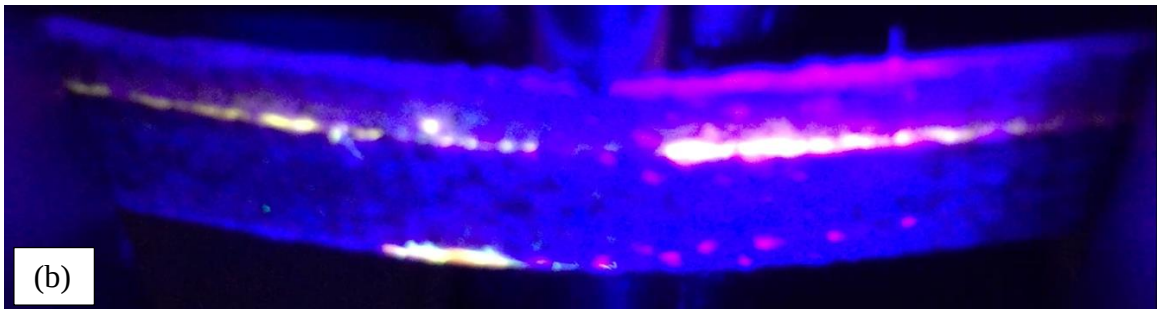

Figure 45: Photographs (a) and (b) of a specimen from sample 9 during three-point bending test showing evident signs of depletion of healing agent (glowing liquid) inside tubes, underneath the loading arm. Image (a) is at the start of the test and (b) is to the end of the test. (Specimen is S9B3)

Figure 45 shows clear signs of depletion of healing agent within the tubes underneath the loading arm of a specimen in sample 9. The tube on the upper side of the photograph (b) shows partial draining of healing agent on the left hand side of the photograph but close to the loading arm. Since the layer of tubes is underneath a layer of fiberglass fabric for the camera, there is reduced clarity of images of the bleeding process.

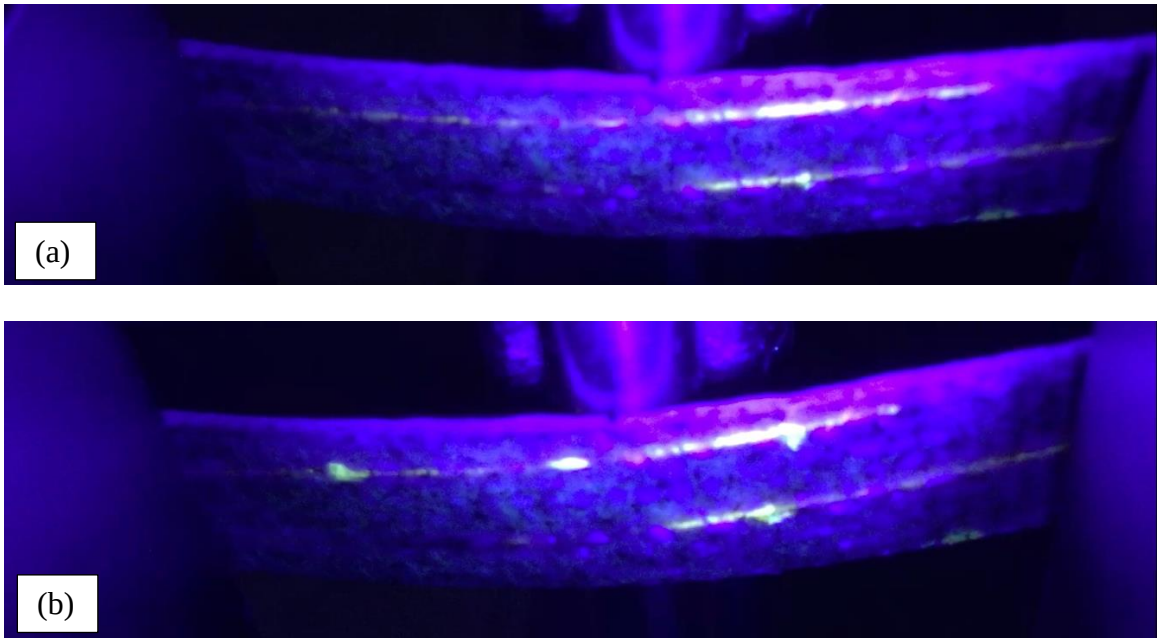

Figure 46: Photographs (a) and (b) of a specimen from sample 9 during three-point bending test showing evident signs of filling of cracks by the healing agent (glowing liquid). Image (a) is at the start of the test and (b) is to the end of the test. Specimen is S9B2

Figure 46 shows photographs during three-point bend test of a specimen from sample 9 clearly showing filling of small cracks by the healing agent. Since the layer of tubes is underneath a layer of fiberglass fabric for the camera, there is reduced clarity of images of the bleeding process.

6.11 Standard deviation and healing efficiency of self-healing samples

Standard deviation of test results of a sample for a number of specimens provide quantification of the variation in the test results. The plots below provide the value of standard deviation of the samples with the white box inside showing the number of specimens tested.

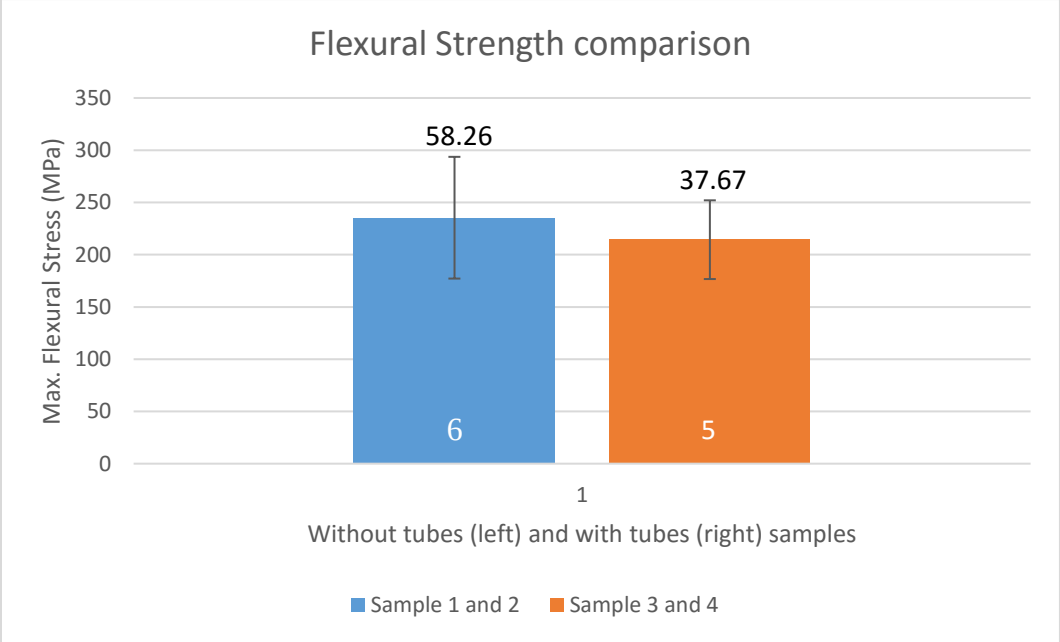

Figure 47: Comparison between Max. Flexural Stress (MPa) of samples with tubes and without tubes showing standard deviation. The white number on the bottom of the bars indicate the number of specimens tested in that sample.

The standard deviation of maximum flexural strength under three-point bending for sample 1 and 2 of 6 specimens without tubes was 58.26 MPa as compared to 37.67 MPa for sample 3 and 4with tubes measured from testing 5 specimens. The average flexural strength as mentioned in section

6.7 for without tubes sample is 235.41 MPa and the average flexural strength with tubes is 214.39 MPa as shown in Figure 47.

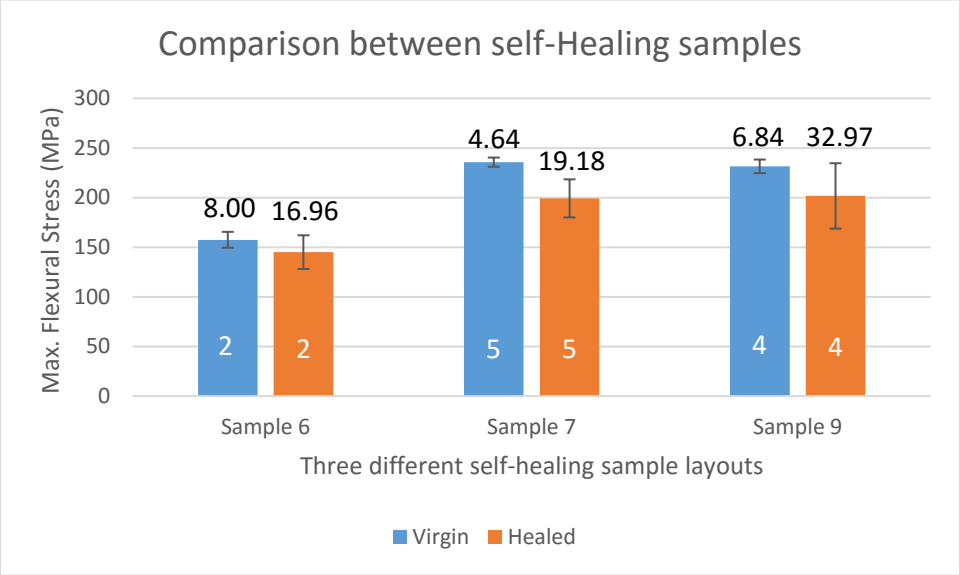

Figure 48: Max. Flexural Stress (MPa) of self-healing samples showing standard deviation. The white number at the bottom of the bars show the number of specimens tested in that sample.

The standard deviation of maximum flexural strength under three-point bending of virgin or undamaged sample 6 with 2 self-healing specimens was 8 MPa; the standard deviation value was 4.64 MPa for sample 7 with 5 self-healing specimens and 6.84 MPa for sample 9 with 4 self-healing specimens as shown in Figure 48. The average flexural strength of undamaged or virgin specimens for self-healing samples is 157.52 MPa, 235.78 MPa and 231.58 MPa for sample 6, sample 7 and sample 8 respectively.

Similarly, the standard deviation of maximum flexural strength under three-point bending of healed samples are 16.97 MPa, 19.18 MPa and 32.97 MPa for sample 6, sample 7 and sample 9 respectively as shown in Figure 48 with orange color bars. The average flexural strength of healed specimens were 145.11 MPa, 199.271 MPa and 201.73 MPa for samples 6, sample 7 and sample 9 respectively.

The standard deviation of healed samples reveal higher variation in test results as compared to standard deviation of virgin or undamaged samples.

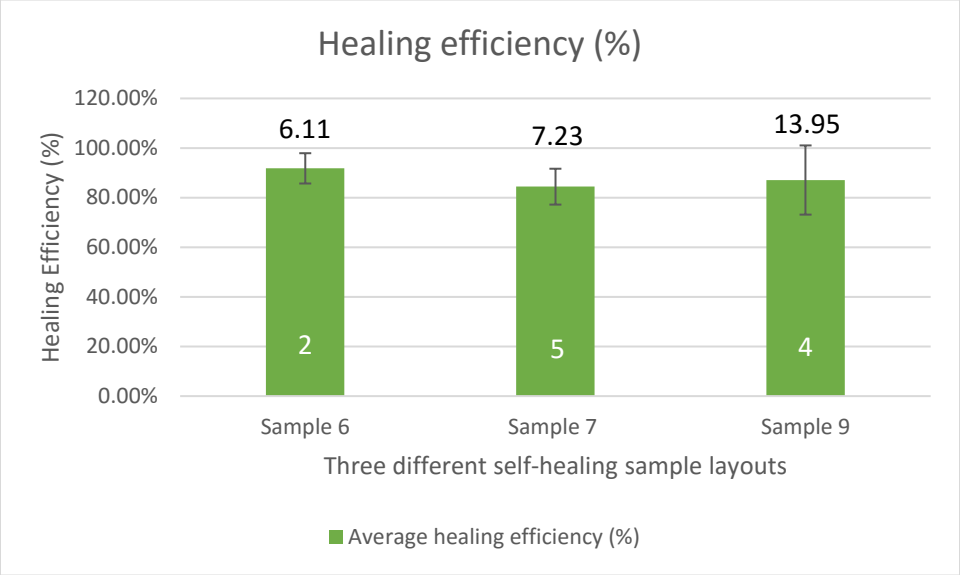

Figure 49: Healing Efficiency (%) of self-healing samples. The white number at the bottom of the bars show the number of specimens tested in that sample.

Healing efficiency in percentage was calculated using the formula mentioned in 3.6. The healing efficiency of sample 6, sample 7 and sample 8 was found to be 91.81%, 84.43% and 87.11% respectively as shown in Figure 49. Further details on differences between the layouts of the three samples are mentioned in section 4.7. The standard deviation of healing efficiency for sample 6 with 2 specimens was found to be 6.11%, standard deviation of healing efficiency for sample 7 with 5 specimens was found to be 7.23% and standard deviation of healing efficiency for sample 9 with 4 specimens was found to be 13.95%.

CHAPTER 7 : WIND TUNNEL TESTS

7.1 Introduction

Wind energy, one among the renewable sources, has the potential to mitigate the issues occurring with fossil fuels as the wind is readily available and can be harnessed with the installation of wind turbines. The energy from the wind rotates the blades which in-turn rotates a turbine generating electrical power. These wind turbines are left unattended after they have been installed and are prone to continual exposure to changes in wind and weather conditions which leads to stress concentrations and small-scale cracks and damages. These minor cracks if left unattended can result in major implications which result in the failure of these blades. The purpose of this part of the project is to design a scaled down wind turbine blade, implement self-healing characteristic into a prototype blade and run the wind turbine in the wind tunnel as a demonstration of the real-life performance of self-healing. A UV-sensitive dye is used to check for movement of the healing agent into cracks. This part of the project is disparate from testing the self-healing in square samples and applying what was learned to develop a self-healing turbine blade.

7.2 Two halves mold design

7.2.1 Blade Design

The initial design intent was to build two dyes to mold two halves of a turbine blade that can be joined to form a full turbine blade. National Advisory Committee for Aeronautics (NACA), NACA 64(2)-415 aerofoil profile was used to design a wind turbine blade. Figure 50 shows a 3D geometry of the wind turbine blade that was drafted using the NACA profile. The 3D geometry was relatively easier to mold as compared to the other designs that were studied.

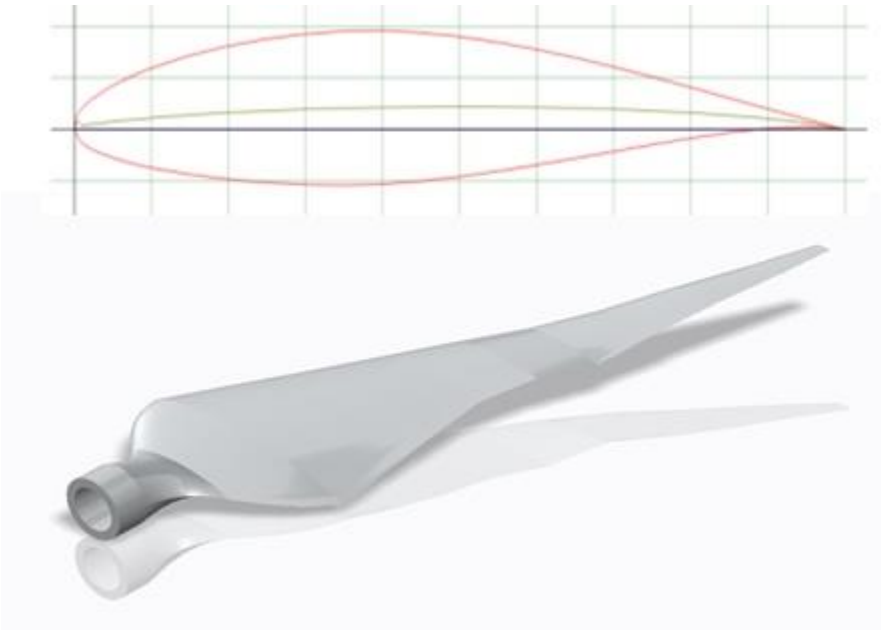

Figure 50: First design iteration of wing profile using NACA 64(2)-415 standard profile

7.2.2 Mold Design

The next step in manufacturing the turbine blade was to manufacture the molds that have a negative profile of the turbine blade. A parting line along the span of the profile (top and bottom) was used to separate the molds. Since, both, upper and lower half of mold possess different designs for aerodynamic reasons, care was taken to implement the changes into the mold design. Figure 52 shows an isometric view of the mold design that was built. The molds had gone through a series of iterations before the final mold geometries were established as seen from Figure 51 through Figure 55.

7.2.2.1 First iteration

In the first iteration, a circular indentation was placed on the top surface of the mold to aid in the vacuum process. One of the things that this mold was lacking was establishing a parting line for the blade (Figure 51). The parting line is the plane in which the two halves of the mold meet. This

is important because if the molds did not stay within the parting line, the blade halves would be too small or too big and would not create a good final part. In this design, the mold extended past the parting line, so the mold was too big to manufacture and it had a high cost associated with it. This iteration was neglected due to those reasons.

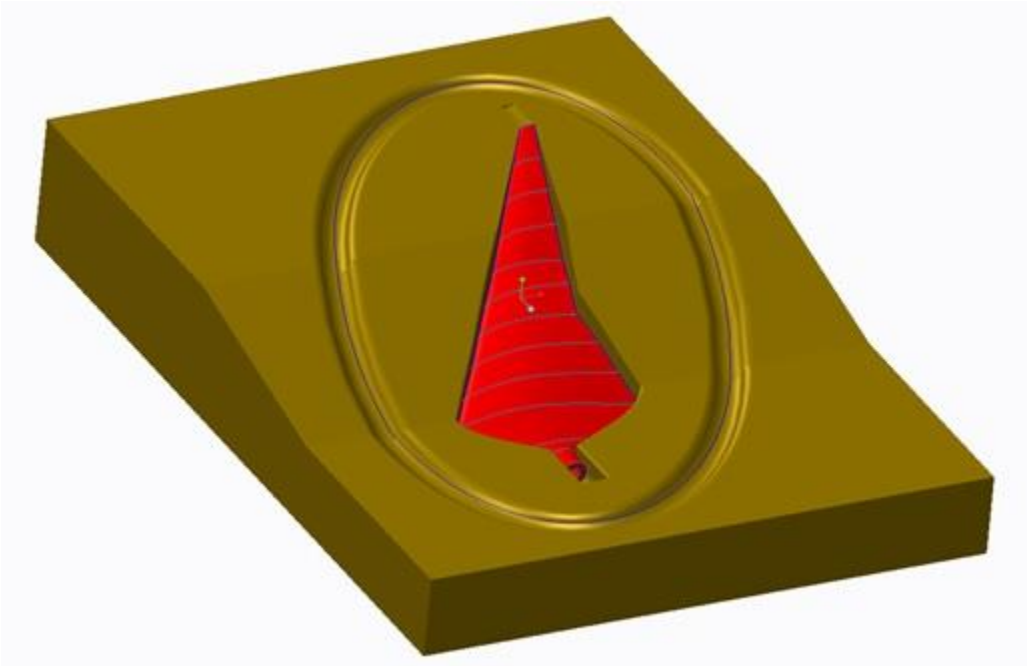

Figure 51: First iteration

7.2.2.2 Second iteration

The second iteration of the mold Figure 52 arrived through a series of design parameters that were established after an in-depth design review of the first iteration.

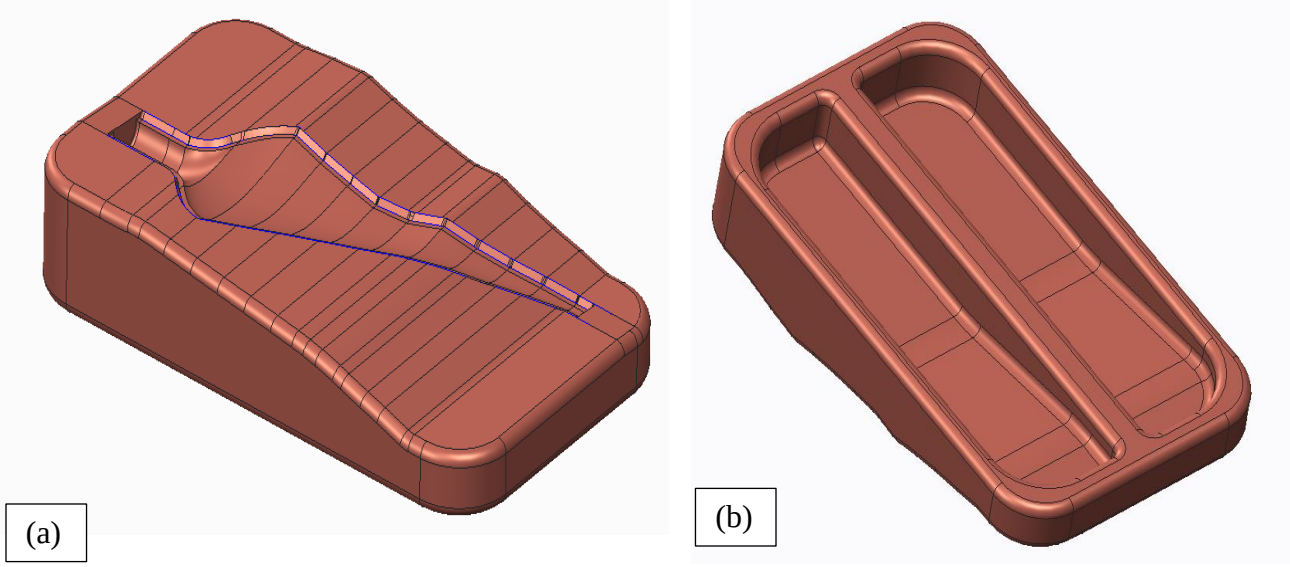

Figure 52: Isometric view of the bottom and top of the mold

The design parameters established were to keep the mold compact in size in order to be able to 3D print it and reduce the amount of material and costs associated with it. The reduction in the amount of material used was achieved by hollowing the mold. Figure 53 shows a cross-sectional view of hollowed mold. An added parameter in this design was creating a key slot feature in the mold which would translate into the molded blade part. The final parameter that was added was creating gates to give excess material some room to run out without affecting the actual part as seen in Figure 55.

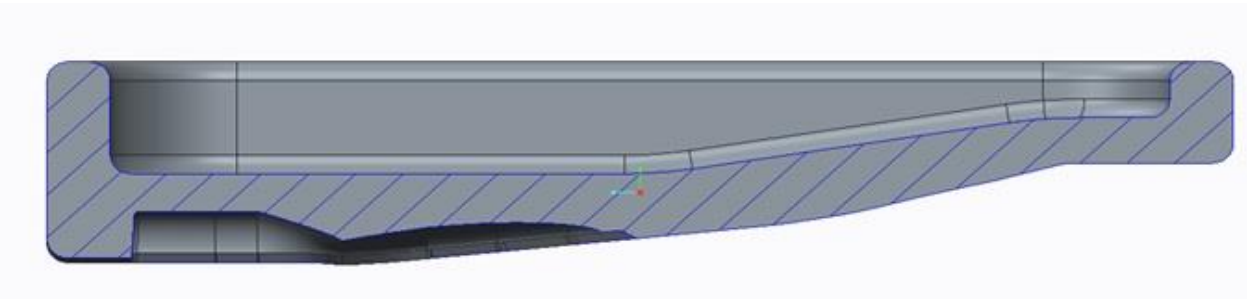

Figure 53: Cross-section of the mold

7.2.2.3 Third iteration

The third and final iteration was driven by the cost of the molds. All the parameters from the previous design were retained. The main change between the first and second iteration was the size of the mold and an additional parameter which was to add a sacrificial area around the blade. This would cause the blade to be slightly oversized which would aid the finished product, since the sacrificial area can be sanded in the molded part to provide a better finish.

The manufacturing process selected was to 3D print the molds using a Fused Deposition Modeling (FDM) printer.

The VARTM process requires molds to be under compression throughout the whole process. Utilizing an FDM printer, the molds would be taking advantage of their loading conditions because the printer prints layer by layer until the part is done. Therefore, under the loading conditions the molds actually become stronger. Figure 54 shows the final design of the mold. The material selected for the molds is Acrylonitrile butadiene styrene (ABS) due to the material's high yield and tensile strength.

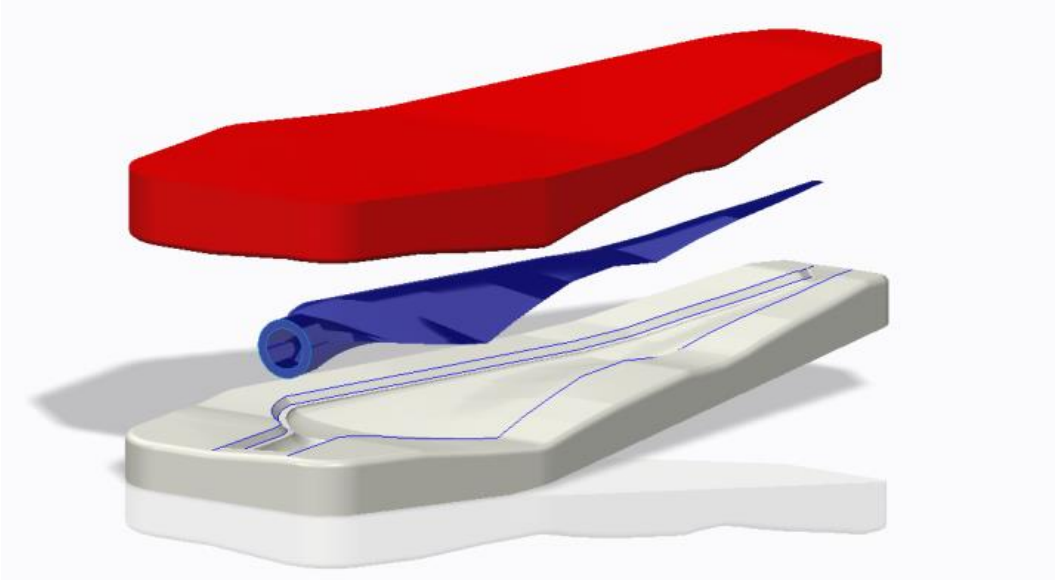

Figure 54: Final mold design; Exploded view displaying bottom and top mold

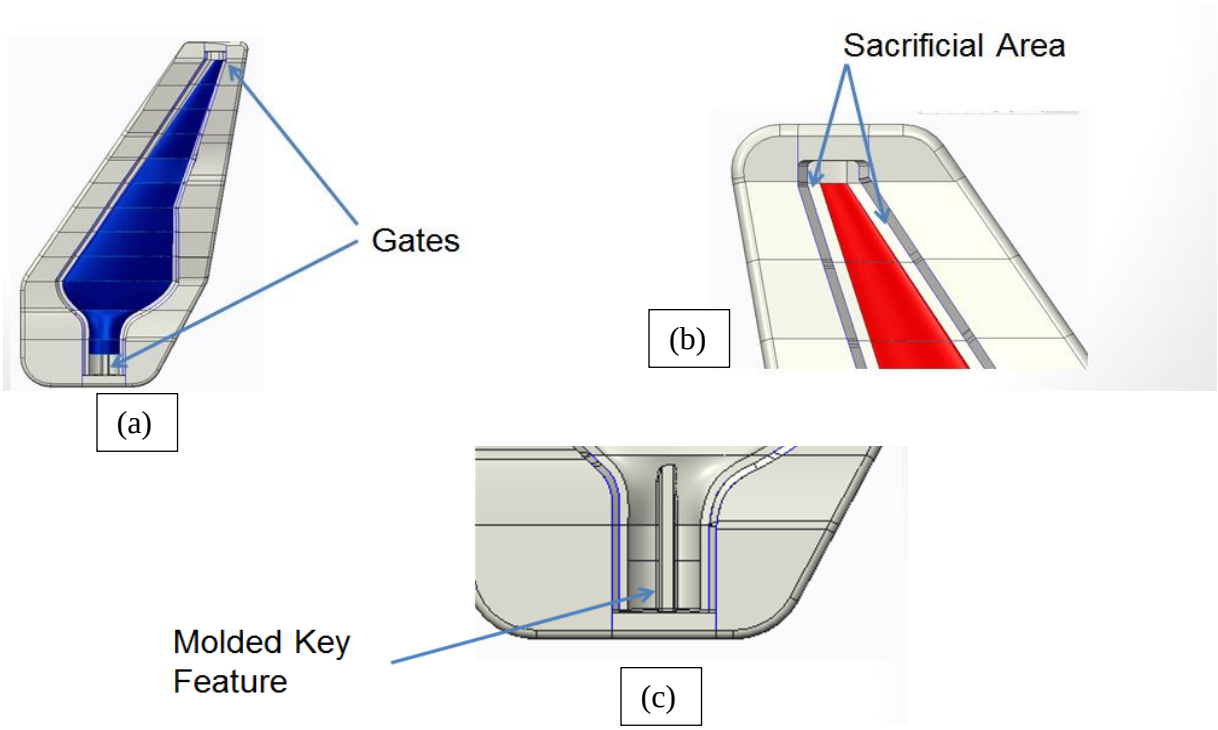

Figure 55: Zoomed images of various key features in the mold

7.2.3 Mold Analysis

The VARTM process utilizes vacuum to create the end product. The vacuum pressure typically needed to create this vacuum is around 80kPa which is a significant amount of pressure the mold has to withstand. In order to ensure the mold does not fail, two analyses were conducted. The first analysis is to specify a minimum thickness needed and the second was a material study and validation of the first.

The first analysis was done through hand calculations. The analysis assumes a simple geometry; the mold has a uniform thickness, the loads are point loads, and a safety factor of 2 was used as the forces will translate to different planes. From the analysis, it was concluded that the minimum thickness required for the mold to withstand the given loading is 7.112 mm. It was decided to specify 12.7 mm at a minimum to take the uncertainty of the analysis out of the equation.

The design was 3D printed from a commercial vendor and the surface of the mold was sanded using 220, 400, 600, 800 and 1000 grit papers to improve the surface finish of the molded blade and also, ease of mold release. Figure 56 shows photograph of two parts of the wind molded using the 3D printed molds.

Figure 56: Photograph of both sides of molded pieces of wind turbine blade inside the 3D printed molds

The vacuum pump was left running until the mold was cured to the leakage in a vacuum bag. Figure 57 and Figure 58 show the molded part that had dry spots due to the intricate shape of the mold.

Figure 57: Turbine blade sample

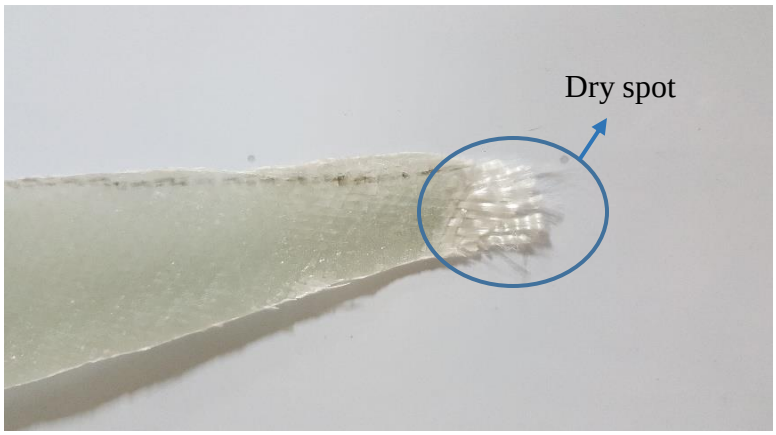

Figure 58: Dry spot at the tip of the blade

The molded parts using the 3D printed mold had multiple issues including problems with vacuum bagging due to the complex shape of the mold, dry spots, higher thickness and hence increased weight in the central regions of the blade. The significant disadvantage of the two part design was the inconsistency in the parting line due to the inherent unevenness of VARTM process and the hence, the two parts could not be joined for without significantly increasing the weight of each blade.

7.3 Shell type design

The second design cycle of a scaled down wind turbine blade involved a 3D printed core over which the fiber reinforced thermoset composite wind turbine blade was molded to form the final composite part. The experience from molding complex blades from the previous design was used in the design and manufacturing of the turbine blades. To achieve the goal of testing and implementing the self-healing process, the design of the blade has been simplified to ease and streamline the manufacturing process.

As compared to the aeroplane wing profile in the previous design, a wind turbine specific aerofoil profile from National Renewable Energy Laboratory (NREL) was used. The blade has been

simplified in comparison to the turbine blades used in industry today. Typical blades used by companies such as GE and Siemens have very complex geometry with both radial pitch and yaw, along with various airfoils throughout the length of the turbine blade to allow for maximum aerodynamic efficiency. Since the focus and scope of the project are on the implementation of the self-healing mechanism, the blade used in this project is an NREL S822 airfoil profile that is tapered along the length of the blade. The NREL S822 airfoil is commonly used on turbines with blade diameters between 1 meter and 5 meters [31]. The details of lift/drag ratio to the angle of attack against the smoothness of the turbine blade are provided in the plot in Figure 59. The angle of attack of 5.5° was chosen for the design.

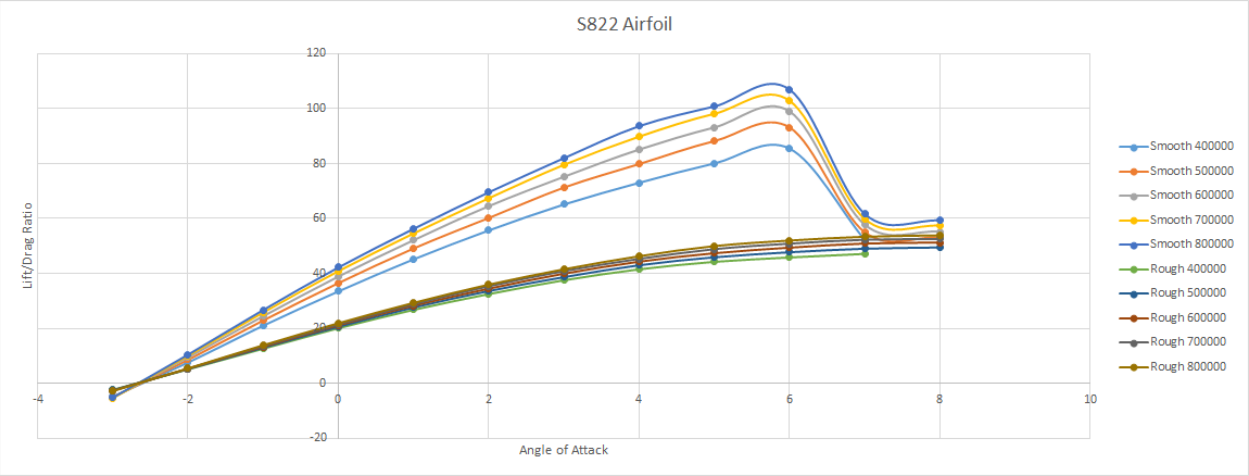

Figure 59: Plotted lift/drag ratio compared to airfoil angle of attack for the NREL S822 airfoil. Curves represent different surface finishes

The blade was then 3D printed and used as the mold to create the fiberglass turbine blades. The blades themselves were constructed out of fiberglass layers that were roughly 2 mm thick. The fiberglass layers were wrapped entirely around the 3D printed mold to create a single uniform piece that doesn't have a parting line. The blade had a draft of 20% from the hub side of the blade to the outside edge of the blade as seen in Figure 60 and Figure 61. The draft in the blade allowed

for less required force to remove the 3D printed core from the fiberglass shell. 3D printing was the chosen manufacturing method for turbine blade core and the turbine hub. 3D printing has several advantages including ease and speed of manufacturing complex shapes. The process provided the ability to vary the angle of attack and other details in quick design cycles if need be.

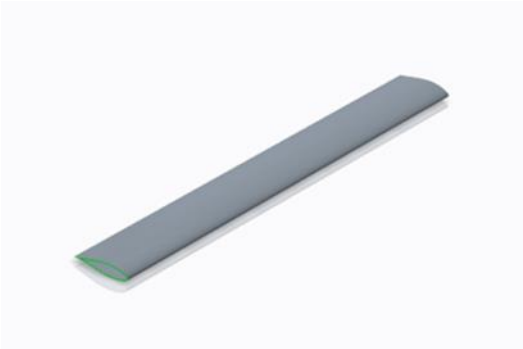

Figure 60: Isometric view CAD model of the scaled down wind turbine blade using NREL aero foil profile

Figure 61: Front view of the 3D printed blade mold

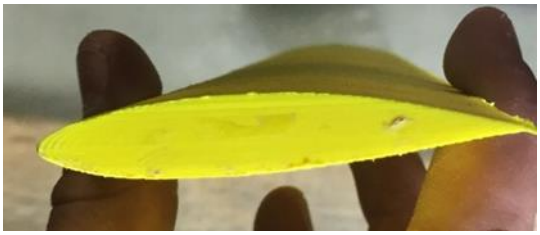

Figure 62: Side view of the 3D blade showing aerodynamic profile

The blade was 3D printed from acrylonitrile butadiene styrene (ABS) material as shown in Figure 61 and Figure 62. ABS has a higher glass transition temperature than other commonly used 3D

printing materials, such as polyvinyl alcohol (PVA). The higher glass transition temperature was required because of the temperatures that are reached during the curing process of the resin. The 3D printed core was polished for easier removal of the vacuum infused shell around it.

Initially, the vacuum infusion process was done with sheets of vacuum bagging material, which was formed to create a bag. The bagging material is hard to seal all four edges consistently. The key to an accurate final product, is maintaining a good vacuum seal throughout the curing process. For the second and third iteration of the fiberglass infusion process, a premade bag that was sealed on both sides was used. The premade bag proved much more successful because only two edges had to be sealed. Once the core is removed, minor surface finishing was performed to eliminate any uniformity issues that arise during the Vacuum Assisted Resin Transfer Molding (VARTM) process. Another change made for the second iteration was to use two resin inlets for the infusion process. The resin infusion process itself takes some time for the resin to flow evenly throughout the whole mold due to the high viscosity of the resin. To account for the low flow rate, one inlet was placed at the base of the blade, and another at the tip. The inlets were in line with the trailing edge of the blade, while the vacuum outlet was in line with the center point of the leading edge of the blade. The two inlet method proved to increase the resin infusion process significantly. Once the VARTM process was complete, the 3D printed blade will then be removed out of the shell to be reused to create future blade iterations.

7.3.1 Hub design

A hub had been designed to fit the above-molded blades. The new design consists of three slots equally sized and spaced that are oriented at the optimal angle of attack for the airfoil chosen. The hub has three NREL S822 profiles cut into it axially spaced at 120 degrees. Each cut was positioned at the angle of attack that provides the greatest lift to drag ratio (5.5°). Slots in the hub were

oversized to account for the increase in the size of the blade from the layers of fiber glass that were being added to create the shell of the blade as seen in Figure 64. Once the blade is slid into the slot, the blades were secured using two set screws. These set screws were inserted at an angle above the back face of the hub; this is to ensure that the set screw is perpendicular to the blade. The set screw approach was chosen to allow for efficient changing of blades between test runs and can be seen in Figure 63.

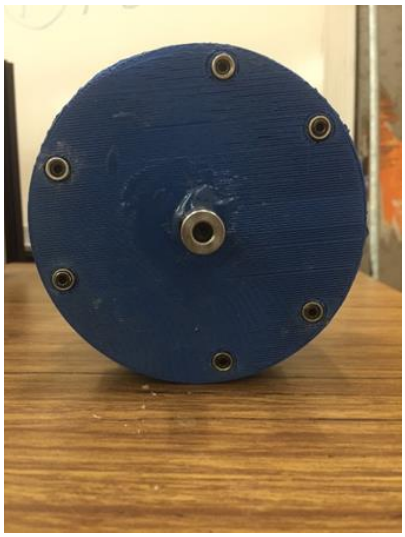

Figure 63: Photograph showing the back view of the 3D printed hub with the set screw location

Figure 64: Side view of the 3D printed hub. View shows the groove for the blade and the coupling used to connect to the motor shaft

The final design is shown in Figure 66 and fabricated wind turbine, as can been seen in Figure 65 was tested inside the wind tunnel at various speeds. The turbine with composite turbine blades was sturdy and had no concerns with running at the maximum wind speed of the wind tunnel. The maximum wind speed was 16.5m/s through the test section of the wind tunnel.

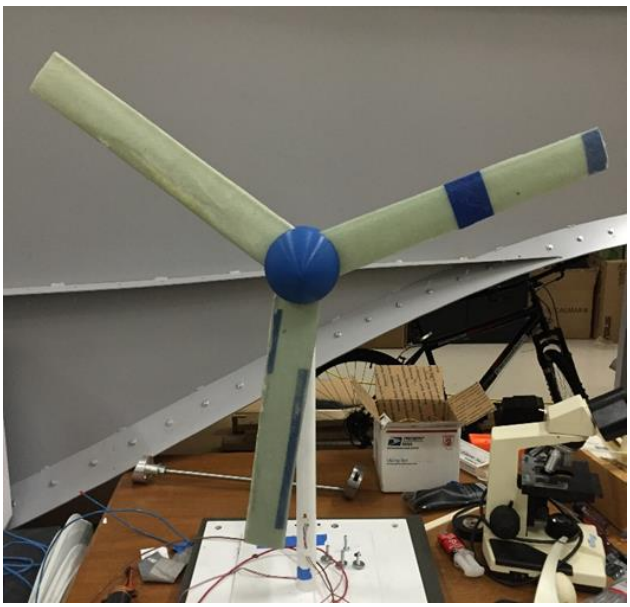

Figure 65: Final prototype assembly. Incorporating the NREL S822 airfoil and a hub designed by the team

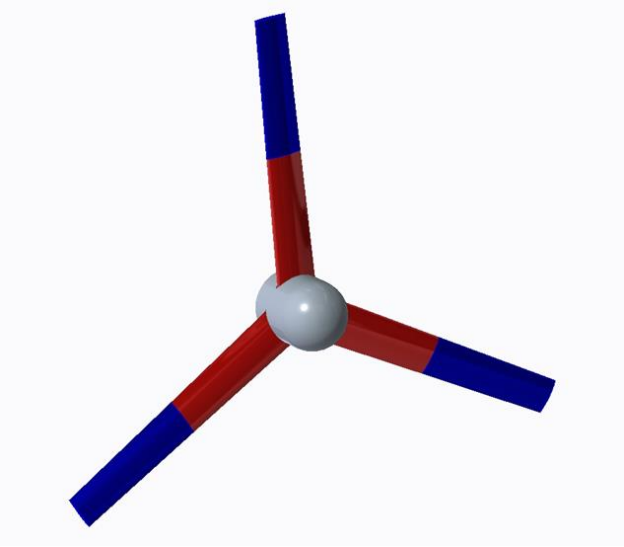

Figure 66: 3D CAD model of the assembly that incorporates a 5.5° angle of attack that is optimal for the NREL S822 aerofoil

Figure 67: Photograph of the wind tunnel used for testing at the University of Wisconsin-Milwaukee

Figure 67 shows a photograph of the wind tunnel used for testing the composite blade wind turbine.

7.4 Self-healing in wind turbine blade

The self-healing analysis in a scaled down wind turbine had two control wings, and one self-healing wing that included self-healing characteristics added into its structure while the other two

blades were without self-healing characteristics. A self-healing blade was manufactured using only two layers of fiber glass as compared to 6 layers of fiber glass used in control blades, for ease of cracking of the tubes containing the healing agent. The blade was manufactured using the same molding technique mentioned in section 7.3.

Maximum stress concentration and cause for damage in wind turbine blades is from high tensile stresses which arise from bending of the turbine blades due to aerodynamic lift on one side of the blade. Most blades tend to break around the center of the turbine blade span and hence, the Borosilicate tubes containing the healing agent for self-healing were implemented at the center of the blade as shown in Figure 68.

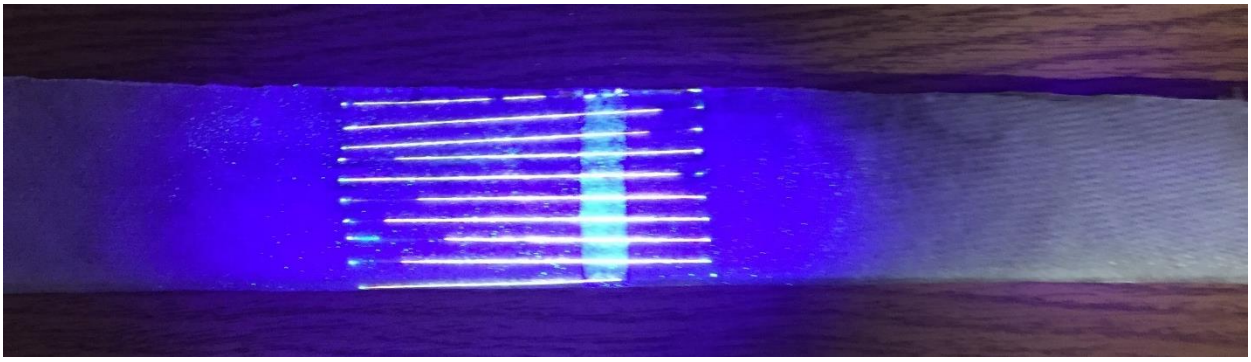

Figure 68: Photograph of scaled down turbine blade showing tubes containing the healing agent for self-healing

The tubes were laid similar to the flat self-healing samples with around 6mm spacing between the tubes and placed all around the central portion of the turbine blade. The tubes were filled with the same concentration as that of flat self-healing molds in section 6.8, 6.9, 6.10 i.e. DCPD mixed with UV reflective dye. Similarly, 1g Grubb's catalyst was dispersed through-out the composite blade. Care was taken to have most of the catalyst around the tubes by laying a small amount of resin-hardener mixture with large portion of 1g catalyst around the tubes prior to the VARTM process. The blade was fixed to the turbine as shown in Figure 69.

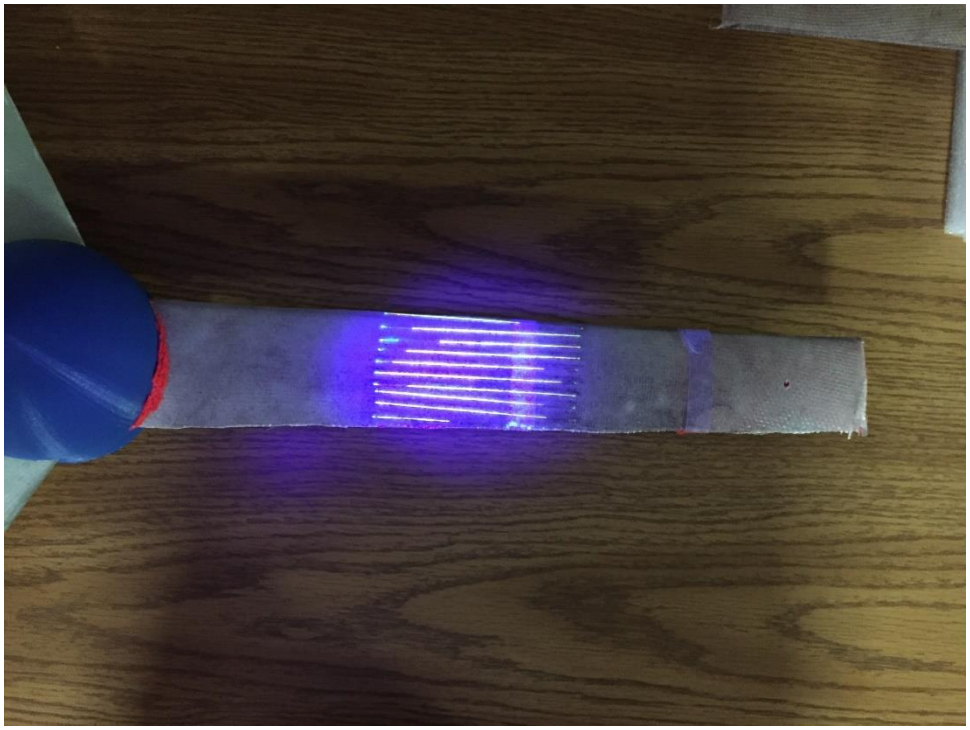

Figure 69: Photograph of a blade with self-healing characteristic fixed to scaled down wind turbine

The prototype was run in the wind tunnel at incremental wind speeds of 9m/s, 12m/s and 16.5 m/s for about an hour and at maximum speed i.e., 16.5 m/s wind speed for about an hour to try and have a crack form naturally under flexural stresses. Inspecting the turbine blades for damage revealed that no visible breakage or any change in the healing agent content in the tubes.

A second trail was performed by adding uneven weights at the tip of the self-healing turbine blade to impart imbalance and increase forces for cracking and subsequent healing of the blades. Figure 70 shows the self-healing sample with weights added at its tip. It can be noted that the blade automatically is lower than the other two blades due to increased weight. The wind tunnel testing is further explained in the following sub-section.

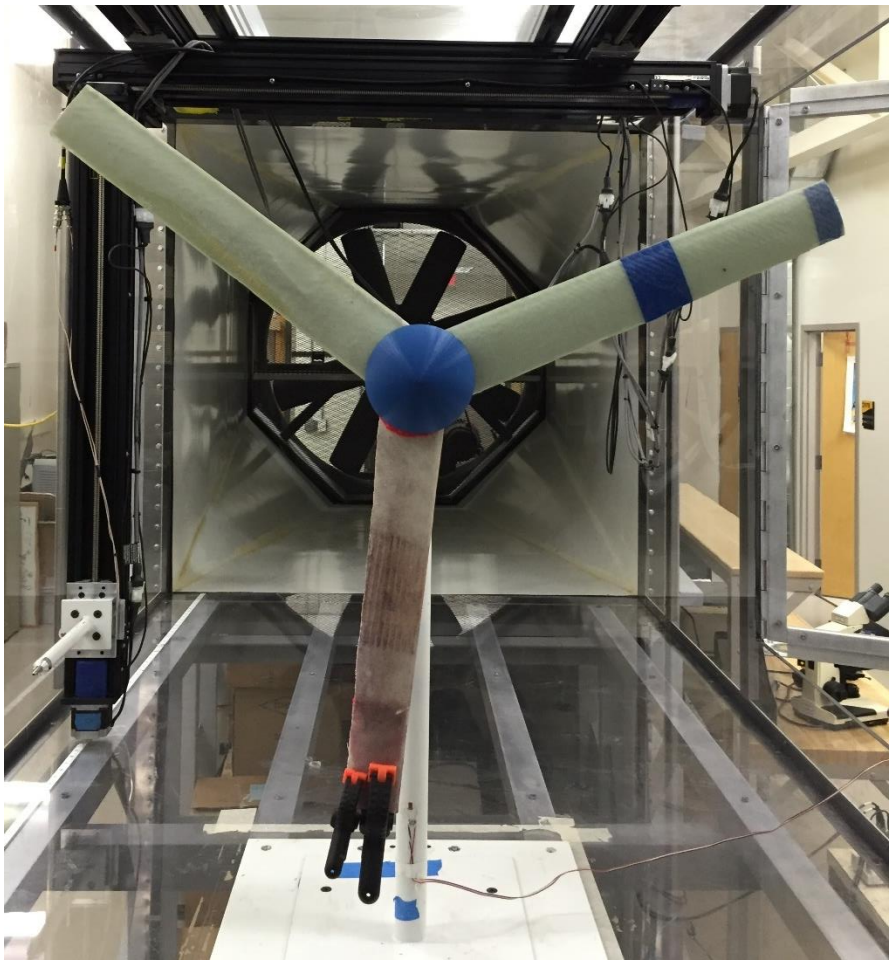

Figure 70: Photographs of self-healing blade with weights added at its tip to add imbalance and stresses on the blade

7.4.1 Wind Tunnel testing of self-healing blade

The scaled down wind turbine was for more than 3 hours, out of which it was run about 2 hours at its maximum wind speed of 16.5m/s through its test section. Extra weights were added to create imbalance and stress the self-healing specimen to impart cracks.

Before wind tunnel test

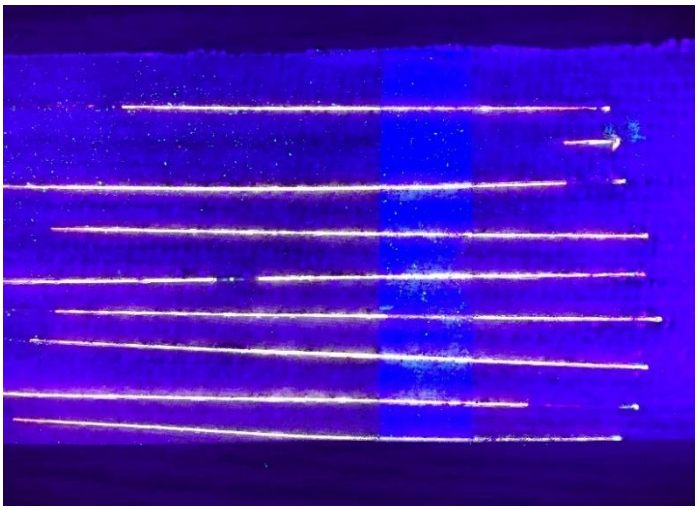

After wind tunnel test

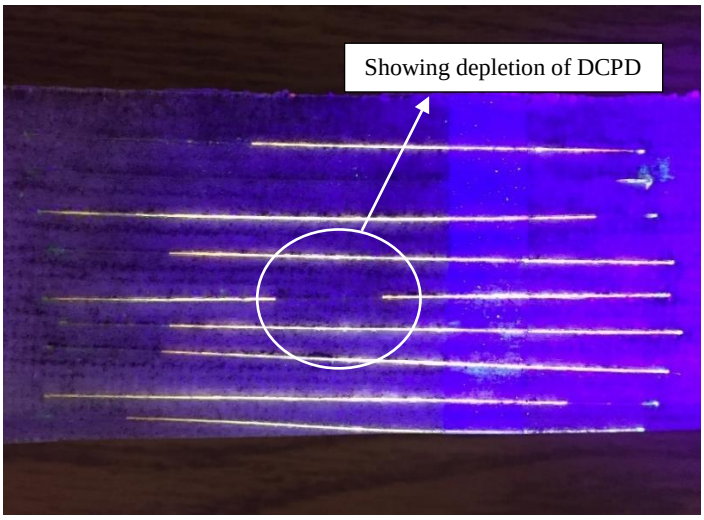

Figure 71: Before and after wind tunnel testing photographs of the section of blade laid with tubes containing healing agent

As can be observed from the photographs presented above, the content of healing agent mixed with UV reflective dye shows minor changes in the DCPD content within the tubes after prolonged wind tunnel testing at high speeds. The composite turbine blade structure proved efficient and sturdy. Decrease in the number of woven fiber glass layers did not deteriorate the strength of the turbine blade significantly. Maximum running speed of 16.5m/s wind speed proved low for the scaled down wind turbine blade fabricated.

Goals accomplished during the length of this scaled down model study include development and improvement of the VARTM process, manufacturing a hub that allows for rapid testing of different blades, molding of a prototype, which incorporates the aforementioned hub and three standard fiberglass blades. Development and implementation of self-healing characteristics within a blade and testing its performance.

CHAPTER 8 : CONCLUSIONS

I. Vacuum Assisted Resin Transfer Molding (VARTM) process is found to be the most effective polymer composite molding technique, supporting the current industry standards.

II. The glass transition temperature of the fiber reinforced thermoset composite material was found to be 67°C from Dynamic Mechanical Analysis under Flexure. However, the storage modulus of the composite was maximum at 57°C. Hence, the operating temperature and temperature increase in the blade due to exothermic reaction during polymerization of the healing agent must preferably be within 57°C for improved durability and performance of the wind turbine blades.

III. Maximum tensile strength was obtained with all the reinforcing glass fiber fabric layers oriented in the same direction and processed using VARTM process in a conventional glass fiber reinforced polymer matrix composite. The tensile strength of the composites with varying fiber orientation within the composite was found to be slightly lower than that of fibers oriented in the same direction. Although, the composite with varying fiber orientation between layers is advantageous with its quasi-isotropic properties. In the case of wind turbine blades subjected to continuous bending, it can be suggested that all the reinforcing fiber fabrics be oriented in the same direction between layers.

IV. Vascular network type of self-healing is chosen for glass fiber reinforced polymer matrix composite. The network can supply the healing agent to the polymer matrix, even between the fiber fabric layers. This type is most suitable as capsules in a capsule-based type of self-healing tend to clump in the interstitial regions of fiber fabrics. Intrinsic type of self-healing is not suitable for thermoset polymer composites.

V. VARTM process proved effective to mold composites with micro-tubes for the self-healing capability. Tubes oriented parallel to the resin flow direction during the VARTM process is the most effective arrangement to implement vascular network type of healing agent distribution system.

VI. Composite with a single, central layer of smaller size (500μm outer diameter) Borosilicate tubes showed around 25% decrease in average tensile strength as compared to average tensile strength of conventional (without tubes) composite.

VII. Composite with a single, central layer of smaller size (500μm outer diameter) Borosilicate tubes showed around 9% decrease in average flexural strength as compared to average flexural strength of conventional (without tubes) composite.

VIII. Self-healing of woven glass fiber reinforced, thermoset polymer composites using 1D vascular-channel type of healing was successful with a minimum average recovery of flexural (three-point bending) strength of 84.52% using a single layer of Borosilicate tubes (500μm outer diameter and 250μm inner diameter) to supply the healing agent coupled with selectively dispersed Grubb's catalyst within the resin matrix.

IX. Average recovery of flexural strength of 92.12% was observed using the tubes as a central layer and 84.52% using tubes as the last layer (i.e. on the tensile loading side of 3-point bending) and 87.11% using tubes as the penultimate layer of glass fiber fabric. (Note: Sampling varies for the average calculation)

X. Movement of healing agent (Dicyclopentadiene) into newly formed cracks and dispersion of healing agent throughout the thickness of the composite (penetrating layers of glass fiber fabrics in-between) at the damage site was demonstrated in real-time while performing

flexural bend test providing visual validation of the mechanism of self-healing in glass fiber reinforced, thermoset polymer composite material.

XI. Consumption of healing agent within the tubes in a prototype model of wind turbine with a self-healing blade after wind tunnel testing was observed verifying the usefulness and potential for self-healing in wind turbine blades

CHAPTER 9 : FUTURE WORK

1. Extending the current one dimensional vascular healing network to two or three dimensional healing network for multiple healing cycles.
2. Feasibility study for commercial application of self-healing in wind turbine blades.
3. Microscopic analysis of the healed specimens to analyze the dispersion of catalyst and DCPD in the damaged region
4. High or positive pressure infiltration of DCPD to improve bleeding of tubes within the composite material.
5. Experimentation and implementation of self-healing characteristic in thermoplastic polymer and polymer composite.

REFERENCES

[1] Dan Utech, "The Promise of Wind Energy," The White House Blog, 12 March 2015. [Online]. Available: https://www.whitehouse.gov/blog/2015/03/12/promise-wind-energy.

[2] U. S. Department of Energy, "Wind Vision," American Wind Energy Association, 2015. [Online]. Available: http://www.awea.org/content.aspx?ItemNumber=7300&RDtoken=61421&userID=&navItemNumber=7077.

[3] S. Campbell, "Annual blade failures estimated at around 3,800," WindPower Monthly, 14 May 2015. [Online]. Available: http://www.windpowermonthly.com/article/1347145/annual-blade-failures-estimated-around-3800. [Accessed 2016].

[4] B. S. Nivedh, "Major Failures in the Wind Trubine Components and the Importance of Periodic Inspections," www.windinsider.com, November 2014. [Online]. Available: http://www.dewi.de/dewi_res/fileadmin/pdf/papers/WindInsider_November_2014.pdf.

[5] C. Smith, "Fires are major cause of wind farm failure, according to new research," Imperial college London, 17 July 2014. [Online]. Available: http://www3.imperial.ac.uk/newsandeventspggrp/imperialcollege/newssummary/news_17-7-2014-8-56-10.

[6] "Caithness Windfarm Information Forum 2015," 2015. [Online]. Available: http://www.caithnesswindfarms.co.uk/.

[7] Joseph Bebon, "GE Investigates Two More Turbine Blade Breaks," North American Wind Power, 13 May 2014. [Online]. Available: http://www.nawindpower.com/e107_plugins/content/content.php?content.12970.

[8] B. Aissa, D. Therriault, E. Haddad and W. Jamroz, "Self-Healing Materials Systems: Overview of Major Approaches and Recent Developed Technologies," *Hindawi Publishing corporation,* 2012.

[9] S. White, N. Sottos, P. Geubelle, J. Moore, M. Kessler, S. Sriram, E. Brown and S. Viswanathan, "Autonomic Healing Of Polymer Composites," *Nature,* vol. 409, no. 6822, pp. 794-797, 2001.

[10] B. Blaiszik, S. Kramer, S. Olugebefola, J. Moore, N. Sottos and S. White, "Self-Healing Polymers and Composites," *www.annualreviews.org,* no. 40, pp. 179-211, 2010.

[11] R. Bogue, "Smart Materials: A Review of Recent Developments," *Assembly Automation,* vol. 32, no. 1, pp. 3-7, 2012.

[12] Y. C. Yuan, T. Yin, M. Z. Rong and M. Zhang, "Self Healing in Polymers and Polymer composites. Concepts, Realization and Outlook: A Review," *eXPRESS Polymer Letters* , vol. 2 , no. 4, pp. 238-250, 2008.

[13] P. Martin, "Wound Healing-Aiming for Perfect Skin Regeneration," *Science,* vol. 276, no. 5309, p. 75–81, 1997.

[14] R. Trask, H. Williams and I. Bond, "Self-Healing Polymer Composites: Mimicking Nature to Enhance Performance," *Bioinspiration & Biomimetics,* vol. 2, no. 1, pp. 1-9, 2007.

[15] M. Q. Zhang and M. Z. Rong, Self-Healing Polymers and Polymer Composites, John Wiley & Sons, Inc., 2011.

[16] M. Kessler and S. White, "Self-Activated Healing of Delamination Damage in Woven Composites," *Composites: Part A,* vol. 32, no. 5, pp. 683-699, 2001.

[17] M. Kessler, N. Sottos and S. White, "Self-Healing Structural Composite Materials," *Composites: Part A,* vol. 34, no. 8, pp. 743-753, 2003.

[18] E. Brown, S. White and N. Sottos, "Microcapsule Induced Toughening in a Self-Healing Polymer Composite," *Journal of Materials Science,* vol. 39, no. 5, pp. 1703-1710, 2004.

[19] S. Van der Zwaag, H. M. Andersson, M. W. Keller, J. S. Moore, N. R. Sottos and S. R. White, In Self Healing Materials—An Alternative Approach to 20 Centuries Materials Science Chap. II, Springer, 2007.

[20] K. S. Toohey, N. R. Sottos, J. A. Lewis, J. S. Moore and S. R. and White, "Self-Healing Materials With Microvascular Networks," *Nature Materials,* vol. 6, no. 8, pp. 581-585, 2007.

[21] P. Brøndsted and R. Nijssen, "Advances in Wind Turbine Blade Design and Materials," *Woodhead Publishing, Elsevier, Cambridge,* 2013.

[22] C.-Y. Huang, R. S. Trask and I. P. Bond, "Characterization and analysis of carbon fibre-reinforced polymer composite laminates with embedded circular vasculature," *Journal of The Royal Society Interface*, vol. 7, pp. 1229-1241, 2010.

[23] M. Motuku, U. K. Vaidya and G. M. Janowski, "Parametric studies on self-repairing approaches for resin infused composites subjected to low velocity impact," IOP Publishing Ltd, 1999.

[24] A. K. Koralagundi Matt, S. Strong, T. ElGammal and R. S. Amano, "Development of Novel Self-Healing Polymer Composites for Use in Wind Turbine Blades," *ASME. Journal of Energy Resources Technology*, vol. 137, no. 5, pp. 051202-5, 2015.

[25] Wikipedia contributors, "Dicyclopentadiene," Wikipedia, The Free Encyclopedia, [Online]. Available: https://en.wikipedia.org/w/index.php?title=Dicyclopentadiene&oldid=710299196.

[26] ASTM D3039 / D3039M-14, "Standard Test Method for Tensile Properties of Polymer Matrix Composite Materials," ASTM International, West Conshohocken, PA, 2014.

[27] ASTM D7264 / D7264M-15, "Standard Test Method for Flexural Properties of Polymer Matrix Composite Materials," ASTM International, West Conshohocken, PA, 2015.

[28] ASTM D5023-15, "Standard Test Method for Plastics: Dynamic Mechanical Properties: In Flexure (Three point bending)," ASTM International, West Conshohocken, PA, 2007.

[29] TA Instruments, "Q800 Dynamic Mechanical Analysis," Q Series Thermal Analysis, [Online]. Available: http://www.tainstruments.com/product.aspx?siteid=11&id=25&n=3.

[30] K. V. Rijswijk, "Vacuum Infusion Technology for Anionic Polyamide-6 Composites," TU Delft, Delft, 2007.

[31] J. Tangler and D. Somers, "NREL Airfoil Families for HAWTs," National Renewable Energy Laboratory, Golden, 1995.

[32] P. Behr, "Will Politics Slow the Wind?," *http://www.scientificamerican.com/article/politics-of-wind-power/*, April 1, 2015.

[33] A. K. Koralagundi Matt, S. P. Strong, J. Guo and R. S. Amano, "Development of Self-Healing Materials for use in Wind Turbine Blades," in *54th AIAA Aerospace Sciences Meeting, AIAA SciTech, (AIAA 2016-0992)*, San Diego, CA, 2016.

[34] P. Denholm, M. Hand, M. Jackson and S. Ong, "Land-use requirements of modern wind power plants in the United States," Golden, CO: National Renewable Energy Laboratory, 2009.

[35] E. Arnett, M. Schirmacher, M. Huso and J. Hayes, "Effectiveness of changing wind turbine cut-in speed to reduce bat fatalities at wind facilities," Bat Conservation International, Austin, TX, 2009.

[36] "Not on my beach, please," *The Economist Newspaper Limited*, 21 August 2010.

APPENDICES

Appendix A : Self-healing test plots and details

The plots of Load (N) vs deflection (mm) of each specimen of the three self-healing samples. The unhealed specimens were allowed to reach their maximum load bearing capacity and the experiment was cut off immediately after a dip in the load. The specimens were left to cure over night for about 24 hours under light weight retain the straightness of the specimens. The healed specimens were tested for their maximum flexural strength after 24 hours. The tests performed on specimens after healing are labelled H towards the end of it.

1 Self-healing results of samples with-tubes as a central layer

The specimens under sample 6 were all prepared from the same mold and hence both the specimens have same conditions. The only difference is the dimensions of the specimens due to minor variations in machine processes.

Table 3: Average Dimensions of specimens used for flexural testing (dimensions are measured at three regions in a specimen and averaged)

SPECIMEN NAME	AVERAGRE WIDTH (mm)	AVERAGE THICKNESS (mm)
S6B1	12.62	2.12
S6B2	12.66	1.95
S6B3	12.63	2.17
S7B1	12.7	2.05
S7B2	12.80	2.07
S7B3	12.98	2

S7B4	12.84	2.04
S7B5	12.98	2.04
S7B6	12.78	2.06
S7B7	12.82	2.02
S9B1	12.93	1.89
S9B2	12.91	2.01
S9B3	12.72	1.98
S9B4	13.01	2.07
S9B5	12.93	2.09
S9B6	12.68	2.07
S9B7	12.91	2.04

1.1 Sample 6; specimen B2 (S6B2)

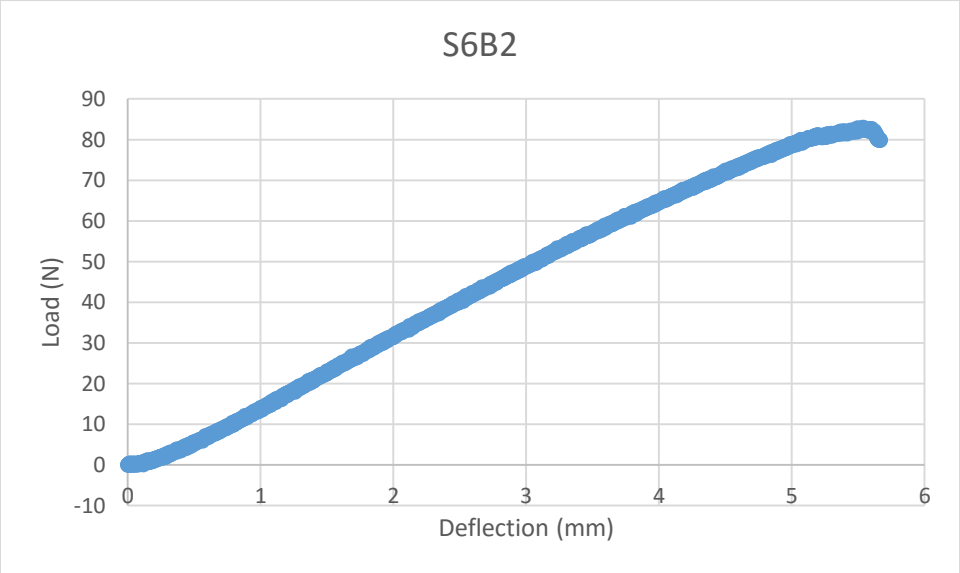

Figure 72: Load (N) vs deflection (mm) plot of the specimen S6B2

Maximum flexural strength of the specimen S6B2 was found to be 165.53MPa with a maximum load bearing capacity of 83.01 N.

1.2 Sample 6, healed specimen B2 (S6B2H)

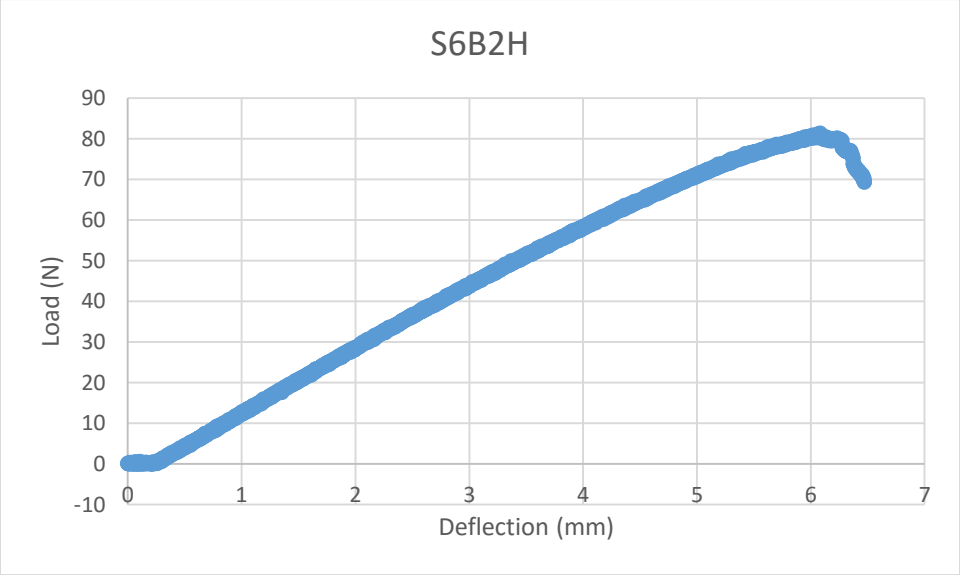

Figure 73: Load (N) vs deflection (mm) plot of the specimen S6B2H

Maximum flexural strength of the specimen S6B2H (after healing) was found to be 162.08MPa with a maximum load bearing capacity of 81.28 N.

1.3 Sample 6, specimen B3 (S6B3)

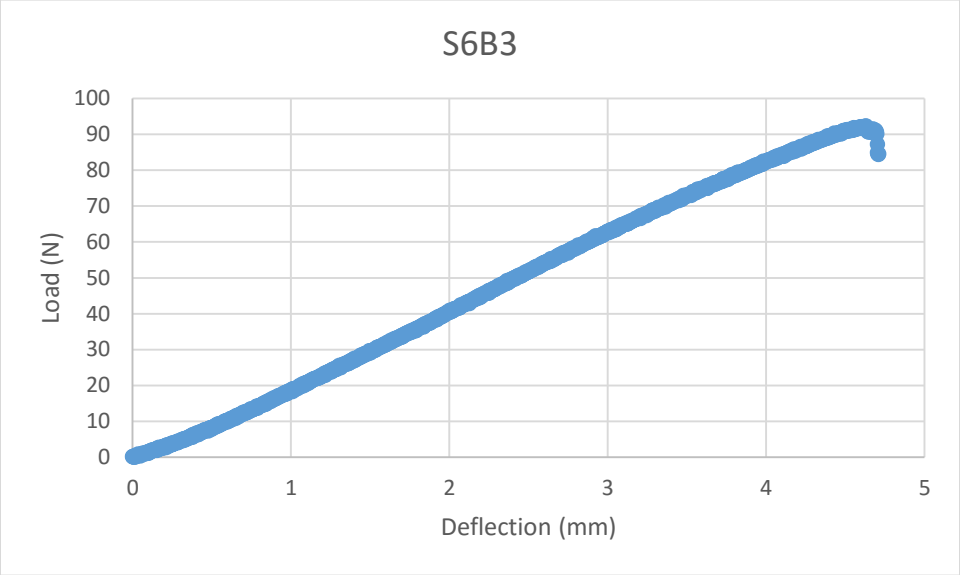

Figure 74: Load (N) vs deflection (mm) plot of the specimen S6B3

Maximum flexural strength of the specimen S6B3 was found to be 149.52MPa with a maximum load bearing capacity of 92.29 N.

1.4 Sample 6, healed specimen B3 (S6B3)

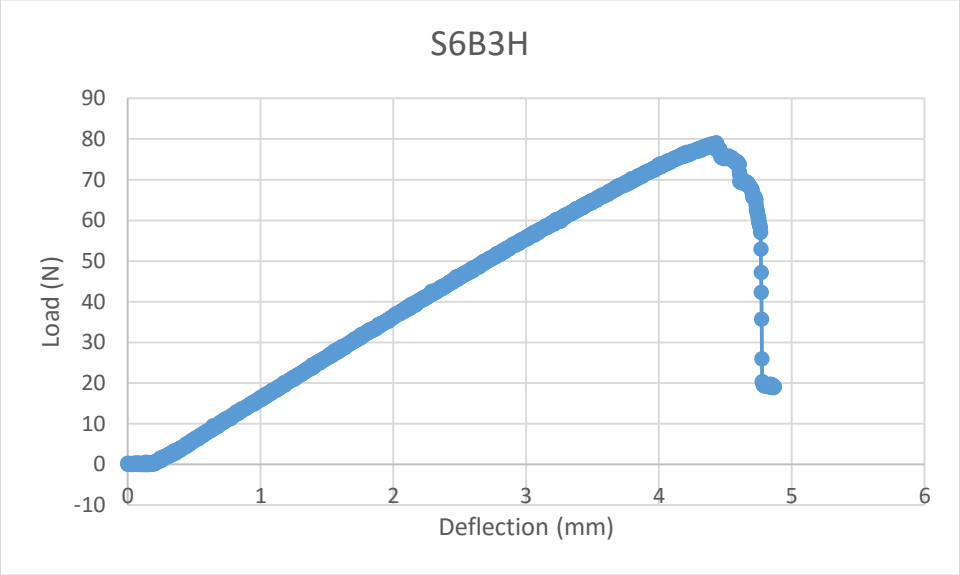

Figure 75: Load (N) vs deflection (mm) plot of the specimen S6B3H

Maximum flexural strength of the specimen S6B3H (after healing) was found to be 165.53MPa with a maximum load bearing capacity of 83.01 N.

2 Self-healing results of samples with tubes as the last layer

2.1 Sample 7, specimen B1 (S7B1)

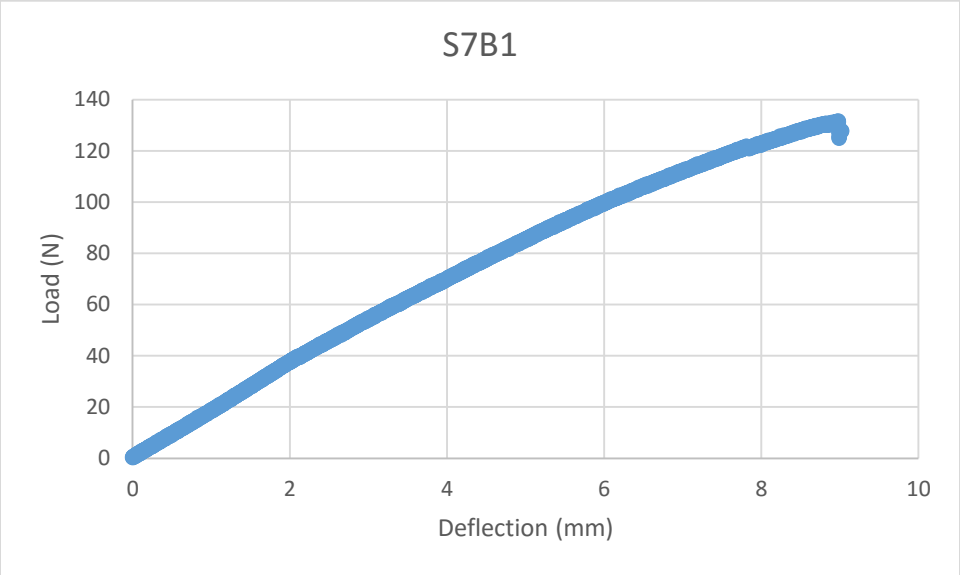

Figure 76: Load (N) vs deflection (mm) plot of the specimen S7B1

Maximum flexural strength of the specimen S7B1 was found to be 237.48MPa with a maximum load bearing capacity of 131.55 N.

2.2 Sample 7, healed specimen B1 (S7B1H)

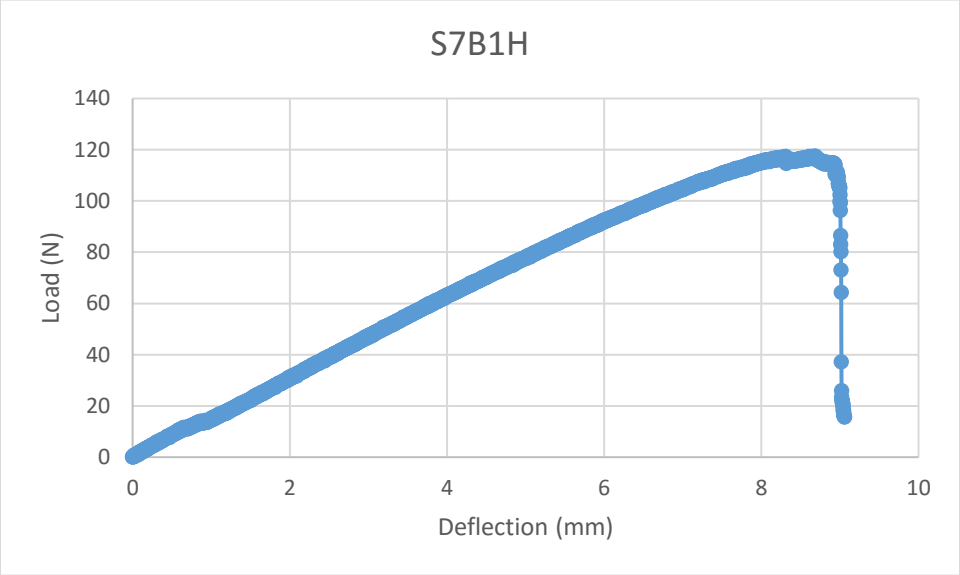

Figure 77: Load (N) vs deflection (mm) plot of the specimen S7B1H

Maximum flexural strength of the specimen S7B1H (after healing) was found to be 212.15MPa with a maximum load bearing capacity of 117.52 N

2.3 Sample 7, specimen B2 (S7B2)

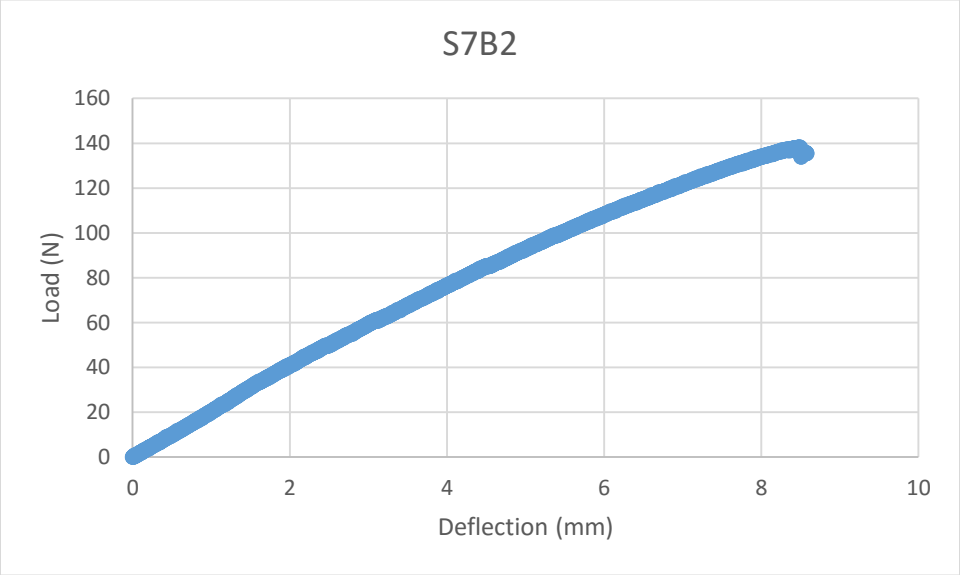

Figure 78: Load (N) vs deflection (mm) plot of the specimen S7B2

Maximum flexural strength of the specimen S7B2 was found to be 241.41MPa with a maximum load bearing capacity of 138.34 N

2.4 Sample 7, healed specimen B2 (S7B2H)

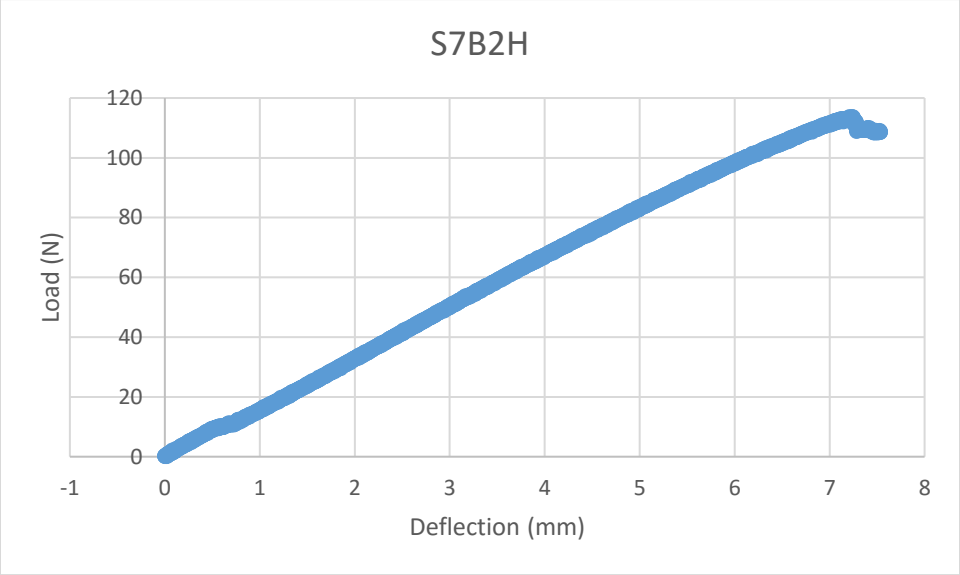

Figure 79: Load (N) vs deflection (mm) plot of the specimen S7B2H

Maximum flexural strength of the specimen S7B2H (after healing) was found to be 198.32MPa with a maximum load bearing capacity of 113.66 N

2.5 Sample 7, specimen B3 (S7B3)

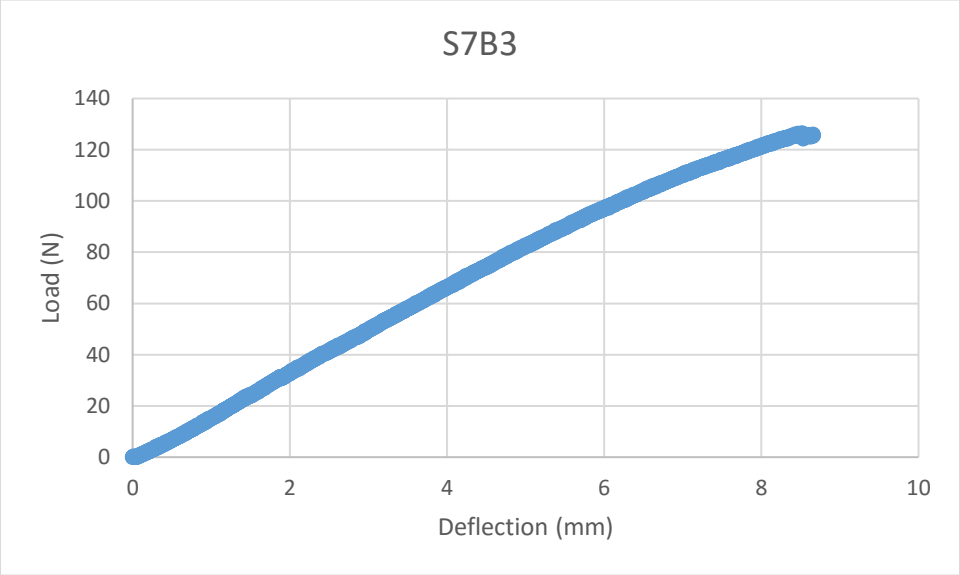

Figure 80: Load (N) vs deflection (mm) plot of the specimen S7B3

Maximum flexural strength of the specimen S7B3 was found to be 234.67MPa with a maximum load bearing capacity of 126.49 N

2.6 Sample 7, healed specimen B3 (S7B3H)

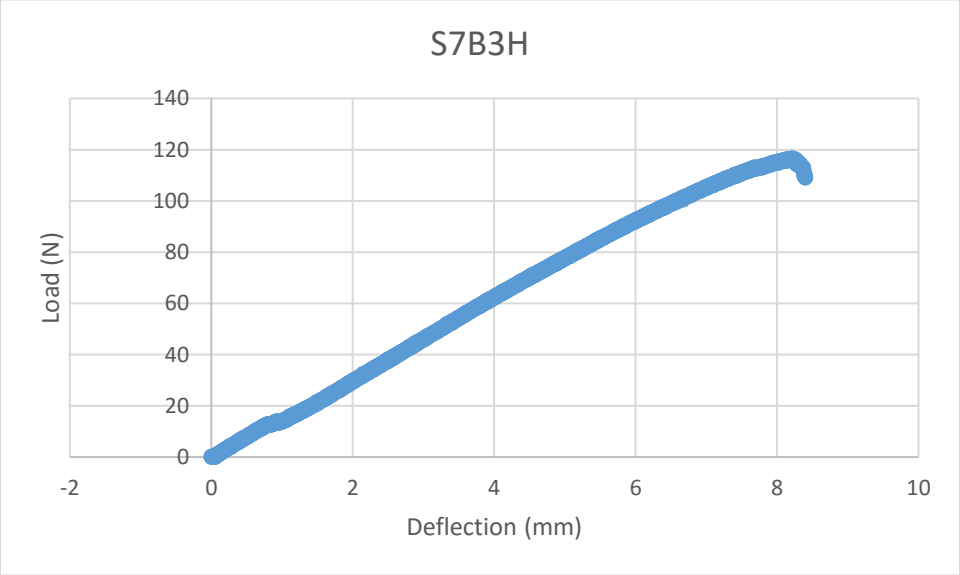

Figure 81: Load (N) vs deflection (mm) plot of the specimen S7B3H

Maximum flexural strength of the specimen S7B3H was found to be 216.58MPa with a maximum load bearing capacity of 116.74 N

2.7 Sample 7, specimen B4 (S7B4)

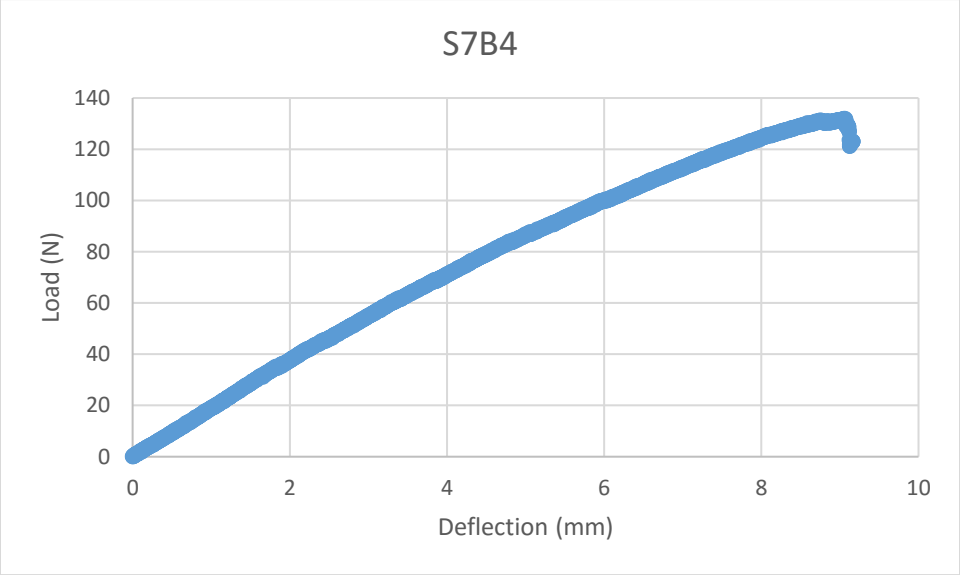

Figure 82: Load (N) vs deflection (mm) plot of the specimen S7B4

Maximum flexural strength of the specimen S7B4 was found to be 237.78MPa with a maximum load bearing capacity of 131.94 N

2.8 Sample 7, healed specimen B4 (S7B4H)

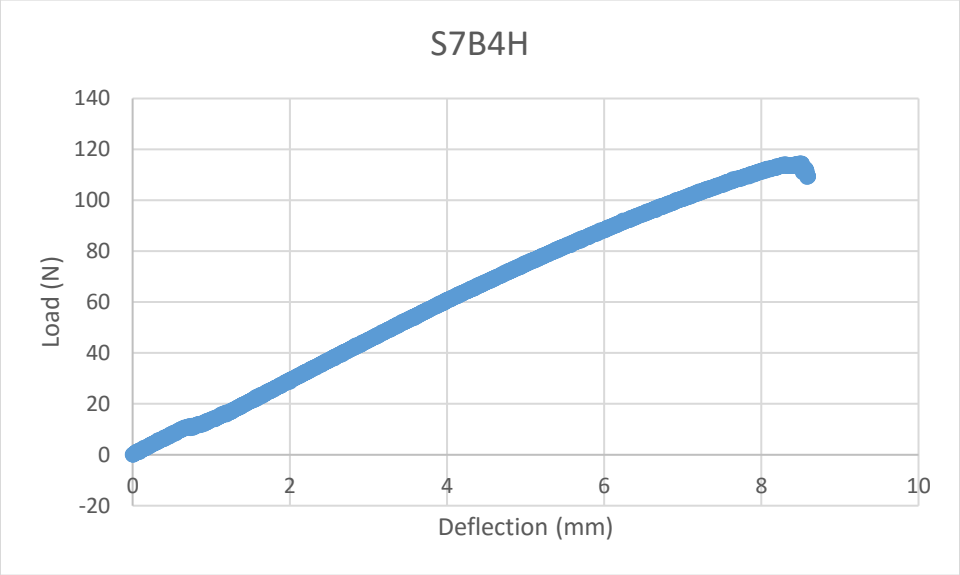

Figure 83: Load (N) vs deflection (mm) plot of the specimen S7B4H

Maximum flexural strength of the specimen S7B4H was found to be 206.38MPa with a maximum load bearing capacity of 114.52 N

2.9 Sample 7, specimen B6 (S7B6)

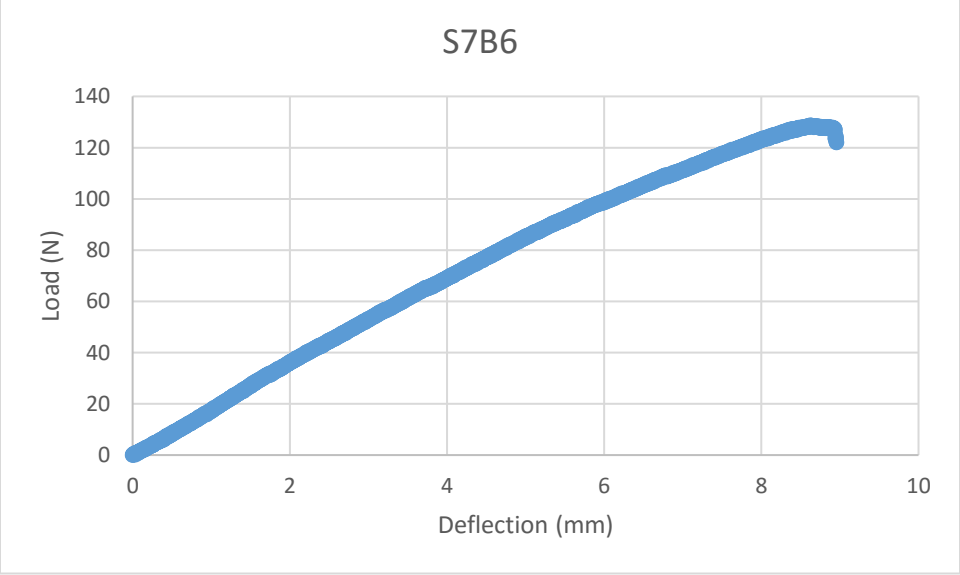

Figure 84: Load (N) vs deflection (mm) plot of the specimen S7B6

Maximum flexural strength of the specimen S7B6 was found to be 227.54MPa with a maximum load bearing capacity of 1128.76 N

2.10 Sample 7, healed specimen B6 (S7B6H)

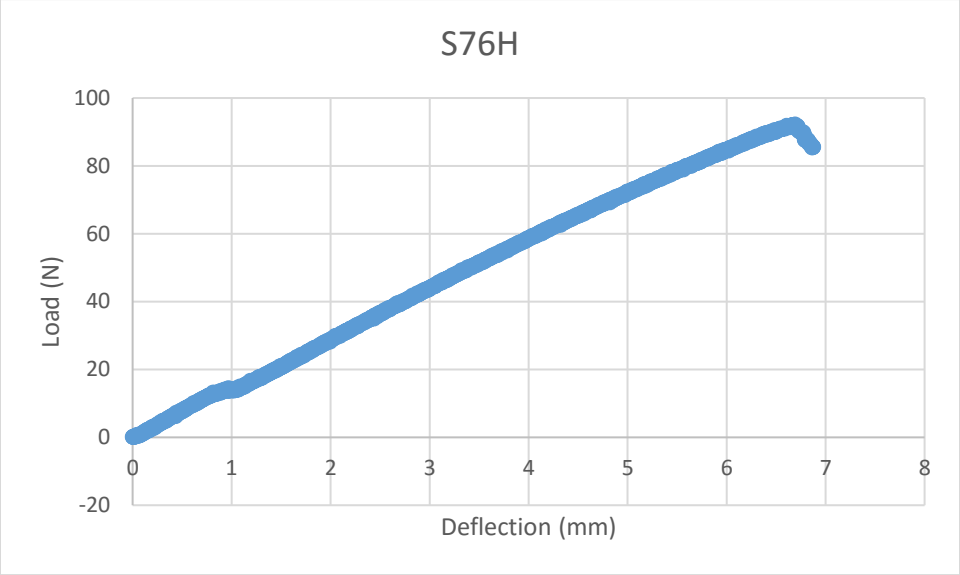

Figure 85: Load (N) vs deflection (mm) plot of the specimen S7B6H

Maximum flexural strength of the specimen S7B6H was found to be 162.91MPa with a maximum load bearing capacity of 92.19N

3 Self-healing results of samples with tubes as the penultimate layer

3.1 Sample 9, specimen B2 (S9B2)

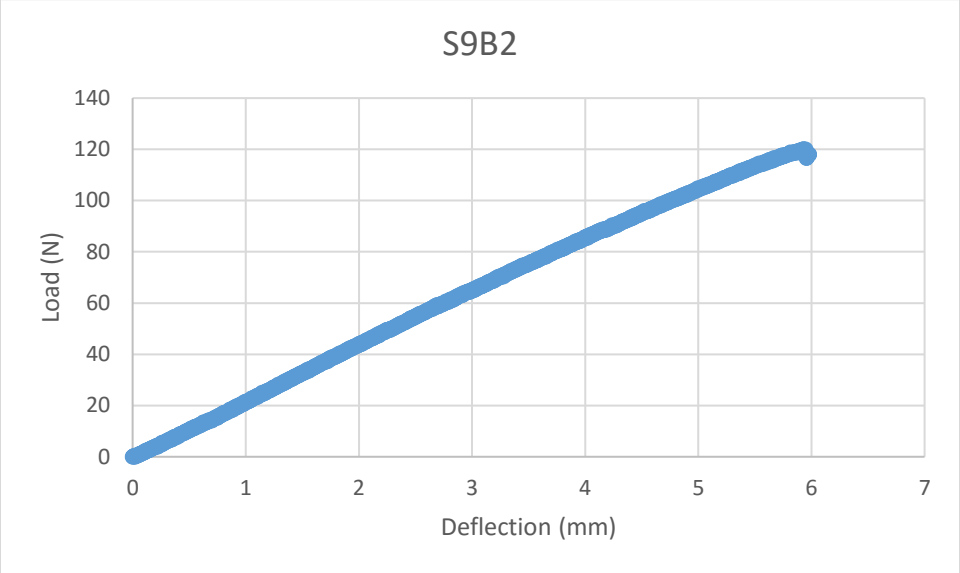

Figure 86: Load (N) vs deflection (mm) plot of the specimen S9B2

Maximum flexural strength of the specimen S9B2 was found to be 221.13MPa with a maximum load bearing capacity of 120.17N

3.2 Sample 9, healed specimen B2 (S9B2H)

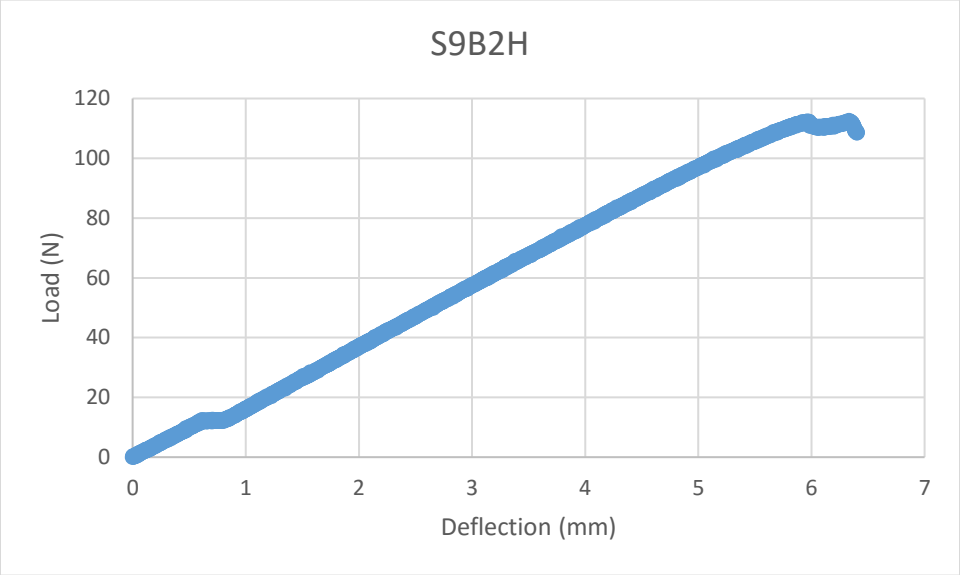

Figure 87: Load (N) vs deflection (mm) plot of the specimen S9B2H

Maximum flexural strength of the specimen S9B2H was found to be 207.19MPa with a maximum load bearing capacity of 112.59N

3.3 Sample 9, specimen B3 (S9B3)

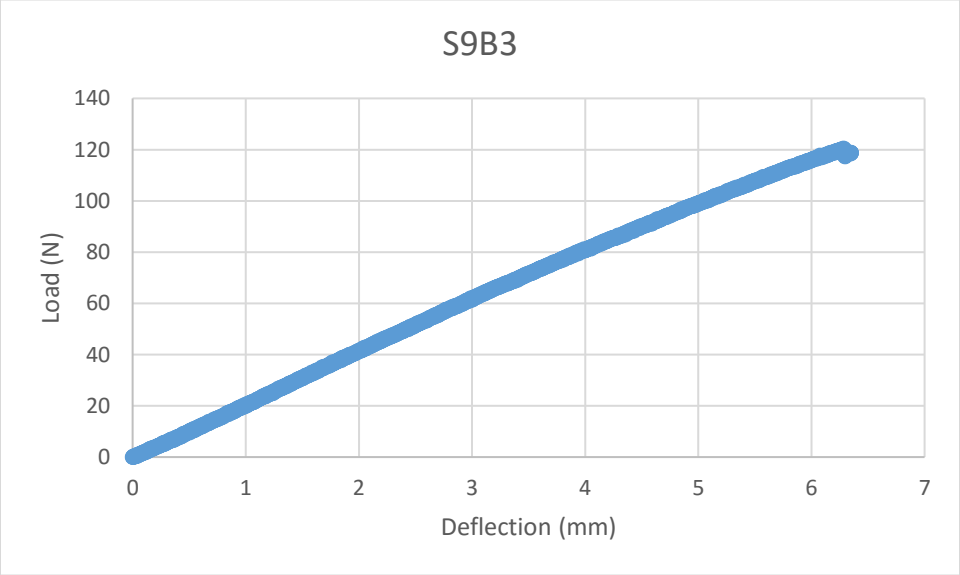

Figure 88: Load (N) vs deflection (mm) plot of the specimen S9B3

Maximum flexural strength of the specimen S9B3 was found to be 232.89MPa with a maximum load bearing capacity of 120.58N

3.4 Sample 9, healed specimen B3 (S9B3H)

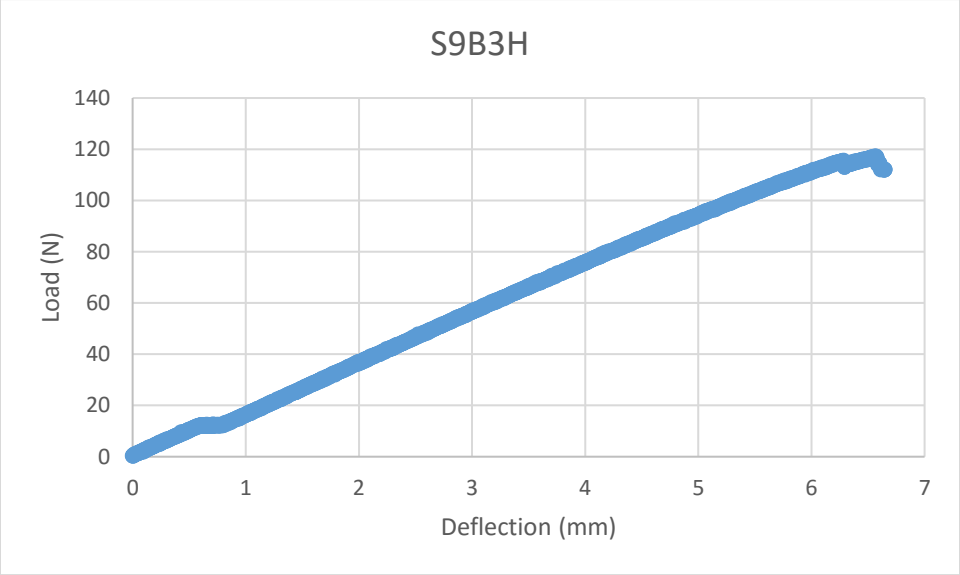

Figure 89: Load (N) vs deflection (mm) plot of the specimen S9B3H

Maximum flexural strength of the specimen S9B3H was found to be 226.54MPa with a maximum load bearing capacity of 117.29 N

3.5 Sample 9, specimen B5 (S9B5)

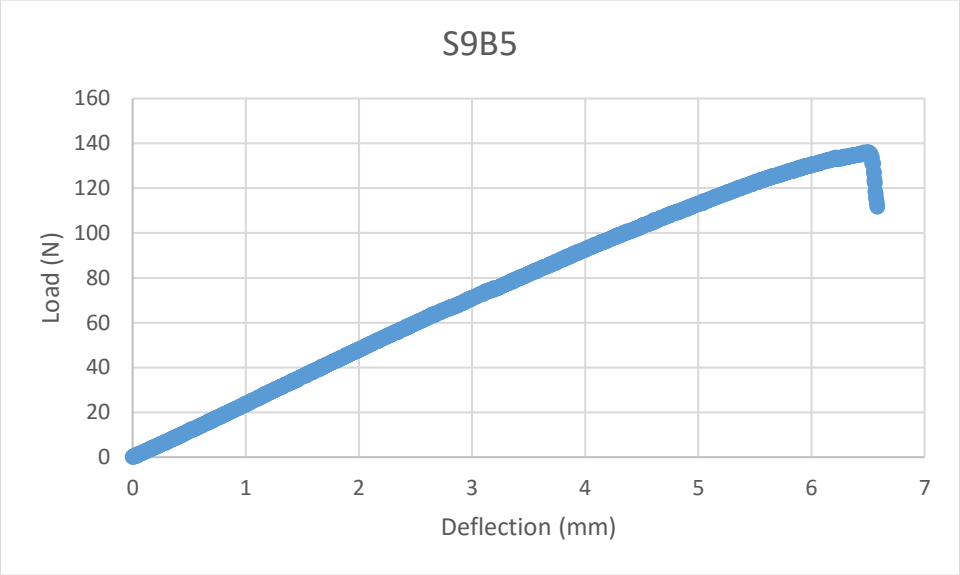

Figure 90: Load (N) vs deflection (mm) plot of the specimen S9B5

Maximum flexural strength of the specimen S9B5 was found to be 232.0MPa with a maximum load bearing capacity of 136.08N

3.6 Sample 9, healed specimen B5 (S9B5)

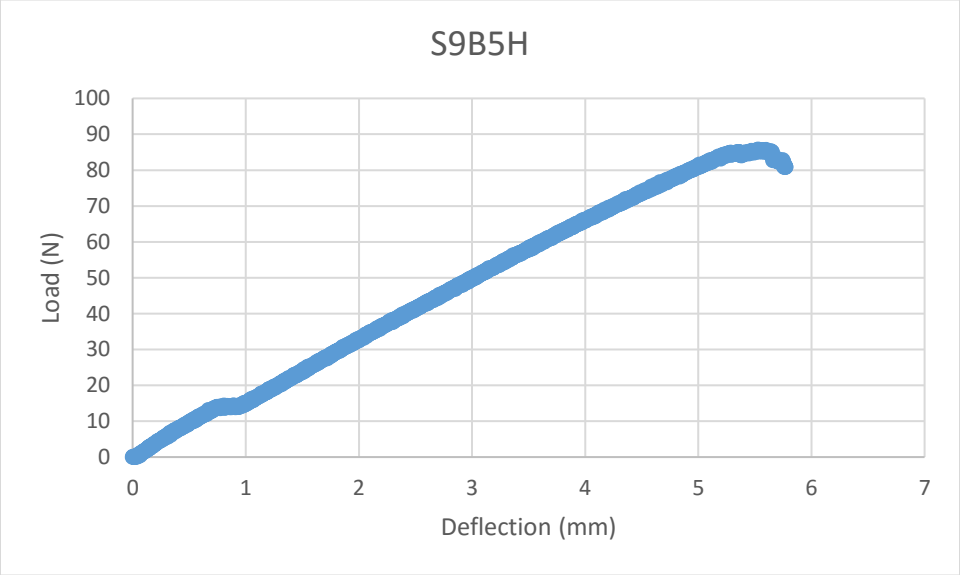

Figure 91: Load (N) vs deflection (mm) plot of the specimen S9B5H

Maximum flexural strength of the specimen S9B5H was found to be 146.31MPa with a maximum load bearing capacity of 85.81N

3.7 Sample 9, specimen B7 (S9B7)

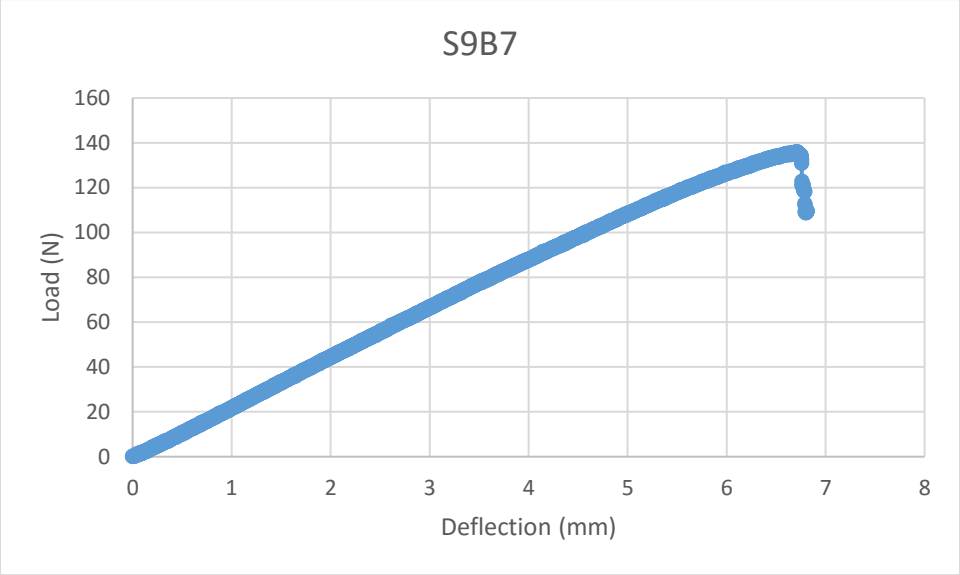

Figure 92: Load (N) vs deflection (mm) plot of the specimen S9B7

Maximum flexural strength of the specimen S9B7 was found to be 240.3MPa with a maximum load bearing capacity of 135.99N

3.8 Sample 9, healed specimen B7 (S9B7H)

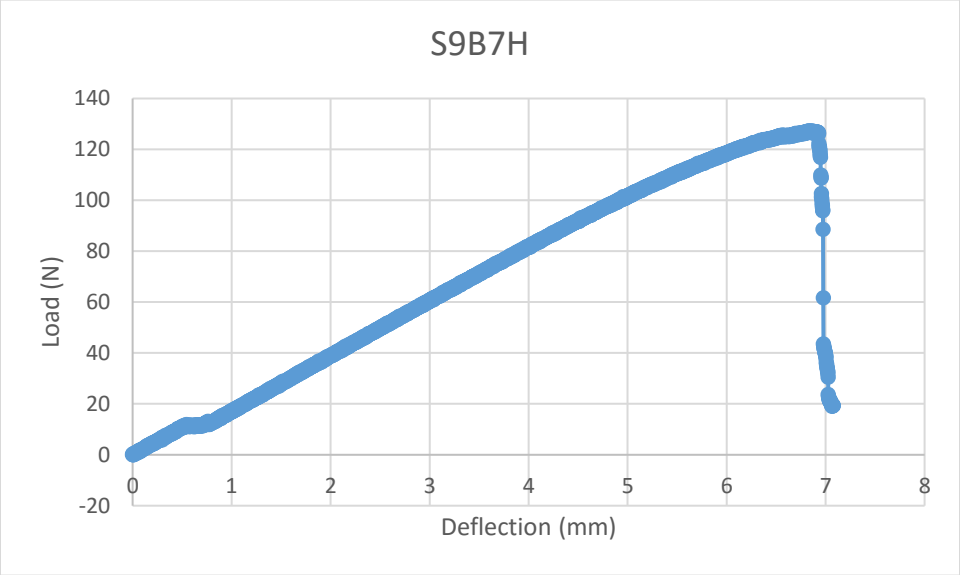

Figure 93: Load (N) vs deflection (mm) plot of the specimen S9B7H

Maximum flexural strength of the specimen S9B7H was found to be 226.85MPa with a maximum load bearing capacity of 127.33N

Appendix B : Best practices employed/learnt during this work

1 Molding through VARTM process

1. It is vital to have the sample under vacuum through its curing duration. The vacuum was left running for up to 24 hours while leaks were inevitable in the vacuum seal.
2. A tolerance of around 5-8mm was provided to in the fiberglass fabrics. The portion in general consists of taper and is cut off after removal from the mold.
3. A layer of wax was smeared over the base of the mold for tack free removal of the mold.
4. Always wear gloves while handling fiber glass/ resin-hardener. Fine fiberglass particles tend to remain unnoticed all over the hands if gloves are not used and can be harmful if consumed or it gets itchy.

5. Use roller to align the fiberglass weave after cutting for maximum consistency of the fiber arrangement in the sample. Roller can also be used for hand lay-up of resin-hardener mixture to remove entrapped air and improve wetting.
6. A twostep process was used while using catalyst during the molding process. A concentrated solution of resin-hardener and Grubb's catalyst solution was poured around the tubes along with usage of roller (only over fibers and not on tubes) to improve the infusion. Figure 94 shows the solution that has been used during the process. Vacuum was then applied and a lean solution of Grubb's catalyst with resin-hardener mixture was used for the VARTM process.

Figure 94: Concentrated Grubb's catalyst mixture used specifically around the tubes

7. Care must be taken to never let the resin mixture or wax to come in contact with vacuum tape. An added layer of vacuum tape is used if the mishap did take place.

8. Clean beakers and other vessels used to mix resin-hardener before it cures and hardens using acetone. Excess resin hardener mixture along with acetone should be disposed in a hazardous waste can and must not be disposed into trash or drain pipes at any circumstances. Curing process is an exothermic process melts trash bags and damages the trashcan. If poured into a drain, the mixture cures and clogs the drainpipe.
9. If there is resin-hardener mixture spillage on the floor, the mixture is easier to remove if allowed to cure and harden (without spreading with a cloth or tissue) and a simple hand tool can be used to chip off the floor surface.
10. Most care and considerable vacuum tape must be used to pierce the inlet and outlet tubes and seal them into the vacuum bag. Care must also be taken that no portion of sealed vacuum bag is over stretched during the process when subjected to vacuum.
11. A hard metal plate covered with wax can be place over the sample with in the vacuum bag to improve the flatness of the sample on the top surface.

2 Filling DCPD into tubes

1. A tube and syringe set-up is used to fill the tubes with DCPD and or DCPD with UV reflective dye mixture. Figure 92 shows the tube and syringe combination.

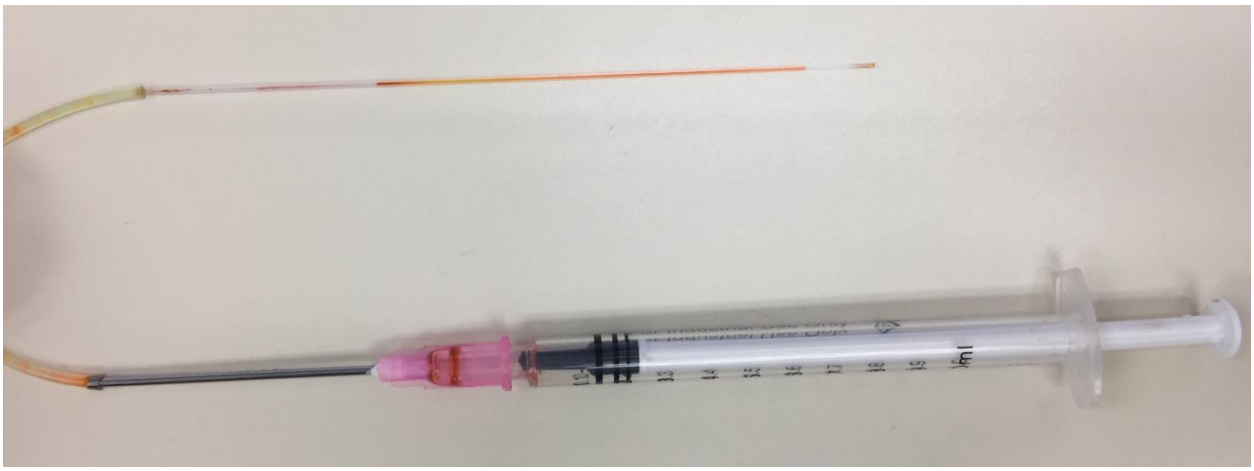

Figure 95: Tube and syringe combination used to fill the tubes with DCPD (colored stains are from UV reflective dye)

2. DCPD is heated for a small duration (3-5min) at medium heat to liquefy the content completely for easy infiltration into the tubes.
3. 2% by volume of a UV reflective dye called UV fluorescent leak detection dye from Tracerline was used along with DCPD to improve the visibility of flow of DCPD inside the molded composite.
4. A double sided tape is used over a ruler to precisely place affix the tubes and for ease of transfer of tubes over the glass fiber samples.
5. The tubes can be infiltrated at positive pressure in a pressurized glove box for improved pressure difference and bleeding of healing agent when cracked.